23525727

MICHIGAN STATE UNIVERSITY LIBRARIES
3 1293 00570 3206

LIBRARY
Michigan State
University

This is to certify that the

dissertation entitled

Spectroscopic Analyses of Supersaturated
Solutions and the Source of Secondary
Nuclei

presented by

Michael K. Cerreta

has been accepted towards fulfillment
of the requirements for

Ph.D. degree in Chemical Engineering

Kris A. Berglund
Major professor

Date Oct 19, 1988

MSU is an Affirmative Action/Equal Opportunity Institution

PLACE IN RETURN BOX to remove this checkout from your record.
TO AVOID FINES return on or before date due.

DATE DUE	DATE DUE	DATE DUE
MAY 10 1993 092		

MSU Is An Affirmative Action/Equal Opportunity Institution

SPECTROSCOPIC ANALYSES OF SUPERSATURATED SOLUTIONS AND THE SOURCE OF SECONDARY NUCLEI

By

Michael Kenneth Cerreta

A DISSERTATION

Submitted to
Michigan State University
in partial fulfillment of the requirements
for the degree of

DOCTOR OF PHILOSOPHY

Department of Chemical Engineering

1988

5454189

ABSTRACT

SPECTROSCOPIC ANALYSES OF SUPERSATURATED SOLUTIONS AND THE SOURCE OF SECONDARY NUCLEI

By

Michael Kenneth Cerreta

Laser Raman, Fourier transform infrared, and UV-Vis spectroscopies were used to investigate crystal growth and nucleation mechanisms and their interrelation. Pure, supersaturated aqueous solutions of ammonium, potassium, and sodium dihydrogen orthophosphate (ADP, KDP, and NaDP, respect.) were found to consist of strongly hydrogen-bonded anion-anion dimers or polymers with structures dissimilar to their crystals. Difficulty in breaking these bonds upon transition from solution to crystal explains the unusually high metastability and growth activation energy, the rate-limiting surface growth mechanism, and rapid z-direction growth that is characteristic of the phosphates. The bulk solution structure of ADP is stable to changes in pH between 2 and 7, and is unaffected by Cr^{+3}, Fe^{+3}, and Al^{+3} habit-modifying ions up to 500 ppm. The pure, supersaturated aqueous solution structures of glycine, lysine, and glutamic amino acids were also found to be distinct from their crystals, but quite sensitive to changes in pH. These results indicate that there is no spectroscopic evidence for quasi-crystalline entities in solution, and that the solute species present in bulk supersaturated solutions may be considered *impurities* that influence crystal growth and nucleation mechanisms.

A laser Raman microprobe was used *in situ* to elucidate the nucleation mechanisms of dextrose from aqueous solution between 20-50°C. Growth of monohydrate dextrose on a parent anhydrous crystal was spectroscopically verified in solutions saturated below 30°C with 2°C undercooling. Single contacts of anhydrous dextrose crystals gave both monohydrate and anhydrous dextrose nuclei in solutions saturated between 40-45°C with 4-6°C undercooling. In this case, growth of the monohydrate phase on an anhydrous parent crystal could not be detected, even after 24 hours. This result precludes an attrition mechanism whereby monohydrate grows on microscopic anhydrous nuclei, and indicates there is a strong relation between the nucleation mechanism and the bulk solution structure.

DEDICATION

To Sophia.

ACKNOWLEDGMENTS

I want to express my sincere gratitude to Professor Kris Berglund, my advisor, without whom I would not know the beauty and workings of crystals, nor the same of friendship.

TABLE OF CONTENTS

CHAPTER 1: INTRODUCTION 1

1-1. Introduction 1

1-2. Literature Cited 4

CHAPTER 2: SURVEY OF THE RELEVANT LITERATURE 5

2-1. General Concepts of Crystal Growth 5

2-1.1 Theories of growth of real and perfect crystals 5
2-1.2 Volume diffusion and growth from solution 10
2-1.3 Surface diffusion and growth from solution 13
2-1.4 Growth rate and industrial crystallizers 15

2-2. General Concepts of Crystal Nucleation 18

2-2.1 Homogeneous and heterogeneous nucleation 18
2-2.2 Secondary nucleation 21
2-2.3 Contact nuclei formation and removal 25

2-3. Raman Spectroscopy and Aqueous Solutions 28

2-3.1 Theory of the Raman process 28
2-3.2 Raman studies of aqueous solutions 31

2-4. Non-Spectroscopic Evidence for Hydrogen Bonding in Dihydrogen Phosphate Solutions 35

2-5. Literature Cited 36

CHAPTER 3: A CONSTANT TEMPERATURE RAMAN CELL FOR THE STUDY OF SUPERSATURATED SOLUTIONS 42

3-1. Introduction 42

3-2. Experimental 43

3-3. Results and Discussion 45

3-4. Conclusions 47

3-5. Acknowledgment 47

3-6. Literature Cited 47

CHAPTER 4: THE STRUCTURE OF AQUEOUS SOLUTIONS OF SOME DIHYDROGEN ORTHOPHOSPHATES BY LASER RAMAN SPECTROSCOPY 48

4-1. Abstract 48

4-2. Introduction 49

4-2.1 Characteristics of dihydrogen orthophosphate crystals and crystal growth 50
4-2.2 Raman spectroscopy and dihydrogen phosphates 56

4-3. Experimental Procedures, Apparatus, and Band Analyses 58

4-4. Results and Discussion 61

4-5. Conclusions 79

4-6. Acknowledgment 80

4-7. Literature Cited 80

CHAPTER 5: THE EFFECT OF IONIC IMPURITIES ON THE AQUEOUS SOLUTION STRUCTURE OF DIHYDROGEN ORTHOPHOSPHATES 84

5-1. Abstract 84

5-2. Introduction 84

5-3. Experimental 85

5-4. ADP Crystals and Crystal Growth 86

5-5. UV-VIS, Raman, and FTIR Spectroscopies 87

5-6. Results and Discussion 90

5-6.1 Pure solutions 90

5-6.2 The effect of pH 95
5-6.3 Effects of metal ions 100

5-7. Conclusions 104

5-8. Acknowledgments 105

5-9. Literature Cited 105

CHAPTER 6: LASER RAMAN AND FOURIER TRANSFORM INFRARED SPECTROSCOPIC STUDIES OF THE CRYSTAL AND AQUEOUS SOLUTION STRUCTURES OF SOME AMINO ACIDS 106

6-1. Abstract 106

6-2. Introduction 106

6-3. Experimental 107

6-4. Raman and Infrared Spectroscopies 108

6-5. Studies of Crystal and Aqueous Glycine 110

6-6. Studies of Crystal and Aqueous Lysine 119

6-7. Studies of Crystal and Aqueous L-Glutamic Acid 126

6-8. Conclusions 131

6-9. Acknowledgments 131

6-10. Literature Cited 131

CHAPTER 7: CONTACT NUCLEI FORMATION IN AQUEOUS DEXTROSE SOLUTIONS 133

7-1. Abstract 133

7-2. Introduction 134

7-3. Production of Secondary Nuclei 135

7-4. Secondary Nucleation and Raman Studies of Dextrose 137

7-5. Experimental Methods and Materials 140

7-6. Results and Discussion 143

7-7. Summary and Conclusions 154

7-8. Acknowledgments 155
7-9. Literature Cited 155

CHAPTER 8: SUMMARY AND CONCLUSIONS 158
8-1. Summary and Conclusions 158
8-2. Proposals for Future Research 160
8-3. Literature Cited 162

APPENDICES 163

APPENDIX A: ON THE VIBRATIONAL BAND ASSIGNMENTS OF AQUEOUS DIHYDROGEN ORTHOPHOSPHATES 164

APPENDIX B: DISTINGUISHING FEATURES OF THE SPECTRA OF CRYSTALLINE AND AQUEOUS DEXTROSE 168

APPENDIX C: RAMAN SPECTRA OF DIHYDROGEN ORTHOPHOSPHATES 170

APPENDIX D: RAMAN SPECTRA OF DEXTROSE 176

CHAPTER 1

INTRODUCTION

1-1. Introduction

According to Mullin [1], "...there are few sections of the chemical industry that do not, at some stage, utilize crystallization as a method of production, purification, or recovery of solid material." Crystallization is the largest unit operation in the chemical process industry. On a scale such as this, any improvement in crystallization operations may bring great benefits to the producer.

Of utmost concern in virtually all crystallization processes is the crystal size distribution (CSD). This characteristic can determine whether crystals will have good flow, handling, packaging, and appearance properties. The factors most important in determining the CSD are the growth and nucleation rates. The CSD may be predicted (in principle) by the population balance technique [2]. In this formalism, the nucleation rate and the growth rate are intimately connected. This means that control of the CSD is not possible unless the mechanisms governing both processes are known.

For crystal growth from the vapor the growth unit is reasonably assumed to be monomolecular. However, for crystal growth from solution, there is no reasonable assumption regarding the state of the growth unit. Whatever form it takes, the growth unit begins its trek to the crystal in the bulk solution. Therefore, a description of the growth process is incomplete unless the structure of the bulk solution is defined.

The debate in the current literature on the mechanism of crystal nuclei formation centers on two hypotheses. One [3] regards the nuclei as pieces "chipped off" a pre-existing or parent crystal by contact with another surface. The other [4] supposes that the presence of a parent crystal stabilizes pre-crystalline clusters that would otherwise dissolve in the bulk solution. Again, a contact dislodges the nuclei. Recently, it has been found [5] that single contacts with dextrose can produce nuclei of two phases; the parent phase, and a hydrated phase. Unless the hydrated phase can grow on the parent phase, this means that the attrition mechanism is not valid for dextrose, and that the pre-crystalline cluster concept would seem to apply.

A promising means of controlling crystal growth and nucleation rates is by the use of impurities. However, very little is known of their influence on growth or nucleation. At present, trial and error is the only course of action.

Knowledge from which crystal growth theories have been derived has come from microscopic observation. The existence of steps on the crystal surface and their peculiar movements have been demonstrated in this way. The inherent limitation of light microscopes to resolve images and the inability to perform electron microscopy experiments _in situ_ have impeded understanding of growth processes.

Raman spectroscopy is an experimental technique yielding information on molecular structure and may be performed in situ. A Raman microprobe can yield this information from specimens as small as 2 μm^2. Using this technique, the objectives of this work are:

1. to study the aqueous bulk solution structure of ammonium, potassium, and sodium dihydrogen orthophosphates, a class of compounds that have received considerable attention in the crystallization literature, from dilute to supersaturated, and to relate this structure to the growth of the crystals;
2. to investigate the effects of the ionic impurities H^+, Cr^{+3}, Fe^{+3}, and Al^{+3}, each known to cause habit modifications in the phosphates, on the dihydrogen phosphate aqueous bulk solution structure, using also infrared and UV-VIS spectroscopies;
3. to study the aqueous solution structure of the amino acids glycine, lysine, and glutamate at neutral, acid, and basic pH, as a measure of the range of applicability of the technique;
4. to use the laser Raman microprobe to determine if the hydrated dextrose phase is capable of growing on the parent dextrose phase.

1-2. Literature Cited

1. J. W. Mullin, Crystallization. (CRC Press, Cleveland, 1971, 2cd ed.).

2. A. D. Randolph and M. A. Larson, Theory of Particulate Processes (Academic Press, New York, 1971).

3. K. Shimizu, K. Tsukamoto, J. Horita, and T. Tadaki, J. Crystal Growth, 69, 1984, 623-626.

4. M. A. Larson and J. Garside, Chem. Eng. Sci., 41(5), 1986, 1285-1289.

5. P. Elankovan and K. A. Berglund, A.I.Ch.E J., 33(11), 1987, 1844-1849.

CHAPTER 2

SURVEY OF THE RELEVANT LITERATURE

2-1. General Concepts of Crystal Growth

Crystal growth occurs only when the environment in which the crystal resides is supersaturated, i.e., when there is more solute present in the environment than would be were the entire system at equilibrium. There are many ways to bring about the growth of crystals. Pamplin [1] lists 37 physically different methods. All of these methods may be considered belonging to one of four catagories:

1. vapor phase growth,
2. solid-state growth,
3. melt growth, and
4. solution growth.

The method employed is chosen to take advantage of the physical properties of the substance being crystallized. Of particular importance here is growth from aqueous solution. Supersaturation in aqueous solution is usually generated by decreasing the temperature of an equilibrium mixture or by evaporating the solvent water.

2-1.1 Theories of growth of perfect and real crystals

The most widely accepted theory describing growth from solution [2] is actually an extension of an earlier theory of growth of real crystals from the vapor [3], which in turn was developed from the theory of growth of perfect crystals. Real crystals are distinguished from perfect crystals by the presence of imperfections in the former. A theory of growth of perfect crystals was first considered by Gibbs in a footnote [4]. As described in [3], this theory was advanced chiefly by Volmer [5], Stranski [6,7], and Becker and Doring [8]. The theory considers that growth of atomically smooth crystal faces occurs by two-dimensional nucleation of growth units on the crystal surface. Burton, Cabrera, and Frank (BCF) [9] showed that because of the high edge energy of the two-dimensional nuclei, relative supersaturations (for definition, see Equation (4-1)) of approximately 50% are required for growth. Since crystals grow at supersaturation ratios of 1% or less, BCF [9] and Frank [10] concluded growth can only be explained if the crystals are not perfect; these are "real" crystals. Two-dimensional nucleation is not required for growth of real crystals since imperfections provide the steps needed for growth. The imperfections take the form of dislocations. A theory of dislocations is given by Hirth and Lothe [11]. Much earlier, Frank [10,12] discussed several possible mechanisms of their origin:

1. surface nucleation of layers in improper and proper positions simultaneously on the same face (this would occur only at high supersaturations, e.g., during initial crystal nucleation),
2. formation of one-dimensional dislocations in the

edge row of a growing terrace (only at high supersaturations),

3. the development of curvature in the growing crystal due to the presence of impurities,
4. the stress developed in a system of dislocations causes the development of others,
5. aggregation of molecular vacancies into flat, collapsed cavities whenever the temperature of the crystal is lowered, and
6. plastic yield under mechanical stress.

The above indicates that a high degree of perfection in growing crystals is possible if the environment of growth is maintained at constant temperature and supersaturation, there are no impurities present, the supersaturation is as low as possible, and the level of mechanical mixing is low. However, absolutely perfect crystals are not possible since the conditions required for their growth would also soon make them imperfect.

By far, the predominant type of dislocation by which real crystals grow is the screw dislocation (Figure 2-1). With this type of dislocation the crystal face always has exposed molecular terraces on which growth can continue indefinitely [10].

The Kossel model [13] of a growing crystal face introduces the idea that growth units diffuse about on the surface of a crystal until a kink site is encountered (Figure 2-2). Incorporation into a kink site is energetically

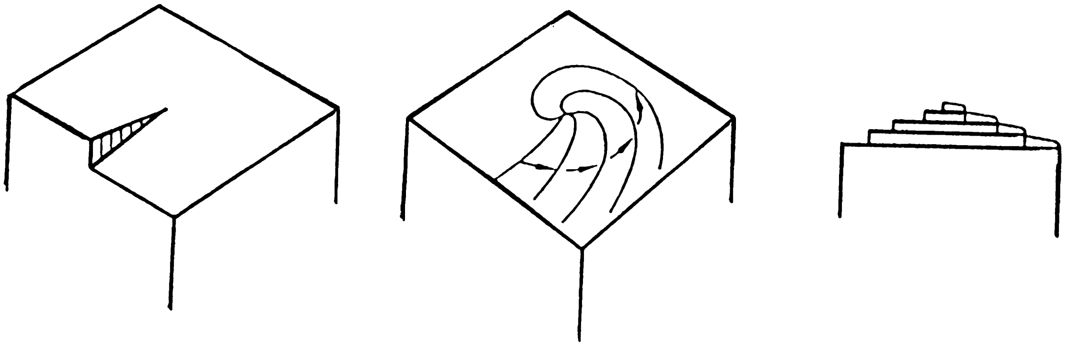

(a) (b) (c)

Figure 2-1. The screw dislocation.

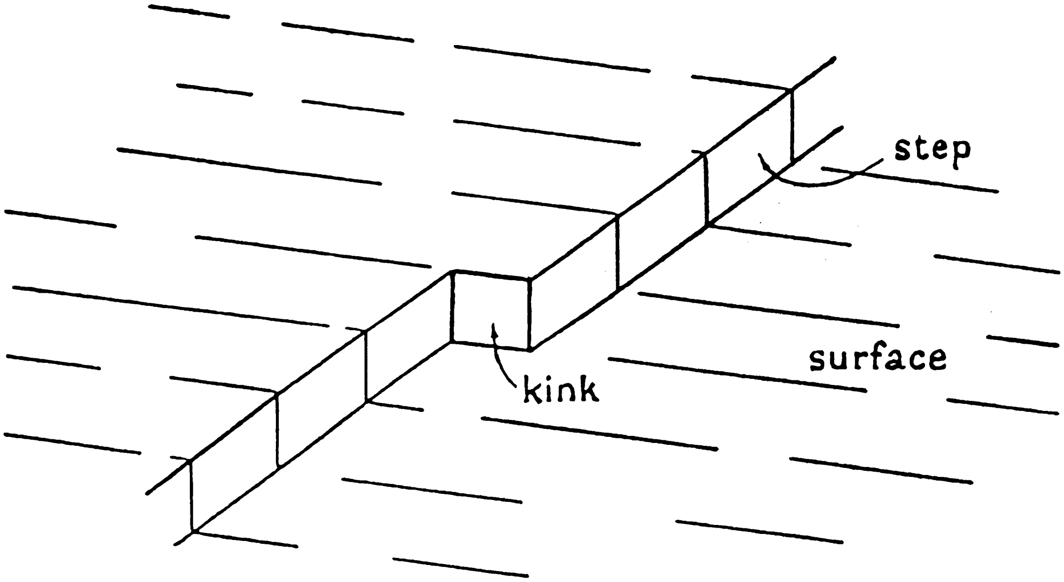

Figure 2-2. The surface of a crystal

more favorable than a flat surface or a step since the surface free-energy of the growth unit is less at a kink. Eventually the entire step is filled. The Kossel model fails because it requires surface nucleation to generate new steps. Burton, Cabrera, and Frank [3] retained the concept of surface diffusion to kink sites to calculate crystal growth rate at any supersaturation. This relationship is given by

$$G = A*\sigma^2*\tanh(B/\sigma) \tag{2-1}$$

where G is growth rate, A and B are constants, and σ is the supersaturation ratio. At low σ, Equation (2-1) approximates to $G = a*\sigma^2$, and at high σ, $G = b*\sigma$, where a and b are constants. These are called the parabolic and linear laws, respectively. These relations were experimentally verified by BCF by measuring the growth rates of Hg, I_2, P_4 (white phosphorus), and $C_{10}H_8$ (napthalene) crystals from their vapor at different supersaturations.

2-1.2 Volume diffusion and growth from solution

Volume diffusion models for crystal growth were introduced by Noyes and Whitney [14] and Nernst [15]. The major assumption is that crystal growth rates are limited by the rate of diffusion of solute through solution. The models fail to explain the varying growth rate of different crystal faces because they do not consider the role of the crystal face in the growth process. The models also assume that crystallization and dissolution proceed at equal rates.

This is quite incorrect, as dissolution is usually much faster than crystallization.

Frank stated in 1949 [10]: "Experimental indications, and such theoretical guesswork as we can make, suggest that the conditions governing the growth from solution of crystals, including ionic crystals, are substantially similar (to growth from the vapor)," but he did not elaborate. BCF [3] briefly treated growth from solution. They recognized that growth unit diffusion would be much slower than in the vapor. It might occur at the edge of a step, on the crystal surface, or through the solution. They chose to concentrate only on volume diffusion and imagined three diffusion fields. The first is a hemispherical diffusion field about kink sites when the growth unit is within the average distance between kinks from a given kink. The second is semi-cylindrical about each step when the growth unit is no farther from a kink site than the average distance between steps. The third is a plane diffusion field when the growth unit resides beyond the distance between steps but still within the so-called unstirred layer of solution about the entire crystal. Equating the fluxes of each field (conservation of mass) gives a growth rate-supersaturation relation of the same form as Equation (2-1), that is, a parabolic relation for low supersaturations and a linear relation for high supersaturations.

Chernov [16] considered growth from solution in more detail than BCF. In the Chernov volume diffusion model, the

steps are treated as line sinks, and kinks are ignored. This requires a semi-cylindrical diffusion field near the crystal. In the BCF model the supersaturation around a step is related to the chemical potential difference between the crystal and solution. Chernov's model assumes the strength of the sink is proportional to the departure from the equilibrium chemical potential of the particles immediately surrounding a sink. In this sense, Chernov's model is probably more correct. Chernov's model results in the same parabolic and linear laws found by BCF, except that the linear law does not pass through the origin.

Bennema [2] analyzed both the BCF and Chernov volume diffusion models and showed their equivalence. In a single paragraph he derived the parabolic and linear laws by reasoning the growth rate of a crystal is proportional to the "flux" of steps passing a certain point on the crystal surface. This flux is given by the product of the advance velocity and density of the steps. The step density is proportional to the supersaturation. For low supersaturations, the diffusion fields of different steps do not interact. The advance velocity is proportional to the supersaturation in this case, and so the parabolic law results. When the supersaturation is high there is interaction between the diffusion fields since growth units can enter more steps. The advance velocity of the steps is independent of the supersaturation and so the linear law results.

2-1.3 Surface diffusion and growth from solution

Bennema [2], BCF [3], and Chernov [16] each felt that an unstirred or boundary layer between the supersaturated solution and the crystal surface must exist. Mullin [17] distinguished between the several kinds of boundary layers about a crystal, e.g., the hydrodynamic boundary layer or the diffusion boundary layer, and discussed their various depths. He estimated the diffusion boundary layer to be maximally 10 microns, the partially disordered solution layer near the interface to be about 0.1 microns, and the adsorbed molecular layers to be about 0.01 microns thick. Bennema [2] estimated this last layer to be 10 to 100 angstroms thick.

Bennema [2] adapted the surface diffusion model of BCF to growth from solution. He assumed:

1. The adsorption layer is of uniform ~10 angstrom thickness.
2. Although two ions may be present, they have the same relaxation time. This is the time required to replenish ions in each layer about the crystal.
3. The first and second diffusion laws of Fick hold in the adsorption layer.
4. For sufficiently low supersaturations the advance velocity of the steps can be neglected.

He then defined the following states of the growth unit:

1. Solvated growth unit in bulk solution.

1a. Activated, partially desolvated growth unit for entering the surface phase.

2. The same partially desolvated growth unit in the adsorption layer.

2a. Activated, partially desolvated growth unit for entering a kink.

3. The same desolvated growth unit half covered with a solvent jacket in the kink.

With these assumptions, the formalism of the BCF surface diffusion model applies and so Equation (2-1) results, except the constants A and B must be evaluated in light of the above. Bennema used Eyring's one-particle kinetic formalism [18] to assist in the evaluation of A and B. The analysis leads once again to linear and parabolic laws relating growth rate to supersaturation.

Since the functional form of the dependence of growth rate on supersaturation is the same for volume diffusion and surface diffusion, how does one determine the true growth mechanism for a given system? The simplest way is to test the dependence of growth rate on the rate of flow of solution past a growing crystal. This was done for ammonium and potassium dihydrogen phosphate [19]. The growth rate was independent of the solution flow rate, so it must be concluded these salts grow by a surface diffusion mechanism under the conditions of the experiment.

Garside [20] introduced the concept of effectiveness factors in crystal growth to give a quantitative measure of the degree of diffusion or surface integration control. The effectiveness factor is defined as

$$n_r = \frac{\text{measured over-all growth rate}}{\text{growth rate expected when the crystal surface is exposed to conditions in the bulk solution}} \qquad (2\text{-}2)$$

As n_r approaches 1, the surface integration process increasingly dominates.

Growth rate as a function of supersaturation is usually cast in the empirical power law form [21]

$$G = k^{*}\sigma^{n} \qquad (2\text{-}3)$$

where n is usually between 1 and 2, but this is by no means necessary. k is usually given in the form of an Arrhenius type expression [21]

$$k = k_o{}^{*}\exp(E_{act}/RT) \qquad (2\text{-}4)$$

E_{act} is the activation energy for crystal growth. Its value can help to distinguish between diffusion and surface integration control by comparison with the activation energy of diffusion.

2-1.4 Growth rate and industrial crystallizers

Growth rate as a function of time was studied by McCabe [22] and McCabe and Stevens [23]. The McCabe Δ-L law results from observations that the growth rate of a crystal is not a function of its size, given all else is constant.

Randolph and Larson [24] established a standard crystallizer by which the performance of industrial crystallizers could be measured and experiments compared. It is called the mixed suspension, mixed product removal (MSMPR) crystallizer. Assuming the applicability of the McCabe Δ-L law, perfect mixing, no classification at withdrawal, constant feed, no crystal breakage or agglomeration, steady-state, constant temperature and constant working volume, then the distribution of crystal sizes within the crystallizer obeys the relationship

$$n(L) = n^{o} * \exp(-L/G\tau) \qquad (2\text{-}5)$$

where L is size, n is the population density (number at size L per unit volume per unit L), n^{o} is the population density at zero size, G is growth rate, and τ is the residence time in the crystallizer. This result is a special case of the population balance technique developed by Randolph and Larson [24]. When ln(n) is plotted with L, a straight line of slope $-1/G\tau$ results, and the growth rate may be calculated. The intercept gives the population density at zero size. The nucleation rate B^{o} is found from

$$B^{o} = n^{o} * G \qquad (2\text{-}6)$$

Thus, the nucleation rate and growth rate may be found with a single experiment.

In many instances Equation (2-5) does not hold even though the assumptions leading to it have apparently been met [24]. Plots of ln(n) with L often show upward curvature

at small sizes. This behavior is suggestive of size-dependent growth, i.e., the McCabe Δ-L law seems in error. Janse and de Jong [25] studied this problem. They seeded a crystallizer with a narrow size distribution of potassium dichromate crystals. After some time, it was found that a much larger spread in crystal sizes was present than could be accounted for by random error. The only reasonable explanation was that crystals of one size exhibit a spread of growth rates. They termed this phenomena "growth dispersion". Earlier, White and Wright found similar results for sucrose [26].

Berglund [27], Ramanarayanan [28], and Berglund et al. [29] followed the growth rate of many individual crystals using photomicrographs. They found growth rate dispersion (as it is now known) exists for contact nuclei of citric acid monohydrate, ammonium dihydrogen phosphate, and potassium nitrate. Most important, they found over the size ranges investigated that individual crystals grow at a constant rate, but growth rate varies from crystal to crystal. This result forms the basis of the constant crystal growth model (CCG) [30]. Berglund and Larson [30] and Larson et al. [31] used the CCG model and gamma distributions for the initial size and growth rates to model growth rate dispersion in MSMPR crystallizers. The crystal size distribution obtained displays the characteristic upward curvature at small sizes.

2-2. General Concepts of Crystal Nucleation

Nucleation, in its broadest sense, refers to the birth of a new phase. The formation of rain or snow from water vapor, a gas bubble from a liquid, or a crystal from solution are examples of nucleation processes. In each case a center for nucleation is required. Rain or snow nucleate on dust particles in the air. The effect of seeding clouds with silver chloride is simply to give ice a sympathetic solid surface upon which to nucleate. Bubbles form from liquids at solid surfaces. Crystals, too, form on surfaces. Because a solution is supersaturated does not mean crystals will nucleate. The nucleation process mechanism greatly depends on the surface used to bring about nucleation. Different mechansims have been classified according to the presence and condition of surfaces in contact with a supersaturated solution.

2-2.1 Homogeneous and heterogeneous nucleation

Working from the framework of equilibrium thermodynamics, Gibbs [4] presented his theory of homogeneous nucleation in 1878. Although it was derived for a vapor condensing to a liquid, the same ideas are extended to crystallization from the melt or solution. Mullin [17] has outlined Gibbs's treatment. When a quantity of material condenses from a homogeneous medium, such as a vapor, work is required to form a surface and the bulk interior of the particle. This work is related to the particle size r by

$$W = \frac{4}{3}\pi r^2\sigma \qquad (2\text{-}7)$$

where W is the work of particle formation and σ is the surface energy of the particle per unit area. The relation between particle size and supersaturation is given by the Gibbs-Thomson relation

$$\ln S = \frac{2M\sigma}{RT\rho r} \qquad (2\text{-}8)$$

where S is the supersaturation ratio defined as the ratio of the concentration of solute actually present in solution, C, to its equilibrium value, C^*, M is the molecular weight, R is the gas constant, T is the absolute temperature, and ρ is the particle density. Solving (2-8) for r and inserting into (2-7) gives the relation between supersaturation and work of particle formation

$$W = \frac{16\pi\sigma^3M^2}{3(RT\rho\ \ln S)^2} \qquad (2\text{-}9)$$

Frank [10] has stated that typically a supersaturation ratio S of 10 is required to nucleate crystals homogeneously.

The number of molecules in a stable nucleus is several thousand. Simultaneous collision of these molecules to form a particle is not at all likely. Instead, the mechanism of homogeneous new-particle formation is thought to occur in a series of bimolecular additions via

$$\begin{array}{llcl} A & + A & = & A_2 \\ A_2 & + A & = & A_3 \\ \vdots & \;\;\vdots & & \vdots \\ A_{n-1} & + A & = & A_n \end{array}$$

where n is the number of molecules needed to form a stable particle.

When extreme precaution is taken to eliminate foreign material, the relation between supersaturation and nucleation holds (i.e., $S \sim 10$) [10]. In practice, supersaturations required to bring about nucleation are far lower. This is not due to any failure of the theory. It is particulate matter (impurities) in solution that provide nucleation sites for the solute. Since a surface is present, the enormous energy required for surface formation is not needed, and so nucleation takes place at lower S. This is called heterogeneous nucleation and is defined as nucleation occuring on a foreign body that is not the solute or isomorphic with it. Homogeneous nucleation results purely from supersaturation.

Ostwald developed a theory of homogeneous nucleation along lines of kinetic reasoning rather than thermodynamic. His ideas may be found in various chapters of his "Lehrbuch". He hypothesized that, within a supersaturated solution, the least-stable phase will nucleate *first*. The most stable phase, that is to say, the crystal, will nucleate *last*. In between, all sorts of species and

structures may form. He also introduced the concepts of supersaturated metastable and labile solutions. A metastable solution is one in which crystals will grow but nucleation will not occur under any circumstances; in a labile solution, both growth and nucleation are possible. A labile solution, then, is necessarily more supersaturated than a metastable one. Ostwald argued that a sharp line paralleling the saturation curve separated the two regimes. Young [32] and later Ting and McCabe [33] showed that nucleation could be induced at any supersaturation. They did not reject Ostwald's concept of metastability and lability, but argued that it had no practical value.

2-2.2 Secondary nucleation

While attempting to test Ostwald's hypothesis of metastable and labile solutions, Miers and Isaac [34] and Young [32] found that crystal nucleation could be induced by strong agitation or by merely dropping a crystal of the solute in a supersaturated solution. The supersaturation required in the latter case was far below that needed for heterogeneous nucleation. Ting and McCabe [33] in 1934 made the first study of supersaturation and crystal formation in seeded solutions. They found that far more crystals of magnesium sulfate heptahydrate were present in an agitated solution than were introduced as seeds. Their work also marked the beginning of studies of crystallization phenomena by chemical engineers made for the benefit of the chemical process industry.

In 1956, Powers [35] found that agitated sucrose solutions produced nuclei by simple fluid shearing of a single sucrose crystal suspended in solution. He was the first to suggest that a parent crystal (one from which the nuclei are descendant) might stabilize pre-crystalline nuclei.

In 1963, Strickland-Constable and Mason [36] performed a variety of experiments with magnesium sulfate heptahydrate. They identified four mechanisms by which a crystal introduced into a supersaturated solution can produce nuclei. They later published a more detailed account of their findings [37]. If a crystal is introduced into solution without any pre-treatment, crystalline dust or abrasion fragments from handling can produce nuclei, which they called "initial breeding". If a crystal pre-treated to remove dust and fragments is placed in a highly supersaturated solution (but below that causing heterogeneous nucleation), needles will grow on it and later break off to produce nuclei. This they called "needle breeding". Investigation of growing crystals of KBr in aqueous solution showed that the crystals grew as polycrystalline aggregates that sometimes broke up to give fresh crystals. This was termed "polycrystalline breeding". The two researchers had eliminated any contacts of the crystals with each other or the vessel in the above studies. When this restriction was lifted, they found that nuclei were produced with great readiness at quite low supersaturations. At first [36] they called this "attrition breeding", but later [37] changed it to "collision breeding" to reflect the fact that the actual mechanism of nuclei formation is not known. It is now known as "contact nucleation". It is now recognized that polycrystalline breeding is not a widespread phenomena, and that fluid shear to produce nuclei is.

In 1964, Melia and Moffitt [38] studied KBr crystallization from aqueous solution. They introduced the terms "primary nucleation" to describe all mechanisms of heterogeneous and homogeneous nucleation, and "secondary nucleation" to describe all means of nucleation that occur only because of the presence of crystals in solution. Figure 2-3 illustrates the relationship between all the various mechanisms of nucleation.

Until about 1975, the focus of research on secondary nucleation involved establishing contact nucleation as the predominant mechanism of new-particle formation in commercial crystallizers. Larson, Timm, and Wolff [39] and Timm and Larson [40] found that nucleation rate was directly proportional to suspension density, which suggests that the number of nuclei produced depended on the amount of solids in suspension. Lal, Mason, and Strickland-Constable [42] conducted sliding contacts with single crystals of magnesium sulfate at very low contact energies to produce nuclei. Clontz and McCabe [41] impacted crystal-crystal and crystal-inert surfaces with a known energy of impact and counted the

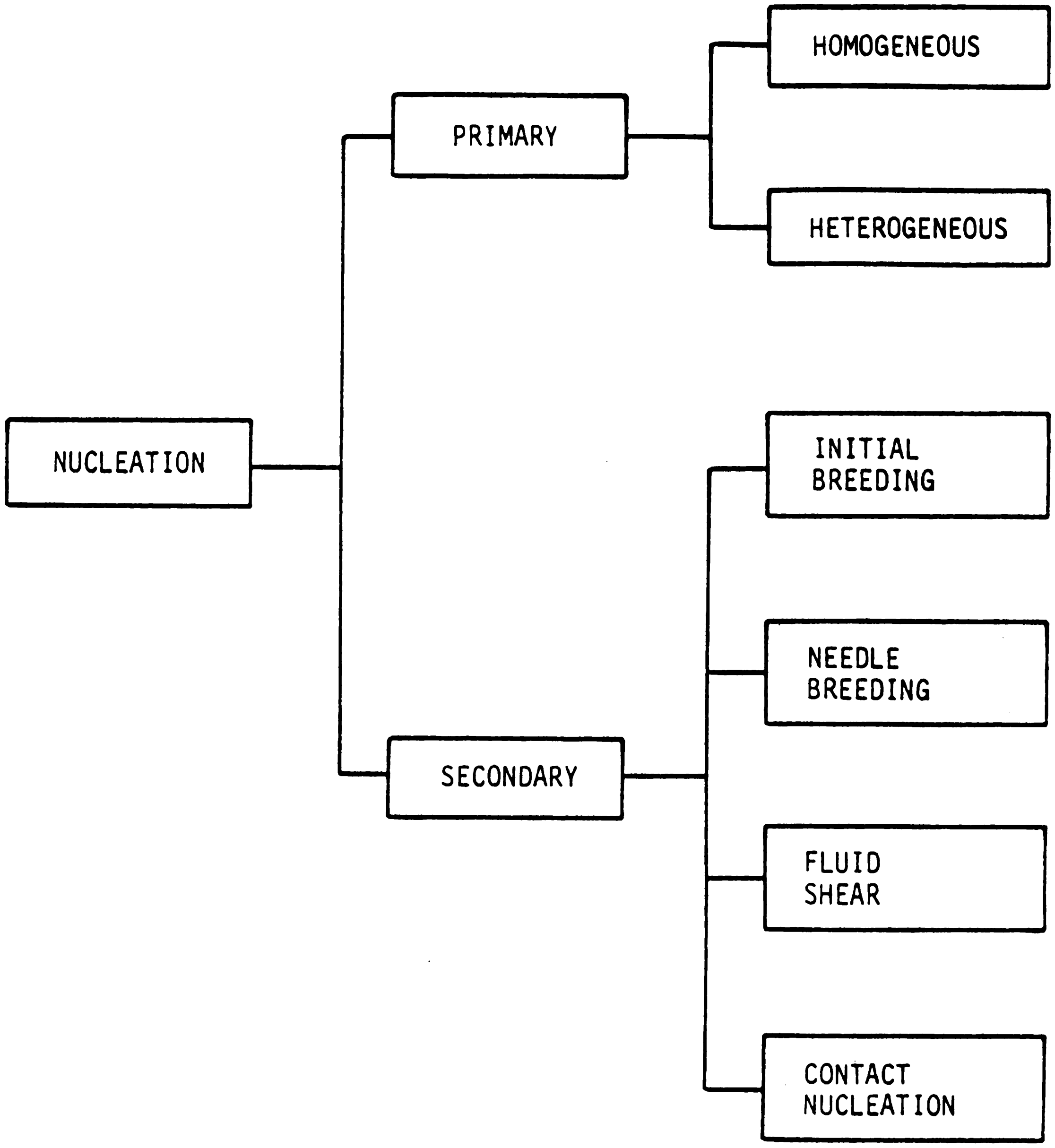

Figure 2-3. Classification of types of nucleation

nuclei that grew to visible size. Their work substantiated the Strickland-Constable survival theory of contact nucleation [43]. This theory holds that the number of nuclei produced by a contact is independent of supersaturation, but that their survival is governed by the Gibbs-Thomson relation, Equation (2-8). Shaw, McCabe, and Rousseau [44] found nucleation rate decreased when polyethylene impellers were used instead of steel impellers.

It was noted early on [37] that, after contacting, smaller crystals did not grow or grew very slowly. Cise and Randolph [45] studied secondary nucleation of potassium sulfate in water with a Coulter counter, a particle-size counting device. They found the number of nuclei were 100 times greater than predicted by the MSMPR model. They concluded the nuclei were born into a measurable size range, the nuclei had a distribution of growth rates (GRD), and small crystals grew very slowly.

2-2.3 Contact nuclei formation and removal

Disagreement over the source of contact nuclei began very soon after the mechanism was discovered [37,46]. One view holds that the source of the nuclei was the parent crystal itself. An attrition mechanism was envisioned where, upon contact, pieces of the parent were flung into solution to become nuclei. A major difficulty with this was that inspection of the parent crystals did not usually show any signs of damage. Second, this process is not conducive to good, well-formed crystals. Third, it was found, as noted earlier, that small attrition fragments did not grow, although large ones did. The concept of "micro attrition" was the answer to these objections. It entails the attrition of less-than-visible nuclei upon contact of a parent crystal.

A second view holds that the parent crystal surface stabilizes the embryo of Gibbs homogeneous nucleation theory. They are able to grow under the protection of the parent until removed by a contact. In this way, the embryo are not subject to the limits on size imposed by the Gibbs-Thomson equation. The arguments against this mechanism remain the same to this day: the "pre-crystalline clusters" have never been detected, and the objection that small attrition particles do not grow should apply even more so to stabilized embryos.

In 1976, Botsaris [47] suggested that the mechanism of contact nucleation is the sum of two mechanisms. The first is the formation of nuclei, and the second is their removal from the parent crystal surface. The second mechanism is clearly the actual contact. Experiments are still being devised to determine the mechanism of nuclei formation.

Denk and Botsaris [48] used the right- and left-handed optical properties of sodium chlorate crystals to determine the source of contact nuclei. In stagnant solutions supersaturated up to 2°C, the fraction of nuclei with the same handedness (d- or l-) as the parent was about one-half.

Above $2^{o}C$ supersaturation all the way to heterogeneous nucleation, 100% of the nuclei were of the same handedness as the parent. In stirred solutions, virtually all the nuclei at any supersaturation had the same d- or l-characteristic as their parent. This result argues strongly for the attrition mechanism.

Garside and Larson [49] used photomicroscopy to observe contact nuclei formation and the parent crystal surface for potash alum and magnesium sufate heptahydrate in water. Crystal attrition was reported to occur very easily and produced many secondary nuclei. Large numbers of particles were produced less than 10 μm in size, and they grew very slowly. In supersaturated solutions nuclei up to 50 μm in size were seen, and they grew normally. This result shows large attrition particles are viable nuclei.

Shimizu and co-workers [50] used isotopic labeling of potash alum (which contains 12 water molecules/potash alum molecule) to investigate the source of contact nuclei. Potash alum crystals were grown from D_2O and contacted in a supersaturated solution containing only H_2O. The nuclei were filtered and analyzed in a mass spectrometer. The nuclei contained far more deuterium than is present in natural water. Once again, the experiment shows nuclei formation can occur by an attrition mechanism.

Mullin and Leci [51] conducted experiments with supersaturated citric acid solutions in temperature-controlled columns 50 cm high and 5 cm in diameter. With time, it was noted that a very small but definite solute concentration gradient formed between the top and bottom of the column. It was concluded that the only way for the gradient to develop was by the formation of molecular clusters which descended the column. These experiments were repeated by Larson and Garside [52] for a number of solutes and in each case the results were the same; a small concentration gradient developed in the column. That molecular clustering is responsible is quite possible, but there is no evidence that the clusters have the structure of their crystals. No effect was observed in undersaturated solutions.

2-3. Raman Spectroscopy and Aqueous Solutions

2-3.1 Theory of the Raman process

An electric dipole is formed when a pair of charges of equal magnitude and opposite sign are separated by a given distance. If the electron cloud about a molecule is not distributed in a symmetrical fashion, it will have a permanent dipole. As the molecule vibrates the dipole moment may change, giving rise to an oscillating dipole at the frequency of the vibration. If the electron cloud is distributed symmetrically about the molecule, some of the unsymmetrical vibrations can distort the electron cloud and produce a dipole which again oscillates with the frequency of the vibration. The oscillating molecular electric dipole may couple to an oscillating electric field of passing

electromagnetic radiation if the frequencies are equal. The molecule then usurps energy from the radiation field. This process is known as infrared absorption since the frequency of the light that produces the effect is in the infrared region.

Alternatively, electric dipoles may be induced in molecules by an electric field, and such dipoles can oscillate and produce electromagnetic radiation. The frequency of the dipole is determined by the frequency of the electric field and the frequency of the molecular vibration. If the electric field inducing the dipole is static, the oscillatory frequency is that of the molecular vibration. However, if the electric field is again of electromagnetic origin, the induced dipole will oscillate and so emit radiation of frequency equal to the frequency of the exciting radiation, and at beat frequencies between that of the molecular vibration and the radiation. The former is Rayleigh scattering and the latter is Raman scattering. For Raman scattering, the molecule may acquire energy from the radiation field (Stokes scattering) or it may depart energy to the radiation field (anti-Stokes scattering). The classical picture just given, and what follows, is that of Long [53].

As a first approximation, it is assumed that the induced dipole moment is proportional to the electric field of the radiation

$$\underline{P} = \underline{\underline{\alpha}} * \underline{E} \qquad (2\text{-}10)$$

where $\underline{P}$ is the induced dipole, $\underline{E}$ is the electric field, and $\underline{\underline{\alpha}}$ is the second-order polarizability tensor. Each of the polarizability tensor components α_{ij} depend on the normal coordinates of vibration, Q. Expanding each component in a Taylor series with respect to the normal coordinates about the equilibrium position of the molecule, and neglecting terms of order two and higher leads to what is called the electrical harmonic approximation

$$(\alpha_{ij})_k = (\alpha_{ij})_o + (\alpha'_{ij})_k Q_k \tag{2-11}$$

where k identifies the k^{th} normal mode and α'_{ij} is the derivative of α_{ij} with respect to Q_k. Assuming the normal coordinates execute simple harmonic motion (mechanical harmonicity), and writing the electric field in sinusoidal form gives for the induced polarization

$$\underline{P} = [\underline{\underline{\alpha}}_o + \{\underline{\underline{\alpha}}'_k Q_{ko} \cos(\omega_k + \phi_k)\}]\underline{E}_o \cos(\omega_o t) \tag{2-12}$$

where Q_{ko} is the normal coordinate amplitude, ω_k is the frequency of the k^{th} normal mode, ϕ_k is a phase factor, ω_o is the frequency of the radiation, t is time, and $\underline{\underline{\alpha}}'$ is the derived polarizability tensor. Using the trigonometric identity $\cos(A)*\cos(B) = \{\cos(A+B) + \cos(A-B)\}/2$ allows Equation (2-9) to be expressed as

$$\begin{aligned}\underline{P} = {} & \underline{\underline{\alpha}}_o \underline{E}_o \cos(\omega_o t) + \\ & \underline{\underline{\alpha}}'_k \underline{E}_o Q_{ko} [\cos\{(\omega_o - \omega_k)t - \phi_k\}]/2 + \\ & \underline{\underline{\alpha}}'_k \underline{E}_o Q_{ko} [\cos\{(\omega_o + \omega_k)t + \phi_k\}]/2\end{aligned} \tag{2-13}$$

The first term on the right accounts for Rayleigh scattering, the second term accounts for Stokes Raman scattering, and the third accounts for anti-Stokes Raman scattering.

The classical analysis of Raman scattering does not predict the proper intensity for the Stokes or anti-Stokes transitions. This is because the molecular vibrations are quantized. Using the Boltzmann distribution law for the population of the vibrational energy levels, Long [53] showed that the intensity of Raman scattered radiation at 90^o to a plane-polarized radiation source is

$$I(90^o) = \frac{A(\omega_o-\omega_k)^4\{45a^2{}_k+7\gamma^2{}_k\}I_oN}{\omega_k\{1 - \exp(B\omega_k/T)\}45} \qquad (2\text{-}14)$$

where A and B are groups of physical constants, a is the trace of the derived polarizability tensor, γ is the anisotropy of the derived polarizability tensor, I_o is the irradiance, T is temperature, and N is the concentration of scattering molecules.

2-3.2 Raman studies of aqueous solutions

Mullin [17] gives a brief review of the structure of liquid water. Bockris and Reddy [54] discuss this subject in more detail. The most accepted view of the water structure is still that of Bernal and Fowler [55]. They proposed a slightly broken down, expanded ice network with free water molecules filling the voids, thus giving water its higher density than ice. The structure is held together by hydrogen bonds, as it is in ice. The bonds are continually breaking and reforming. Bockris and Reddy [54] estimate that the hydrogen bond length in liquid water is 2.92 angstroms. The hydrogen bond length in ice is 2.76 angstroms [56].

One of the first theories of ions in solution was the very crude Born model [57] which assumes only that the water is a structureless continuum and the ions are charged spheres. The Debye-Huckel theory [58] was published only three years later and remains the most reliable theory of ions in solution. The problem with both models is they are applicable only to very dilute solutions, up to 0.01N in favorable cases. Obviously, they are of little use in predicting the behavior of solutions from which soluble salts crystallize.

In 1946, Redlich [59] reviewed the subject of the dissociation of strong electrolytes. He argued that of the methods available for the determination of degree of dissociation, like apparent molal volume, molal refractivity, extinction coefficient, heat of dilution, and heat capacity, only the Raman spectra are reliable. Because of the necessary reduction in the number of vibrational degrees of freedom when a molecule such as NH_4NO_3 dissociates in solution, unambiguous information is obtained regarding the species present. More important is the change in molecular symmetry. Redlich measured the intensity of alkali nitrate Raman bands at various concentrations [60]. He found them to be linear with concentration and took this as proof of complete dissociation. Redlich stated the uncertainties in such measurements were 5% or more. Vollmar [61] repeated the study and found small deviations from linearity which he interpreted in terms of the influence of hydrated cations on the nitrate ion.

Mathieu and Lounsbury [62] noted the splitting of the degenerate 1387 cm^{-1} band in concentrated nitrate solutions. They attributed this to the lowering of the symmetry of the nitrate ion produced by an anisotropic ionic atmosphere. Lee and Wilmshurst [63] also studied this band and believed the splitting was due to the formation of solvent-separated ion pairs.

Pitha and Jones [64-66] considered the problem of fitting the Raman and infrared vibrational contours of ions in solution to synthetic bands. They investigated Lorentzian (Cauchy) and Gaussian individual, sum, product, and convolution functions. They concluded that the sum and product functions generally gave the most satifactory fit. Bulmer et al. [67] modeled Raman baselines from spectra of ionic solutions. They investigated polynomials, cubic splines, and decaying exponentials. They felt the best approximation to the baseline was a combination exponential-polynomial function.

Irish and Davis [68], Irish et al. [69], and Riddell et al. [70] used band fitting techniques to study the behavior of nitrate solutions over wide concentration ranges and in D_2O. They postulated the existence of three distinct

structure regimes within ionic solutions:

1. free, aquated ions,
2. solvent-separated ions, and
3. contact ion pairs.

Rothschild [71] used carefully measured Raman band contours to describe the motional characteristics of large molecules in the pure, condensed phase on the picosecond time scale. This was accomplished through the Fourier transform of the isotropic and anisotropic parts of the parallel and perpendicular polarized Raman spectra. In essence, he was measuring the vibrational time correlation function (I_{iso}) and the convolution of the rotational and vibrational time correlation function (I_{an}). Frost and James [72-76] extended Rothschild's analysis to the study of nitrates in aqueous solution. They measured rotational reorientational relaxation times with various cations. The Fourier transform technique also functioned as a sensitive test for the number of composite bands within the 1050 cm^{-1} band envelope. They identified four components and assigned three of them to the three structures of Irish given above, and the fourth to a structure they called an ion aggregate. Similar results were found for perchlorates [77] and sulfates [78-79], except no mention of ion aggregates was made.

Hussmann et al. [80] used laser Raman microscopy to scan near a growing crystal of $NaNO_3$. Using the Fourier transform technique, they found the same species present in supersaturated solution as did Frost and James. There was no detectable difference between the spectra of supersaturaed and saturated solutions. McMahon et al. [81] studied supersaturated KNO_3 solutions. The addition of 200 ppm Cr^{+3} to the solutions was found to decrease the intensity of the 1050.5 cm^{-1} band. This band is attributed by Irish and Davis [68] to the solvent-separated ion pair species, and so its behavior in the presence of Cr^{+3} impurity suggests the cation disrupts ordered species in supersaturated solutions.

2-4. Non-Spectroscopic Evidence For Hydrogen Bonding In Dihydrogen Phosphate Solutions

In general, methods other than Raman or IR are used to attempt to justify hydrogen bonding based on the behavior of the substance in question compared to similar compounds that are known not to hydrogen bond. The three most common methods are conductance, potentiometric titration, and isopiestic.

Smith and Huffman [82], Bassett [83], and Elmore et al. [84] attempted to fit conductance data for monomers of the phosphoric acid dissociation system to the theoretical models of Foss [85] and Wooster [86]. Each reported the fit was not satisfactory. When dimers were envoked, and in [84] trimers, reasonable agreement between the data and the theories were found. There were no conductance studies in the literature arguing for the monomer.

According to the theory of Robinson et al. [87], if association is correct, any mixture of dihydrogen phosphate salt plus another strong electrolyte will show the same positive free-energy of mixing. Isopiestic, or free-energy of mixing measurements [88,89] were also unanimous in their conclusions. $NaClO_4$ [88] and NaCl [89] were the strong electrolytes used.

There is disagreement over the results of potentiometric titration experiments. Baldwin and Sillen [90] and Mesmer and Baes [91] found nothing unusual in their titrations of phosphoric acid solutions. Ferroni [92], Childs [93], and Wilson [94] all found that titration curves of phosphoric acid at different concentrations crossed at about pH 1.5 to 2.5, which according to the theory of Carpeni [95] confirms the existence of dimers. There are roughly as many potentiometric studies supporting dimer formation as opposed.

On balance, the majority of work done on the dihydrogen phosphate problem supports the existence of dimer formation in aqueous solution.

2-5. Literature Cited

1. B. R. Pamplin. Crystal Growth, 2nd ed. (Pergamon Press, Oxford, 1980), Chapter 1.

2. P. Bennema, J. Cryst. Growth, 1, 1967, 278.

3. W. K. Burton, N. Cabrerra, and F. C. Frank, Philos. Trans. R. Soc. London, A:243, 1951, 299.

4. J. W. Gibbs. Collected Works (Longmans Green and Co., London), p. 325, footnote.

5. M. Volmer. Kinetik der Phasenbildung (Steinkopff, Dresden, 1939).

6. I. N. Stranski, Z. Phys. Chem., Abt. A:136, 1928, 259.

7. I. N. Stranski, Z. Phys. Chem., Abt. B:26, 1934, 31.

8. R. Becker and W. Doring, Ann. Phys., (Leipzig), 24, 1935, 719.

9. W. K. Burton, N. Cabrera and F. C. Frank, Nature, 163, 1949, 398.

10. F. C. Frank, Discuss. Faraday Soc., 5, 1949, 48.

11. J. P. Hirth and J. Lothe. Theory of Dislocations, 2nd ed. (J. Wiley, New York, 1982), Chapters 1 and 2.

12. F. C. Frank, Z. Elektrochem. Angew. Phys. Chem., 5, 1952, 429.

13. W. Kossel, Ann. Phys., (Leipzig), 21, 1934, 457.

14. A. A. Noyes and W. R. Whitney, Z. Phys. Chem., Abt. A:23, 1897, 689.

15. W. Nernst, Z. Physik. Chem., Abt. A:47, 1904, 52.

16. A. A. Chernov, Sov. Phys., Usp., Engl. Transl., 4(1), 1961, 116.

17. J. W. Mullin. Crystallisation, 2nd ed. (CRC Press, Cleveland, 1972), Chapters 5 and 6.

18. S. Glasstone, K. J. Laidler, and H. Eyring. The Theory of Rate Processes (McGraw Hill, New York, 1941).

19. J. W. Mullin and A. Amatavivadhana, J. Appl. Chem., 17, 1967, 151.

20. J. Garside, Chem. Eng. Sci., 26, 1971, 425.

21. S. J. Jancic and P. A. M. Grootscholten. Industrial Crystallization (D. Reidel Publishing Co., Dordrecht, 1984).

22. W. L. McCabe, Ind. Eng. Chem., 21, 1929, 30.

23. W. L. McCabe and R. P. Stevens, Chem. Eng. Prog., 47, 1951, 168.

24. A. D. Randolph and M. A. Larson. Theory of Particulate Processes (Academic Press, New York, 1971).

25. A. H. Janse and E. J. deJong. Industrial Crystallization, J. W. Mullin, Editor (Plenum Press, New York, 1976).

26. E. T. White and P. G. Wright, Chem. Eng. Prog. Symp. Ser., 67(110), 1970, 81.

27. K. A. Berglund, Ph.D. Dissertation, Iowa State University, Ames, Iowa, 1981.

28. K. A. Ramanarayanan, Ph.D. Dissertation, Iowa State University, Ames, Iowa, 1982.

29. K. A. Berglund, E. L. Kaufman and M. A. Larson, AIChE J., 29(5), 1983, 867.

30. K. A. Berglund and M. A. Larson, AIChE J., 30(2), 1984, 280.

31. M. A. Larson, E. T. White, K. A. Ramanarayanan, and K. A. Berglund, AIChE J., 31(1), 1985, 90.

32. S. W. Young, J. Amer. Chem. Soc., 33, 1911, 148-162.

33. H. H. Ting, and W. L. McCabe, Ind. Eng. Chem., 26(11), 1934, 1201-1207.

34. H. A. Miers, and F. Isaac, J. Chem. Soc., 89, 1906, 413.

35. H. E. C. Powers, Nature, 178, 1956, 139-140.

36. R. F. Strickland-Constable, and R. E. A. Mason, Nature, 197, 1963, 897-898.

37. R. E. A. Mason, and R. F. Strickland-Constable, Trans. Faraday Soc., 62, 1966, 455-461.

38. T. P. Melia, and W. P. Moffitt, Ind. Eng. Chem., Fund., 3(4), 1964, 313-317.

39. M. A. Larson, D. C. Timm, and P. R. Wolff, AIChE J., 14(3), 1968, 448-452.

40. D. C. Timm, and M. A. Larson, AIChE J., 14(3), 1968, 452.

41. N. A. Clontz, and W. L. McCabe, AIChE Symposium Ser., 67(110), 1971, 6-17.

42. D. P. Lal, R. E. A. Mason, and R. F. Strickland-Constable, J. Crystal Growth, 5, 1969, 1.

43. R. F. Strickland-Constable, AIChE Symposium Ser., 68(121), 1972, 1-7.

44. B. C. Shaw, W. L. McCabe, and R. W. Rousseau, AIChE J., 19(1), 1973, 194.

45. M. D. Cise, and A. D. Randolph, AIChE Symposium Ser., 68(121), 1972, 42-56.

46. H. E. C. Powers, Chem. and Ind., 14, 1962, 627-631.

47. G. D. Botsaris. Industrial Crystallization, J. W. Mullin, Ed. (Plenum Press, New York, 1976), 3-22.

48. E. G. Denk, and G. D. Botsaris, J. Crystal Growth, 13/14, 1972, 493-499.

49. J. Garside, and M. A. Larson, J. Crystal Growth, 43, 1978, 694-704.

50. K. Shimizu, K. Tsukamoto, J. Horita, T. Tadaki, J. Crystal Growth, 69, 1984, 623-626.

51. J. W. Mullin, and C. L. Leci, Phil. Mag., 19, 1969, 1075-1077.

52. M. A. Larson, and J. Garside, Chem. Eng. Sci., 41(5), 1986, 1285-1289.

53. D. A. Long. Raman Spectroscopy (McGraw Hill, New York, 1977).

54. J. O. M. Bockris and A. K. N. Reddy. Modern Electrochemistry (Plenum/Rosetta, New York, 1970).

55. J. D. Bernal and R. H. Fowler, J. Chem. Phys., 1, 1933, 515.

56. G. C. Pimentel and A. L. McClellan. The Hydrogen Bond (W. H. Freeman and Co., New York, 1960).

57. M. Born, Z. Phys., 21, 1920, 45.

58. P. Debye and E. Hunkel, Z. Phys., 24, 1923, 305.

59. O. Redlich, Chem. Rev., 39, 1946, 333.

60. O. Redlich and J. Bigeleisen, J. Am. Chem. Soc., 65, 1943, 1883.

61. P. M. Vollmar, J. Chem. Phys., 39, 1963, 2236.

62. J. P. Mathieu and M. Lounsbury, Discuss. Faraday Soc., 9, 1950, 196.

63. H. Lee and J. K. Wilmshurst, Aust. J. Chem., 17, 1964, 943.

64. J. Pitha and R. N. Jones, Can. J. Chem., 44, 1966, 3031.

65. J. Pitha and R. N. Jones, Can. J. Chem., 45, 1967, 2347.

66. J. Pitha and R. N. Jones, Can. J. Chem., 44, 1966, 14.

67. J. T. Bulmer, D. E. Irish, F. W. Grossman, G. Herriot, M. Tseng, and A. J. Weerheim, Appl. Spectrosc., 29(6), 1975, 506.

68. D. E. Irish and A. R. Davis, Can. J. Chem., 46, 1968, 943.

69. D. E. Irish, D. L. Nelson, and M. H. Brooker, J. Chem. Phys., 54(2), 1971, 654.

70. J. D. Riddell, D. J. Lockwood, and D. E. Irish, Can. J. Chem., 50, 1972, 2951.

71. W. G. Rothschild, J. Chem. Phys., 65(1), 1976, 455.

72. D. W. James and R. L. Frost, Can. J. Spectrosc., 23(1), 1978, 5.

73. D. W. James, R. L. Frost, R. Appleby, and M. T. Carrick, Can. J. Spectrosc., 27(3), 1982, 82.

74. D. W. James, R. L. Frost, and M. T. Carrick, J. Raman Spectrosc., 13(2), 1982, 115.

75. R. L. Frost and D. W. James, J. Chem. Soc., Faraday Trans. I, 78, 1982, 3223.

76. D. W. James and R. L. Frost, J. Phys. Chem., 86(19), 1982, 3840.

77. R. L. Frost and D. W. James, J. Chem. Soc., Faraday Trans. I, 78, 1982, 3235.

78. A. C. Hayes, P. Kruus, and W. A. Adams, J. Solution Chem., 13(1), 1984, 61.

79. P. Kruus, A. C. Hayes, and W. A. Adams, J. Solution Chem., 14(2), 1985, 117.

80. G. A. Hussmann, M. A. Larson, and K. A. Berglund. Industrial Crystallization 84, S.J. Jancic and E.J. de Jong, Eds. (Elsevier Science Publishers, Amsterdam, 1984), p. 21.

81. P. M. McMahon, K. A. Berglund, and M. A. Larson. Industrial Crystallization 84, S.J. Jancic and E.J. DeJong, Eds. (Elsevier Science Publishers, Amsterdam, 1984), p. 229.

82. A. J. Smith and E. O. Huffman, Chem. Eng. Data Ser., 1, 1956, 99.

83. H. Bassett, J. Chem. Soc., 1958, 2949.

84. K. L. Elmore, J. D. Hatfield, R. L. Dunn, and A. D. Jones, J. Phys. Chem., 69(10), 1965, 3520.

85. R. M. Foss, J. Am. Chem. Soc., 80, 1958, 3163, 1959, 2659.

86. C. B. Wooster, J. Am. Chem. Soc., 59, 1937, 377.

87. R. A. Robinson, R. H. Wood, and P. J. Reilly, J. Chem. Thermodyn., 3, 1971, 461.

88. R. H. Wood and R. F. Platford, J. Solution Chem., 4, 1975, 977.

89. C. W. Childs, C. J. Downs, and R. F. Platford, Aust. J. Chem., 2:, 1973, 863.

90. W. G. Baldwin and L. G. Sillen, Arkiv Kemi, 31, 1968, 391.

91. R. E. Mesmer and C. F. Baes, J. Solution Chem., 3, 1974, 307.

92. G. Ferroni, Electrochim. Acta, 21, 1976, 283.

93. C. W. Childs, J. Phys. Chem., 73, 1969, 2956.

94. J. M. Wilson, R. A. Robinson, and H. S. Ayling, J. Am. Chem. Swc., 69, 1942, 1469.

95. G. Carpeni, J. Chim. Phys., Phys.-Chim. Biol., 66, 1969, 327.

CHAPTER 3

A CONSTANT-TEMPERATURE RAMAN CELL FOR THE STUDY OF SUPERSATURATED AQUEOUS SOLUTIONS*

3-1. Introduction

In order that the phenomena of crystal nucleation and growth from solution can be fully understood, the current knowledge of supersaturated solution structure must be extended. Previous studies on Raman spectroscopy of aqueous metal nitrate solutions [1,2] indicated the presence of solvated ions, solvent separated ion pairs, contact ion pairs, and ion agglomerates as a function of concentration. Unfortunately, the concentration range of these studies did not include supersaturated solutions. It is the purpose of this work to describe an experimental technique which allows the study of supersaturated solutions.

The amount of supersaturation that a solution can support is characteristic of the solute; however, the behavior of all supersaturated solutions of soluble compounds is qualitatively the same. In the present work we desired to study the supersaturation regime wherein no nucleation occurs. This is known as the metastable regime, and crystal growth will occur if a seed crystal is introduced into such a solution [3]. The technique of

---

* a paper published by P. M. McMahon, M. K. Cerreta, K. A. Berglund, and M. A. Larson in App. Spectrosc., 40(2), 1986, 282-283.

attaining such metastable solutions requires the careful cooling of a saturated solution. Therefore, precise control of temperature is necessary to obtain Raman spectra of such supersaturated solutions.

3-2. Experimental

The constant-temperature cell used in the present work consists of a water-jacketed, square-quartz sample holder. The sample holder is 10-mm-o.d. square-quartz tubing with a wall thickness of less than 1 mm. The circular water jacket consists of 25-mm-o.d. quartz tubing with 7-mm inlet and outlet tubes attached. We left one end open to fill and clean the cell. The cell is closed with a Teflon-coated rubber stopper with an Omega Small Surface Thermistor inserted through it. The thermistor extends into the cell to approximately 5 mm from the region illuminated by the laser. The cell is shown in Figure 3-1, with dimensions. Temperature control was maintained at 30^{o} $\pm 0.02^{o}$ by circulating water through the jacket. The sample cell is held in place with the use of the kinematic base of the SPEX Harney-Miller apparatus.

All spectra were taken with the use of a SPEX #1403 double monochromator equipped with a standard sample illuminator and a Laser Mate to remove laser plasma lines. A standard 90^{o} collection geometry was used in all cases. All samples were illuminated by 400 mW from the 514.5 nm line of a Spectra Physics Model 165 Ar^{+} laser.

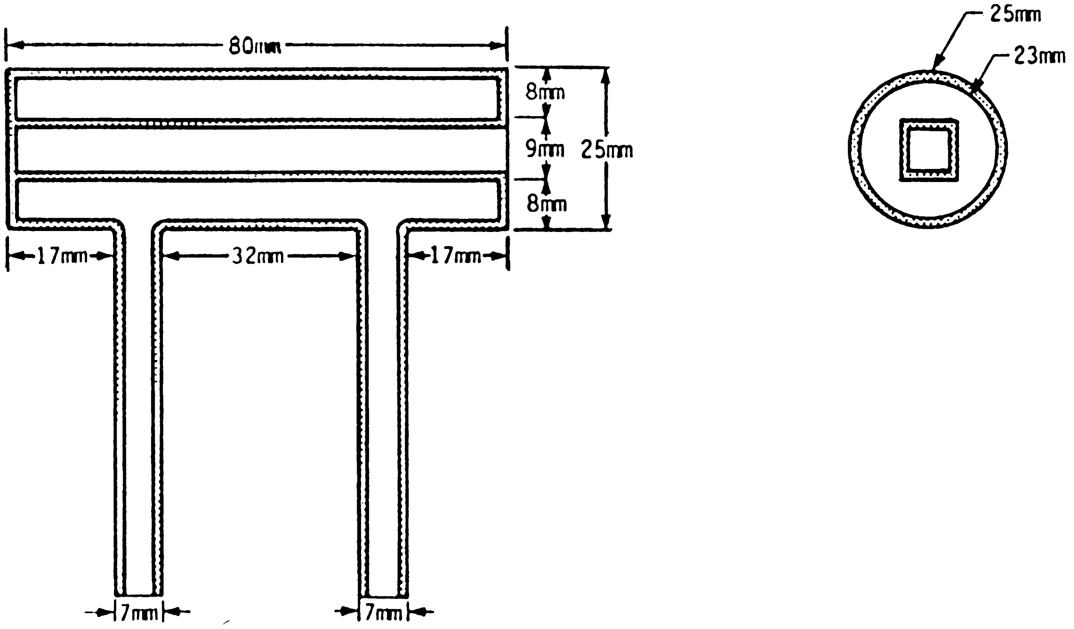

Figure 3-1. Schematic of the constant-temperature Raman cell used in the present study.

Aqueous solutions of two compounds, namely, potassium nitrate and ammonium dihydrogen phosphate (ADP), were studied. All solutions were prepared from reagent-grade material dissolved in distilled-deionized water. Saturated solutions were prepared by stirring solutions containing excess crystals at a known temperature. The solution was filtered, then cooled to the desired temperature in the cell. The amount of cooling established the degree of supersaturation. The bandpass width for the potassium nitrate solutions was 0.5 cm^{-1} and for the ADP solutions was 1.0 cm^{-1}. Multiple scans were signal averaged to obtain spectra with high signal-to-noise ratios (generally in excess of 100:1).

3-3. Results and Discussion

Typical results for the ν_1 [P-$(OH)_2$ symmetric stretch] and the ν_3 [P-$(O)_2$ symmetric stretch] bands of the H_2PO_4- ion in ADP solutions are presented in Figure 3-2 (assuming approximate T_d symmentry). The shape and position of the bands studied continue to be strong functions of concentration into the supersaturated regime. The structure of the aqueous solution is approaching that of an anion-anion dimeric or polymeric state with increased concentration [4]. This is particularly evident by the movement of the ν_1 band of ADP to higher wavenumbers and the hydrogen-bonding-induced asymmetry of the ν_3 band. Full analyses and discussion of these results as well as those for potassium nitrate are presented elsewhere [4-6].

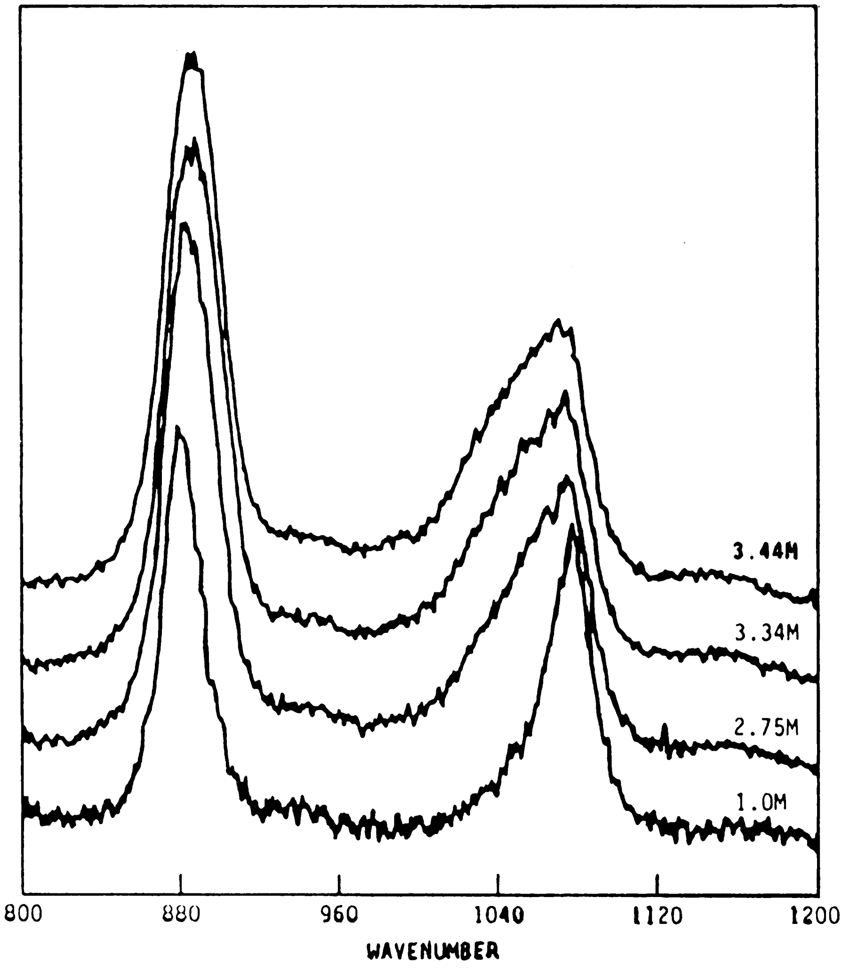

Figure 3-2. Raman spectra of the ν_1 band (left) and the ν_3 band (right) of $H_2PO_4^-$ in ADP solutions at 30°C. Saturation is 3.19 M.

3-4. Conclusions

In summary, it has been demonstrated that high-quality Raman spectra can be obtained for supersaturated solutions. The device used is capable of very precise temperature control. Current research indicates that concentration-dependent phenomena occur in supersaturated solutions and can be studied with the use of Raman spectroscopy. Future work will deal with the concentration and nature of the species which are responsible for the observed phenomena.

3-5. Acknowledgment

This work was supported by the National Science Foundation under grants #CPE-8111685 and #CPE-8204977. The assistance of Dr. Glenn Schrader of Iowa State University in providing the Raman spectrometer for this work is appreciated.

3-6. Literature Cited

1. D. E. Irish and A. R. Davis, Can. J. Chem., 46, 1968, 943.
2. R. L. Frost and D. W. James, J. Chem. Soc., Faraday Trans., 78, 1982, 3223.
3. J. W. Mullin. Crystallization (Butterworths, London, 1972), p. 35.
4. M. K. Cerreta and K. A. Berglund, 1985 Annual Meeting of AIChE, Chicago, Ill., November 10-15, 1985.
5. P. M. McMahon, M.S. thesis, Iowa State University of Science and Technology (1984).
6. P. M. McMahon, K. A. Berglund, and M. A. Larson, Process Tech. Proc., 2, 1984, 229.

CHAPTER 4

THE STRUCTURE OF AQUEOUS SOLUTIONS OF SOME DIHYDROGEN ORTHOPHOSPHATES BY LASER RAMAN SPECTROSCOPY*

4-1. Abstract

Powdered crystals and pure, aqueous solutions of ammonium, sodium, and potassium dihydrogen orthophosphates in concentrations ranging from 0.01M to supersaturated were investigated at 30^0C using laser Raman spectroscopy between 700 cm^{-1} and 1350 cm^{-1}. With increasing solute concentration, the peak position of the 875 cm^{-1} $P-(OH)_2$ symmetric stretch band increases. Extreme asymmetry in the 1075 cm^{-1} $P=(O)_2$ symmetric stretch band developes to lower energy. The integrated intensity ratio of the 875 cm^{-1} band to the 1075 cm^{-1} band envelope remains constant. These observations are consistent with anion-anion association via hydrogen bonds. Deconvolution of the spectral bands shows only 40% and 20% of the phosphates exist as monomers in saturated potassium and ammonium solutions, respectively, and that anion association does not cease with the dimer. The spectra provide no evidence of quasi-crystalline entities in solution. The necessary breaking and reforming of hydrogen bonds during the growth process can explain rapid z-direction growth, growth activation energy, and the rate-limiting surface growth mechanism.

---

* a paper published by M. K. Cerreta and K. A. Berglund in J. Crystal Growth, 84, 1987, 577-588.

4-2. Introduction

Potassium and ammonium dihydrogen phosphate crystal growth has been well-characterized [e.g., 1-16] and several efforts have been made to theoretically model their growth [1,3,9,12,17]. Due to the absence of experimental work identifying the species present in solution or on the surface of the growing crystal, many of the physical characteristics of the growth unit have been assumed, e.g., its size, state of hydration, or concentration. The solution structure problem is ubiquitous in crystallization and presents difficulties in reliably applying the general theory of crystal growth developed by Burton, Cabrera, and Frank [18] and extended to growth from solution by Bennema [19]. Similarly, the growth rate and birth rate parameters in the population balance technique of Randolph and Larson [20] are intimately related to the solution structure. Laser Raman spectroscopy is a technique capable of providing much of the information that has been assumed. Here, the Raman spectra are used to identify the species present in pure, aqueous solutions of sodium, potassium, and ammonium dihydrogen orthophosphates (NaDP, KDP, and ADP, respectively) from dilute to supersaturated concentrations. The implications for crystal growth are examined by relating and contrasting the solution and crystal structures on the molecular level.

4-2.1 Characteristics of Dihydrogen Orthophosphate Crystals and Crystal Growth

ADP and KDP crystallize from aqueous solution in anhydrous form. NaDP crystallizes in either of anhydrous, monohydrate, or dihydrate forms; only the anhydrous form will be considered here for comparative purposes. X-ray diffraction studies at room temperature have determined NaDP crystals to be monoclinic [21] while ADP and KDP crystals are tetragonal and isomorphic [22,23]. The hydrogen atom positions have been found by neutron diffraction [24-26]. For ADP and KDP, each phosphate is hydrogen bonded through its oxygens and hydroxyls to four other phosphates (Figure 4-1). These are among the strongest hydrogen bonds known [27] with oxygen-to-oxygen distances of 2.49 angstroms. The ammonium ion forms much weaker hydrogen bonds to the phosphates. Each nitrogenous hydrogen makes a hydrogen bond to an oxygen of two separate phosphates. One bond is approximately parallel to the ab plane of Figure 4-1 with a nitrogen-to-oxygen length of 2.91 angstroms, while the second bond is parallel to the c-axis and is 3.17 angstroms in length [22]. For NaDP, Catti and Ferraris [21] found that some of the phosphates in the unit cell are linked by two hydrogen bonds of 2.50 angstroms each, forming a kind of "dimeric" unit. The remaining hydroxyls or oxygens each form three weaker hydrogen bonds to other phosphates.

Since the growth characteristics of NaDP have not been studied, the remainder of this section will focus on ADP and KDP. The natural habit of these isomorphs consists of a

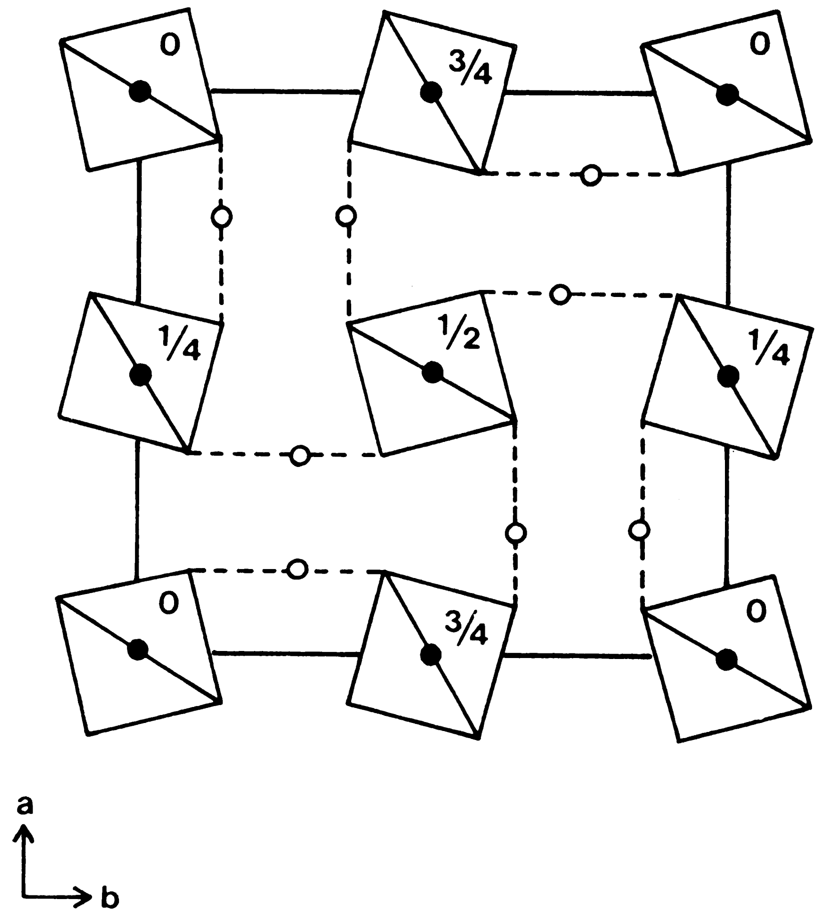

Figure 4-1. The arrangement of phosphate groups and hydrogen bonds in the unit cell of ammonium and potassium dihydrogen phosphates.

The nine small squares are tetrahedral phosphate groups. The black dots are phosphorous, and oxygens occupy the vertices. The fractions signify the height above the ab plane in the unit cell. The small open circles are hydrogen atoms and hydrogen bonds are depicted by broken lines. The cations are located 1/2 unit cell above and below the phosphate groups. The single large square is for reference only.

tetragonal prism capped at either end by tetragonal pyramids and is shown in Figure 4-2.

Mullin and Amatavivadhana [1] measured the solubility and diffusivity between 20^{o}C and 40^{o}C for ADP and KDP. They found no dependence of growth rate on time or solution velocity for their range of experimental conditions. The growth rate of any face varied parabolically with supersaturation for either substance. The activation energies for growth and diffusion are listed in Table 4-1. The growth rate dependence on supersaturation and the data of Table 4-1 suggest growth of ADP and KDP is limited by a surface mechanism [1,18,19]. The growth rate along the z-axis was four to five times greater for ADP than KDP. KDP was reported capable of supporting a much higher relative supersaturation than ADP.

ADP and KDP exhibit discontinuous growth behavior with varying supersaturation. At very low (but measureable) supersaturation, no growth of any face occurs [1-5], although Dam et al. [6,7] found z-direction growth at any σ and attributed the results of others to the presence of trace impurities. σ is defined here as the relative supersaturation

$$\sigma = \frac{C - C^{*}}{C^{*}} \qquad (4-1)$$

where C is the solute concentration and C^{*} is the equilibrium concentration at the specified temperature. At slightly higher σ {101} growth commences but not {100}; the

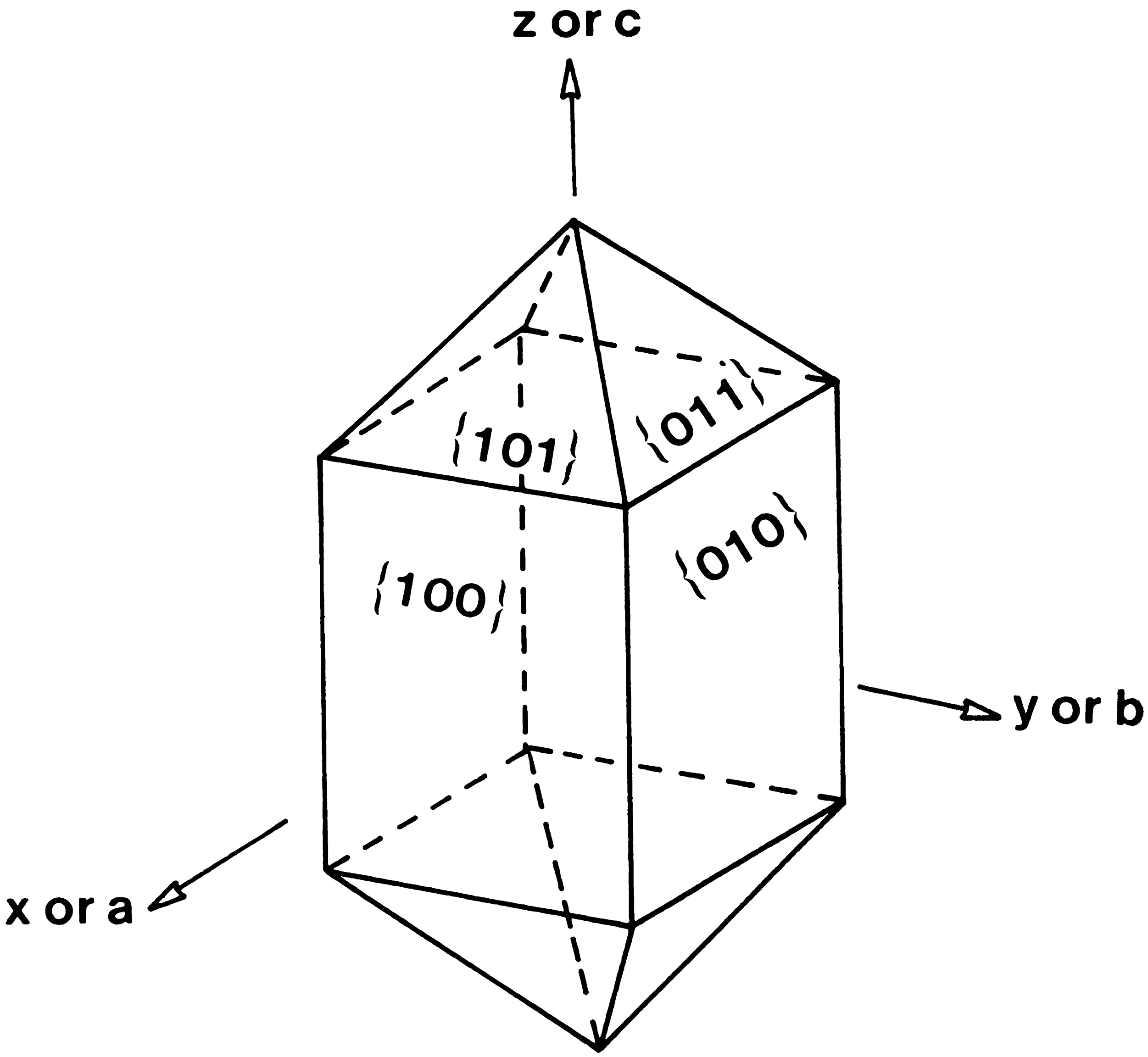

Figure 4-2. The natural habit of ADP and KDP crystals.

Table 4-1. Activation energies for growth and diffusion [1]

	Growth (kcal/mole)		Diffusion (kcal/mole)
	z	xy	
ADP	12.2	-	2.4
KDP	8.1	6.0	3.8

{100} faces taper in the [001] direction. As σ is increased further, the tapering diminishes and {100} growth begins.

Growth of the {100} faces has been fairly well characterized. Dislocation studies [8-11,15] conclusively prove the faces advance by a screw dislocation mechanism at low to medium supersaturations. Chernov et al. [12] used laser Michelson interferometry to study {100} face growth of ADP and showed surface diffusion is unimportant. A variety of microscopic observation experiments of growing ADP crystals revealed elliptical surface layers emanating from well-defined growth centers when σ is between approximately 0.02 and 0.07 [3,5,11,13]. Propagation is most rapid in the [010] direction. Estimates of layer heights, which increased with increasing σ, ranged from 0.05 to 3 microns. Layer velocity was independent of time, solution velocity, and layer height. Davey and Mullin [3,13] concluded the macrosteps were bunches of small steps, perhaps even mono-layers. Above σ=0.07, their photographs show the elliptical layers giving way to faster moving parallel layers without well-defined growth centers. The improved photographic detail of Ristic et al. [5] revealed the parallel layers to be two-dimensional nucleation islands, indicating the predominance of a new growth mechanism. Dam et al. [6] used reflection differential interference contrast microscopy to study growing crystals of KDP. They measured step heights as low as 0.01 microns. For σ=0.15 they found low steps moved faster than high ones in the [010] direction with the reverse true for $\sigma=0.05$. Growth in the [001] direction showed little or no dependence of layer velocity on step height.

Growth of the {101} faces remains a puzzle. Growth in the z-direction is many times more rapid than in the x- or y-directions [1], yet the few screw dislocations which exist in the pyramidal regions do not terminate at pyramid surfaces [8,10,11,14,15]. Several growth mechanisms have been postulated, such as surface nucleation or layer growth originating from the {100} faces [11]. Dam et al. [6] and Van Enckevort et al. [16] dispute this and suggest ADP and KDP {101} faces grow by dislocations that generate spiral steps and triangular growth hillocks. Bhat et al. [10] found that crystal growth rate and size can determine instances such that mixed dislocations may emerge at face intersections and function as growth centers. This entire matter is still unresolved. Dam et al. [6] measured step heights as low as 80 angstroms.

4-2.2 Raman Spectroscopy and Dihydrogen Phosphates

Raman spectroscopy is a vibrational spectroscopy yielding structural information on the nature of molecular interactions. It is similar to infrared spectroscopy but differs in that photons are inelastically scattered from a vibrating molecule rather than absorbed. The energy exchange between photon and molecule is the energy difference between vibrational states of a particular normal mode. Raman scattered light is dispersed by a spectrometer according to its energy (frequency) and recorded as symmetric bands in a spectrum. Each band corresponds to a normal mode in a specific environment. Vibrations that distort the molecule's equilibrium symmetry rotate the plane-polarized laser light in proportion to the degree of symmetry distortion. This feature can be used to determine band parameters of overlapping bands by measuring the spectrum produced perpendicular to the polarization of the incident laser beam. In general, the integrated intensity of a band is proportional to the concentration of the species responsible for the band, provided the Raman transition parameters for that vibration are constant.

Group theoretical considerations show the "free" dihydrogen phosphate ion has C_{2v} symmetry with 15 non-degenerate vibrations, all of which are Raman active and 13 of which are IR active. These vibrations have been assigned to their corresponding bands in aqueous solution [28-37], and a normal mode coordinate analysis has been performed [38]. More recent studies have focused on changes in the aqueous solution spectra brought about by concentration perturbations [39-43]. Preston and Adams [41] report the integrated intensity of the 875 cm^{-1} band ($P-(OH)_2$ symmetric stretch) and the 1075 cm^{-1} envelope ($P=(O)_2$ symmetric stretch) increase linearly with concentration up to 2M for KDP and NaDP and up to 3M and possibly higher for ADP.

In view of the preceding discussions, this investigation was undertaken to determine the species present in aqueous dihydrogen phosphate solutions and relate the results to the growth of the crystals using laser Raman spectroscopy. In very dilute solutions, one expects only "free" aquated ions to exist. As the solutions become more concentrated, the interactions that ensue should alter the molecular environment and the corresponding Raman spectrum. In all, spectra of solutions ranging in concentration from 0.01M to 6.01M were recorded, including five that were supersaturated. The $P=(O)_2$ and $P-(OH)_2$ symmetric stretches were followed since both are prominent in the Raman, and both should be highly sensitive to environmental perturbations.

4-3. Experimental Procedures, Apparatus, and Band Analyses

All solutions were prepared with reagent grade ADP, KDP, and NaDP from Fisher Scientific Company. Doubly distilled water was passed through a Barnstead D8904 organic removal cartridge and a Barnstead D8901 deionization cartridge prior to use. Undersaturated solutions were prepared gravimetrically. Supersaturated solutions were made by saturating with excess crystals for a period of at least 48 hours with the saturator bath temperature controlled by a Haake Model E2 immersion circulator. A magnetic stirbar provided the agitation in a 1-liter Pyrex vessel. The saturated solutions were filtered under vacuum using Whatman No. 4 filter paper and transferred to a specially designed quartz Raman cell capable of temperature control to ± 0.02°C [44].

After heating to approximately 10^{o}C above saturation for 30 minutes, the solution was cooled to 30.00^{o}C, the temperature at which all spectra were recorded. The solute concentration was varied from 0.01M (ADP) to 6.01M (NaDP). Solid samples of ADP and KDP were prepared by grinding reagent grade crystals to a fine powder (to remove any orientational effects) and were inserted into capillary tubes.

Raman spectra were obtained using the 514.5 nm line of a Spectra Physics Model 164-08 argon ion laser as the excitation source, operated between 400 and 500 mW. The spectrometer was a Spex 1403 double-monochromator equipped with a Spex 1459 UVISIR Illuminator, a Spex 1460 Lasermate for the removal of unwanted plasma lines, a Research Incorporated photomultiplier, and 90 degree collection optics. The light scattered at 90 degrees was focused through a polarization scrambler onto the entrance slit. Slit widths varied from 1.5 cm^{-1} for the powders and relatively concentrated solutions to 4.0 cm^{-1} for very dilute solutions. The spectrometer was calibrated using the 546.07 nm emission line of mercury. The perpendicular polarized spectra were measured by placing a polarization analyzer after the sample but before the polarization scrambler. CCl_4 was used for calibration and gave a polarization ratio of ~0.0 for the highly polarized band at 459 cm^{-1} and 0.75 for the highly depolarized band at 314 cm^{-1}. The spectrometer control and data acquisition were computerized using in-house programs. Depending on the solute concentration, each sample was scanned 5 to 20 times. The wavenumber interval never exceeded 1.0 cm^{-1}.

Baseline corrections for spectra above 0.05M were made by subtracting the lowest intensity count from each point in the spectrum and fitting "free" baseline regions to a single Gaussian band using the Simplex method of Nelder and Mead [45]. After subtracting the baseline, the resulting vibrational bands were fit to weighted Lorentzian-Gaussian sum functions of the form

$$I(\nu) = I^{o}\{\{z*\exp[-\ln(2)[(\nu-\nu^{o})/H]^{2}]\} + \{(1-z)/[1+[(\nu-\nu^{o})/H]^{2}]\}\} \qquad (4-2)$$

where I is intensity, ν^{o} is wavenumber, I^{o} is peak intensity, z is a weighting factor, ν^{o} is peak position, and H is half-width at half-maximum. Below 0.1M, reliable data analyses were not possible because of severe baseline curvature due to the broad water librational band.

The spectral parameters for each band were initially estimated from the unpolarized spectrum or with the aid of the perpendicular polarized spectrum. To accurately determine the band parameters, a grid search was used to minimize the sum-of-squares difference between the experimental band profile and the synthetic band profile. The algorithm is similar to the Simplex method but less likely to find a local minimum. Several different initial guesses were used to insure a global minimum was found. Band areas were calculated by integrating the analytic expression for each particular band. The differences between areas found from analytic representations and dilute solution experimental profiles were insignificant.

4-4. Results and Discussion

Figure 4-3 shows the Raman spectra of aqueous dihydrogen phosphates between 700 cm^{-1} and 1350 cm^{-1} at several salt concentrations. At any concentration below 0.05M the Raman spectra of all dihydrogen phosphates show the 875 cm^{-1} and 1075 cm^{-1} bands are of nearly equal peak intensity, half-width at half-maximum, and band shape. This indicates H_2PO_4- exists as a "free" aquated ion. With increasing concentration the peak position of the 875 cm^{-1} band increases to 894 cm^{-1} (for 6.0M NaDP), the 1075 cm^{-1} band developes extreme asymmetry on the low wavenumber side and decreases in peak intensity relative to the 875 cm^{-1} band. The weak 945 cm^{-1} ($P-(OH)_2$ asymmetric stretch), 1150 cm^{-1} ($P=(O)_2$ asymmetric stretch), and extremely weak 1230 cm^{-1} (P-O-H in-plane deformation) bands are better observed in the IR [36,39].

Cation-phosphate association can not be responsible for the changes in the 875 cm^{-1} and 1075 cm^{-1} bands of Figure 4-3. Preston and Adams [41] present a thorough discussion of this. The asymmetry in the 1075 cm^{-1} band is visible at phosphate concentrations as low as 0.1M. They found that the addition of 1M NaCl to 0.1M and 1.0M NaDP did not increase the asymmetry of the 1075 cm^{-1} band or reduce its

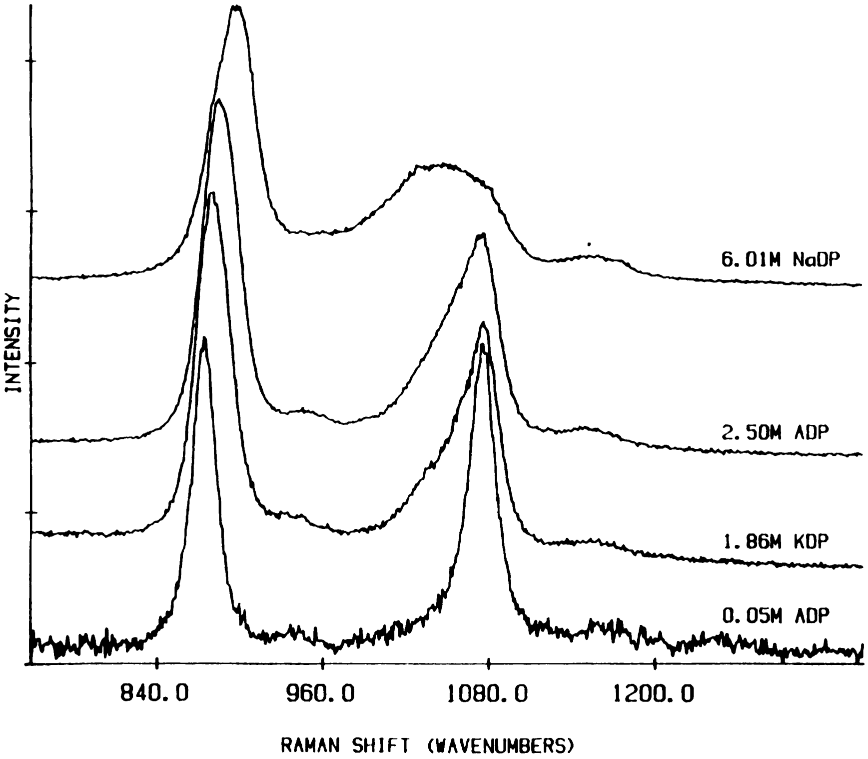

Figure 4-3. The Raman spectra of aqueous dihydrogen phosphates.

intensity. The changes in band parameters of any phosphate were cation nonspecific to 2M; in the present study, the 1.86M spectra of all three salts are completely identical.

In the supersaturated region, it is reasonable to assume that the cation is somewhere very near the anion. *Ab initio* quantum mechanical calculations revealed the cation takes up a position directly between the lone oxygens [46]. The Na-O distance is about 2.25 angstroms and the Na-O interaction is 95% coulombic. Adding a water of hydration would weaken the interaction somewhat, as was found for beryllium and lithium ions. The larger ammonium and potassium ions (the Pauling radii are 0.95, 1.33, and 1.48 angstroms for Na^+, K^+, and NH_4+, respectively [47]) are expected to behave similarly. However, the coulombic interaction would be ~100% for the potassium ion, the ammonium ion would probably engage in hydrogen bonding, and the distance of approach would be greater than for sodium. The cation-oxygen interaction in the crystals support this [21-23]. James and Frost [48] measured vibrational and rotational relaxation times for aqueous nitrate solutions. Unlike all other cations, the ammonium ion did not perturb the nitrate until the NH_4+ concentration was 5 or 6M. By virtue of its size, geometry, and ability to hydrogen bond, the ammonium ion remains in the water lattice until highly concentrated.

Hydrogen bonding between anions accounts for the spectral changes of Figure 4-3 when simple harmonic oscillator concepts are applied to the molecular vibrations. As the OH group of one phosphate comes into proximity with the lone oxygen of another phosphate, some electron density is withdrawn from the P=O linkage to establish the hydrogen bond. This weakens the P=O bond (thereby reducing the force constant), and the hydrogen increases the effective mass of the lone oxygen. The combined effects lower the $P=(O)_2$ symmetric stretch oscillator frequency resulting in a new band as evidenced by the increasing asymmetry of the 1075 cm^{-1} band with increasing salt concentration. As monomers enter into hydrogen bonding the 1075 cm^{-1} band decreases in intensity relative to the 875 cm^{-1} band. The Raman spectra of powdered and saturated solution ADP are compared in Figure 4-4. Only the P-(OH) stretch band appears in the solid-state spectrum at 921 cm^{-1}. The 1075 cm^{-1} band is no longer discernible, although the asymmetry to higher wavenumbers undoubtably comprises this and other bands. IR spectra of solid NaDP show a very strong band at 1053 cm^{-1} that has been assigned to the hydrogen bonded $P=(O)_2$ symmetric stretch vibration [36].

In the $P-(OH)_2$ symmetric stretch, the OH group vibrates as a unit with molecular weight 17. When it is hydrogen bonded to another oxygen, electron density is withdrawn from the O-H bond, increasing the strength of the P-OH bond. For this reason the oscillator frequency is increased by 20 cm^{-1} over the range of concentrations studied. The intensity of the 875 cm^{-1} band does not decrease because the bond

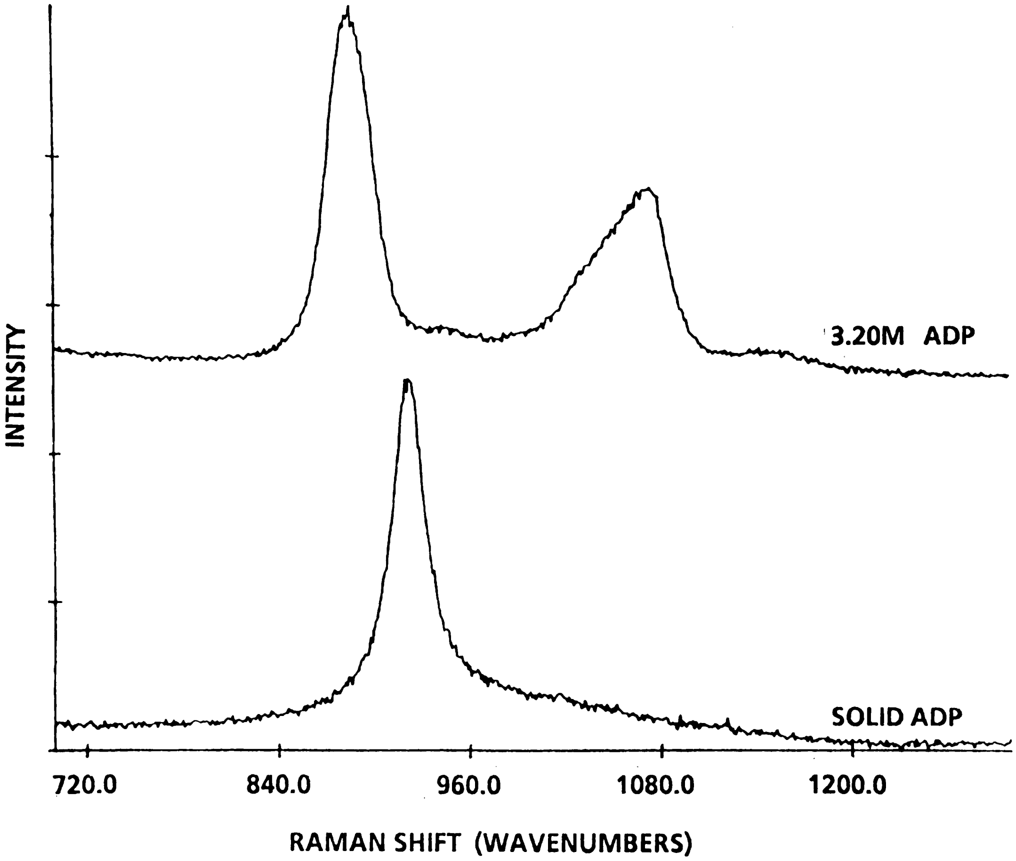

Figure 4-4. The Raman spectra of powdered-crystal and saturated-solution ADP.

containing the vibration is well removed from the site of hydrogen bonding, whereas the P=O bond is directly adjacent to it.

Two results of the band deconvolution analysis are presented graphically in Figure 4-5. For both Figures 4-5a and 4-5b, the lowest set of bands are the synthetic bands. When summed they give the total spectrum, shown just above and overlayed with the experimentally measured band profile. At the top is the difference between the total synthetic spectrum and the experimental spectrum. Figure 4-5 dramatically contrasts the changes in the 1075 cm^{-1} envelope with increasing concentration.

The synthetic band parameters are gathered in Tables 4-2 thru 4-5. They vary in a reasonable and systematic manner. The peak position of the hydrogen-bonded $P=(O)_2$ symmetric stretch vibration gradually lowers from 1063 cm^{-1} in dilute solution to 1038 cm^{-1} in concentrated solution. This and the increase in its half-width at half-maximum indicate that probably more than one type of species is present, although separate bands cannot be resolved. Since the band area (1075 cm^{-1} + 1050cm^{-1}) increases linearly with solute concentration up to the limits specified earlier, below these limits the ratio of the band areas (1050 cm^{-1})/(1050 cm^{-1} + 1075cm^{-1}) gives the fraction of anions participating in hydrogen bonding. At approximately 1.8M, 60% of the phosphates are involved in dimers or polymers, and this rises to 80% at 3.2M ADP. Although Preston and Adams [41]

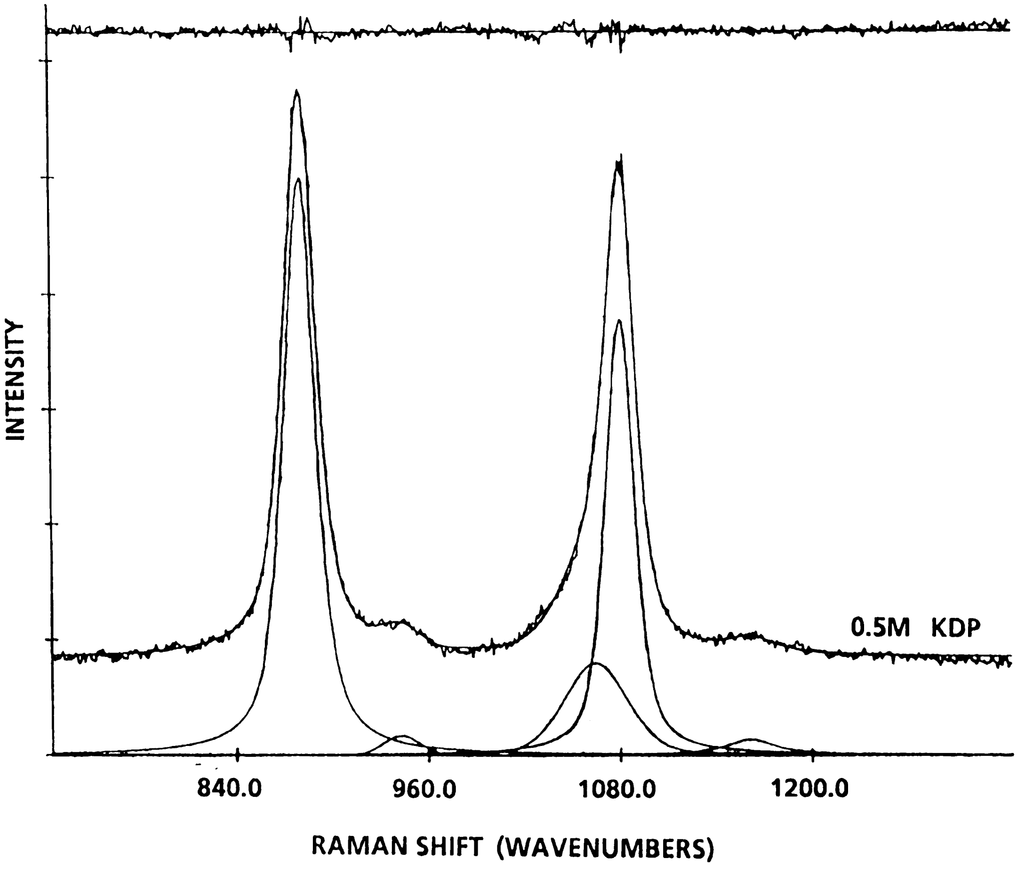

Figure 4-5a. The deconvoluted spectrum of 0.5 M KDP.

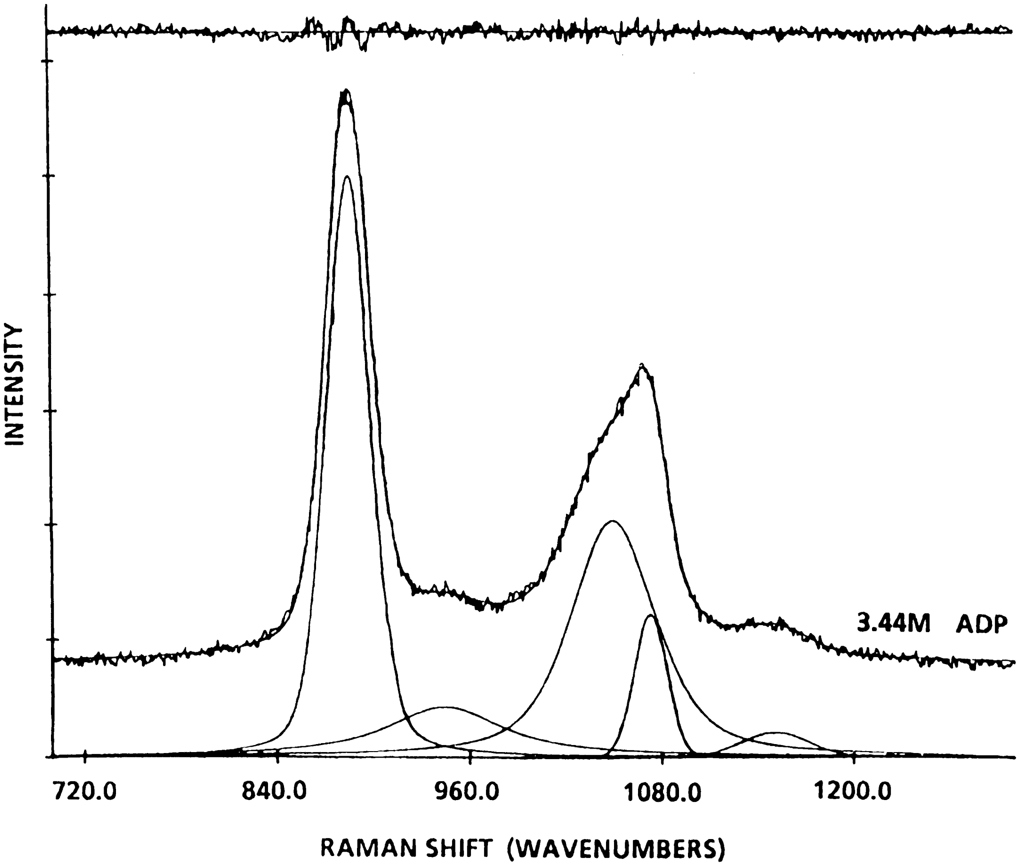

Figure 4-5b. The deconvoluted spectrum of supersaturated 3.44 M ADP.

Table 4-2. Band Positions From Dihydrogen Phosphate Vibrational Band Deconvolution

Concentration	Band Position (cm^{-1})				
(mole/l)	$875cm^{-1}$	$945cm^{-1}$	$1050cm^{-1}$	$1075cm^{-1}$	$1150cm^{-1}$
0.01 ADP[a]	875.0	-	-	1076.1	-
0.05 ADP[a]	875.0	-	-	1076.3	-
0.10 KDP	876.1	944.8	1062.7	1076.5	1166.8
0.50 KDP	877.3	943.0	1061.7	1077.2	1161.8
1.00 ADP	879.5	940.0	1055.6	1075.1	1158.6
1.50 ADP	880.3	940.0	1053.0	1075.5	1157.6
1.86 KDP,[b,c] ADP, NaDP	881.7	940.0	1054.5	1077.0	1155.1
2.50 ADP	883.1	940.0	1050.7	1076.3	1151.6
3.20 ADP[c]	884.6	947.0	1052.1	1074.0	1155.3
3.30 ADP[c]	885.0	940.6	1050.9	1074.0	1148.5
3.44 ADP[c]	887.2	944.5	1051.5	1075.2	1150.6
4.60 NaDP	889.0	947.0	1045.0	1075.8	1158.4
6.01 NaDP[c]	893.8	947.0	1038.0	1073.5	1162.0

[a] Not deconvoluted due to severe baseline curvature.

[b] Only 1.86M KDP was deconvoluted. The spectra of all three salts are identical within the spectral noise.

[c] Supersaturated. At 30°C, the solubilities are 1.79M, 3.19M, and 6.00M for KDP, ADP, and NaDP, respectively.

Table 4-3. Half-Widths At Half-Maximum From Dihydrogen Phosphate Vibrational Band Deconvolution

Concentration	Half-Width At Half-Maximum (cm^{-1})				
(mole/l)	875cm^{-1}	945cm^{-1}	1050cm^{-1}	1075cm^{-1}	1150cm^{-1}
0.01 ADP[a]	~10	-	-	~10	-
0.05 ADP[a]	~10	-	-	~10	-
0.10 KDP	10.6	12.1	16.7	10.7	14.4
0.50 KDP	11.8	13.5	23.5	10.8	18.7
1.00 ADP	13.0	33.7	25.7	11.3	29.0
1.50 ADP	13.6	38.7	26.2	12.4	24.9
1.86 KDP,[b,c] ADP, NaDP	14.5	46.9	31.3	12.1	34.4
2.50 ADP	15.0	56.7	29.1	13.1	30.7
3.20 ADP[c]	16.3	45.2	32.3	11.6	24.5
3.30 ADP[c]	15.6	56.4	31.0	12.9	18.3
3.44 ADP[c]	16.2	44.0	31.7	12.3	25.0
4.60 NaDP	17.4	38.0	35.9	14.7	26.6
6.01 NaDP[c]	18.6	23.1	47.4	14.2	23.5

[a] Not deconvoluted due to severe baseline curvature.

[b] Only 1.86M KDP was deconvoluted. The spectra of all three salts are identical within the spectral noise.

[c] Supersaturated. At 30°C, the solubilities are 1.79M, 3.19M, and 6.00M for KDP, ADP, and NaDP, respectively.

Table 4-4. Lorentzian-Gaussian Weighting Factor From Phosphate Vibrational Band Deconvolution

Concentration (mole/l)	Weighting Factor Z 875cm^{-1}	945cm^{-1}	1050cm^{-1}	1075cm^{-1}	1150cm^{-1}
0.01 ADP[a]	-	-	-	-	-
0.05 ADP[a]	-	-	-	-	-
0.10 KDP	.61	.00	.00	.69	.00
0.50 KDP	.68	.00	.22	.55	1.00
1.00 ADP	.39	.00	.12	.54	1.00
1.50 ADP	.45	.27	.06	.61	.00
1.86 KDP,[b,c] ADP, NaDP	.34	.00	.01	.41	.74
2.50 ADP	.20	.00	.28	.40	.52
3.20 ADP[c]	.28	1.00	.50	.00	.00
3.30 ADP[c]	.20	.68	.35	.08	.00
3.44 ADP[c]	.27	1.00	.57	.00	.00
4.60 NaDP	.21	1.00	.70	.00	.12
6.01 NaDP[c]	.37	1.00	.42	.35	.21

[a] Not deconvoluted due to severe baseline curvature.

[b] Only 1.86M KDP was deconvoluted. The spectra of all three salts are identical within the spectral noise.

[c] Supersaturated. At 30°C, the solubilities are 1.79M, 3.19M, and 6.00M for KDP, ADP, and NaDP, respectively.

Table 4-5. Band Area Ratios From Phosphate Vibrational Band Deconvolution

Concentration (mole/l)	Area Ratios $\frac{A_{875}}{A_{1050} + A_{1075}}$	$\frac{A_{1050}}{A_{1050} + A_{1075}}$
0.01 ADP[a]	~1	.00
0.05 ADP[a]	~1	.00
0.10 KDP	0.93	.08
0.50 KDP	1.07	.29
1.00 ADP	1.00	.39
1.50 ADP	1.09	.43
1.86 KDP,[b,c] ADP, NaDP	1.03	.60
2.50 ADP	0.91	.65
3.20 ADP[c]	1.01	.84
3.30 ADP[c]	1.06	.79
3.44 ADP[c]	0.94	.85
4.60 NaDP	0.79	.88[d]
6.01 NaDP[c]	0.85	.94[d]

[a] Not deconvoluted due to severe baseline curvature.

[b] Only 1.86M KDP was deconvoluted. The spectra of all three salts are identical within the spectral noise.

[c] Supersaturated. At 30°C, the solubilities are 1.79M, 3.19M, and 6.00M for KDP, ADP, and NaDP, respectively.

[d] These values are not reliable since band areas are not linear with concentration in this range [41].

found that the integrated intensities of the NaDP bands were not linear with concentration above 2M (verfied in the present study), it is clear from Figure 4-3 that a larger fraction of anions take part in hydrogen bonding in concentrated NaDP solutions than in supersaturated ADP solutions. The results for all deconvoluted spectra are presented in Figure 4-6. The uncertainties in the data of Figure 4-6 are impossible to state explicitly since the ordinate values depend most heavily upon the baseline subtracted. Varying the baseline between reasonable extremes produced changes in percent hydrogen bonded phosphates of no more than ±5% at any concentration.

A wide variety of structural types are possible for the anion-anion interaction in aqueous solution. Single, double, and triple hydrogen bonds may form, and each of these may take on several conformations. Ionic aggregates with the structure of the crystal are not likely. There is no evidence of a solid-state band around 920 cm^{-1} in supersaturated ADP or KDP solutions. The crystal structure of NaDP is quite different from the isomorphic ADP and KDP, but the spectra of all three salt solutions at 1.86M (at which KDP is supersaturated) are completely identical. At the solution temperature investigated, NaDP actually crystallizes as the dihydrate. There is good evidence for the double-bonded structure shown in Figure 4-7, although other structure types cannot be discounted. Crystals of monoclinic NaDP include anions associated into "dimeric"

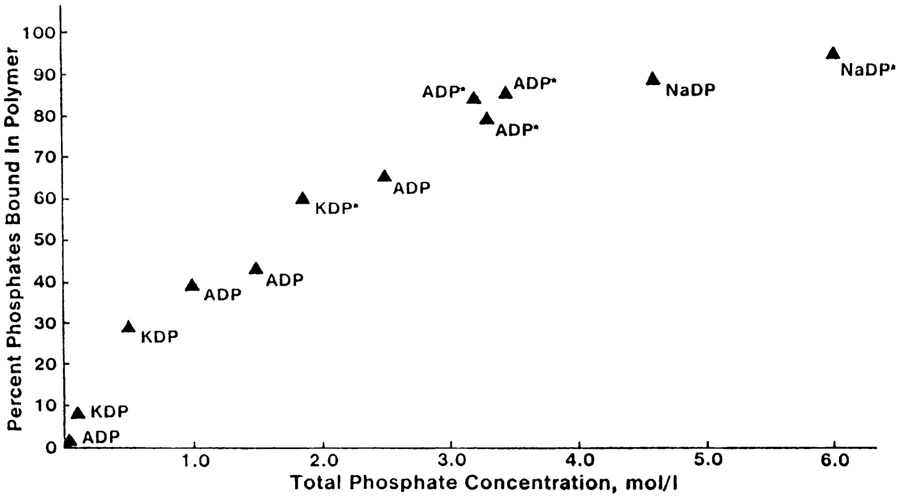

Figure 4-6. Percent of phosphates in solution participating in hydrogen bonding at various concentrations.

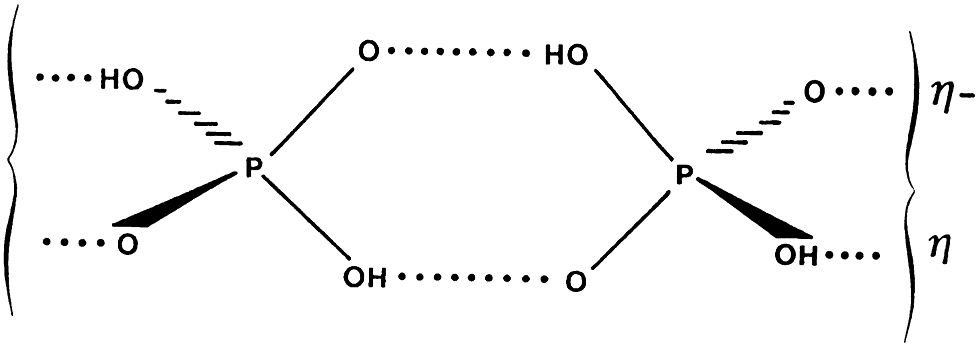

Figure 4-7. The double-bonded structure of dihydrogen phosphates in aqueous solution.

units as in Figure 4-7 [21]. A wide angle x-ray scattering study of 85% phosphoric acid by Wertz and Cook [49] showed H_3PO_4 dimerizes in the form of Figure 4-7. The hydrogen bonded oxygen-to-oxygen length was measured to be 2.6 angstroms, which is still short for hydrogen bonds and indicates a very stable structure. Finally, this hydrogen bonded framework has been found for carboxylic acids [27] and the structurally homologous sulfuric acid [50].

The value(s) of n in Figure 4-7 is still to be determined. If the anion association process ceased with the dimer, then the equilibrium between monomer (M, mol/liter) and dimer (D, mol/liter) may be expressed

$$M + M = D \tag{4-3}$$

$$Q_d = \frac{D}{M^2} \tag{4-4}$$

where Q_d is the concentration quotient. Q_d is used since the actual equilibrium constant must depend on activities, not concentrations. Between 0.1M and 3.44M, the area ratio of the 875 cm^{-1} band to the 1050 cm^{-1} + 1075 cm^{-1} sum band is very close to 1, averaging 1.01 (Table 4-5). This implies that the relative molar scattering factor is the same for all three bands, i.e., the proportionality constants between concentration and band intensity are equal. The concentration ratio of dimer to monomer is therefore

$$\frac{D}{M} = \frac{A_{1050}}{2A_{1075}} \qquad (4\text{-}5)$$

where A is the area of the band identified by the subscript. Since $C_o = M + 2D$, where C_o is the formality of the salt, Q_d may be written as

$$Q_d = \frac{D}{M} * \frac{1}{M} = \frac{D}{M} * \left(\frac{1}{C_o}\left(\frac{2D}{M} + 1\right)\right)$$

$$= \frac{A_{1050}}{2A_{1075}}\left(\frac{1}{C_o}\left(\frac{A_{1050}}{A_{1075}} + 1\right)\right) \qquad (4\text{-}6)$$

When evaluated with the data of Table 4-5, Q_d varies erratically between 0.43 and 5.41. Since a monomer-dimer composition should result in a systematic variation of Q_d, it must be concluded that n may be other than 2. The peak position and half-width at half-maximum behavior of the 1050 cm^{-1} and 875 cm^{-1} bands are also consistent with a distribution of values for n.

Several aspects of ADP and KDP crystal growth are better explained if the polymer structure of Figure 4-7 acts as a constituent of the growth unit in supersaturated solution rather than the monomer. O-HO hydrogen bond energies usually fall within the range 2 to 7 kcal/mole, with those between liquid water at 3.4 kcal/mole [27]. The O--O distance in ice is 2.76 angstroms [27]. Because of the very short hydrogen bond length in crystalline ADP or KDP, the O-HO bond energy is certainly 7 kcal/mole or greater. Comparison of Figures 4-1 and 4-7 shows that at least two and possibly more strong hydrogen bonds must be broken and reformed upon transition of the solute from solution to crystal. Where and how this occurs is not known, but if it occurs on the crystal surface just prior to lattice incorporation, it explains the unimportance of surface diffusion noted by Chernov et al. [12]. Further, this implies that desolvation of the phosphate is not rate-limiting for crystal growth since some waters of hydration are preferentially replaced by other phosphates, even at very low concentrations.

The rapid growth in the z-direction as compared to the x- or y-direction is explained by the fact that the strong hydrogen bonds in the crystal which must reform after breaking are roughly in the xy-plane. If the activation energy for crystal growth is related to the breaking of hydrogen bonds, it becomes clear why the value for ADP is greater than for KDP. Supersaturated ADP solutions have many more phosphates involved in hydrogen bonding and so more bonds must be broken and reformed than in KDP solutions.

Step sizes of hundreds of angstroms are more easily rationalized by growth units of similar dimensions, although this does not preclude the existence of relatively small growth units. Evidence of large, molecular clusters in supersaturated solution has been reported for citric acid by Mullin and Leci [51] and for several compounds by Larson and Garside [52]. An important result for the dihydrogen phosphates is that the structure of the clusters or polymers formed in solution bears little resemblance to the crystal structure.

Obviously, further spectroscopic studies of this system are necessary. The change in growth mechanism of the {100} face of ADP at $\sigma=0.07$ is yet to be explained on a molecular basis. Raman spectra of other dihydrogen phosphates such as cesium (monoclinic) and lithium (orthorhombic) will help to establish trends in the solution structure. It may be expected that dihydrogen arsenates, monohydrogen phosphates, or hydrogen bonding compounds in general will display similar solution behavior. The Raman spectra of solutions containing impurities such as chromium should provide insight into the taper effect found in ammonium and potassium dihydrogen phosphate crystals.

4-5. Conclusions

Interpretation of the Raman spectra of aqueous dihydrogen orthophosphate salt solutions shows that monomolecular units are accompanied by phosphate polymers of varying size. The anions are linked by strong hydrogen bonds in a fashion dissimilar to the crystal. The breaking and reforming of these bonds upon lattice incorporation explains many of the characteristics of dihydrogen orthophosphate crystal growth, including the faster growth rate in the z-direction than the x- or y-direction; the larger activation energy for crystal growth of ADP compared to KDP; and the rate-limiting surface growth mechanism.

4-6. Acknowledgments

The authors thank the National Science Foundation for support making this work possible through Grant No. CPE-8409458. The Upjohn Company is also thanked for the graduate fellowship support of M.K. Cerreta. This work was performed in the Shared Laser Laboratory at Michigan State University.

4-7. Literature Cited

1. J. W. Mullin and A. Amatavivadhana, J. Appl. Chem., 17, 1967, 151.
2. J. W. Mullin, A. Amatavivadhana, and M. Chakraborty, J. Appl. Chem., 20, 1970, 153.
3. R. J. Davey and J. W. Mullin, J. Cryst. Growth, 29, 1975, 45.
4. J. Garside and R. I. Ristic, J. Cryst. Growth, 61, 1983, 215.
5. R. I. Ristic, J. Garside, and B. Zizic, J. Cryst. Growth, 69, 1984, 442.
6. B. Dam and W. J. P. Van Enckevort, J. Cryst. Growth, 69, 1984, 306.
7. B. Dam, P. Bennema, and W. J. P. Van Enckevort, J. Cryst. Growth, 74, 1986, 118.
8. V. G. Lutsau, Ju. M. Fishman, and I.S. Res, Krist. Tech., 5(3), 1970, 445.
9. R. J. Davey, R. I. Ristic, and B. Zizic, J. Cryst. Growth, 47, 1979, 1.
10. H. L. Bhat, K. J. Roberts, and J. N. Sherwood, J. Appl. Crystallogr., 16, 1983, 390.
11. J. L. Torgesen and R. W. Jackson, Science, 148, 1965, 952.
12. A. A. Chernov, L. N. Rashkovich, and A. A. Mkrtchan, J. Cryst. Growth, 74, 1986, 101.

13. R. J. Davey and J. W. Mullin, J. Cryst. Growth, 26, 1974, 45.

14. C. Belouet, E. Dunia, and J. F. Petroff, J. Cryst. Growth, 23, 1974, 243.

15. C. Belouet and W. T. Stacy, J. Cryst. Growth, 44, 1978, 315.

16. W. J. P. Van Enckevort, R. Jannsen-Van Rosmalen, and W. H. Van der Linden, J. Cryst. Growth, 49, 1980, 502.

17. M. Aguilo and C. F. Woensdregt, J. Cryst. Growth, 69, 1984, 527.

18. W. K. Burton, N. Cabrerra, and F. C. Frank, Philos. Trans. R. Soc. London, A:243, 1951, 299.

19. P. Bennema, J. Cryst. Growth, 1, 1967, 278.

20. A. D. Randolph and M. A. Larson. Theory of Particulate Processes (Academic Press, New York, 1971).

21. M. Catti and G. Ferraris, Acta Crystallogr., B30, 1974, 1.

22. A. A. Khan and W. H. Baur, Acta Crystallogr., B29, 1973, 2721.

23. J. West, Z. Kristallogr., 74, 1930, 306.

24. R. N. P. Choudhary, R. J. Nelmes, and K. D. Rouse, Chem. Phys. Lett., 78(1), 1981, 102.

25. L. Tenzer, B. C. Frazer, and R. Pepinsky, Acta Crystallogr., 11, 1958, 505.

26. G. E. Bacon and R. S. Pease, Proc. R. Soc. London, A:220, 1953, 397.

27. G. C. Pimentel and A. L. McClellan. The Hydrogen Bond (W. H. Freeman and Co., New York, 1960).

28. C. S. Venkateswaran, Proc. Indian Acad. Sci., A3, 1936, 25.

29. A. Simon and F. Feher, Z. Anorg. Allg. Chem., 230, 1937, 289.

30. A. Simon and G. Schulze, Z. Anorg. Allg. Chem., 242, 1939, 313.

31. J. P. Mathieu and J. Jacques, C. R. Seances Acad. Sci., Ser. C, 215, 1942, 346.

32. P. S. Narayanan, Proc. Indian Acad. Sci., A28, 1948, 469.

33. F. A. Miller and C. H. Wilkens, Anal. Chem., 24, 1954, 1253.

34. D. E. C. Corbridge, J. Appl. Chem., 6, 1956, 456.

35. J. V. Pustinger, W. J. Cave, and M. L. Nielsen, Spectrochim. Acta, 1959, 909.

36. A. C. Chapman and L. E. Thirlwell, Spectrochim. Acta, 20, 1964, 937.

37. E. Steger and K. Herzog, Z. Anorg. Allg. Chem., 331, 1964, 169.

38. A. C. Chapman, D. A. Long, and D. T. L. Jones, Spectrochim. Acta, 21, 1965, 633.

39. E. Steger, K. Herzog, and J. Klosowski, Z. Anorg. Allg. Chem., 432, 1977, 42.

40. C. M. Preston and W. A. Adams, Can. J. Spectrosc., 22, 1977, 125.

41. C. M. Preston and W. A. Adams, J. Phys. Chem., 83(7), 1979, 814.

42. W. A. Adams, C. M. Preston, and H. A. M. Chew, J. Chem. Phys., 70(5), 1979, 2074.

43. P. Haufe, J. Solution Chem., 14(2), 1985, 73.

44. P. M. Mcmahon, M. K. Cerreta, K. A. Berglund, and M. A. Larson, Appl. Spectrosc., 40(2), 1986, 282.

45. J. A. Nelder and R. Mead, Comput. J., 7, 1965, 308.

46. P. Liebman, G. Loew, A. D. McLean, and G. R. Pack, J. Am. Chem. Soc., 104(3), 1982, 691.

47. F. A. Cotton and G. Wilkinson. Advanced Inorganic Chemistry, 4th ed. (John Wiley and Sons, New York, 1980).

48. D. W. James and R. L. Frost, Faraday Discuss. Chem. Soc., 64, 1978, 48.

49. D. L. Wertz and G. A. Cook, J. Solution Chem., 14(1), 1985, 41.

50. A. Goypiron, J. de Villepin, and A. Novak, J. Chim Phys., Phys.-Chim. Biol., 75(9), 1978, 889.

51. J. W. Mullin and C. L. Leci, Philos. Mag., 19, 1969, 1075.

52. M. A. Larson and J. Garside, Chem. Eng. Sci., 41(5), 1986, 1285.

CHAPTER 5

THE EFFECT OF IONIC IMPURITIES ON THE AQUEOUS SOLUTION STRUCTURE OF SOME DIHYDROGEN ORTHOPHOSPHATES*

5-1. Abstract

The effect of ionic impurities on the aqueous solution structure of supersaturated ammonium dihydrogen phosphate (ADP) has been studied at 28°C using UV-VIS, Laser Raman, and Fourier transform infrared spectroscopies. Using NH_4OH and H_3PO_4 to adjust the solution pH, the spectra indicate that dimeric dihydrogen phosphate anions are stable between pH 2.12 and pH 7.30, although certainly somewhat less so at elevated pH. The presence of the dimers may account for the difficulty in growing well-formed ADP crystals at natural pH 3.8 and low supersaturations. The UV-VIS spectra show that Cr^{+3} and Fe^{+3} ions, added as their chlorides from 100 ppm to 1000 ppm, interact strongly with the dihydrogen phosphate anions. The results for Al^{+3} are indeterminate.

5-2. Introduction

It is common knowledge that even trace quantities of impurities in crystallization suspensions can greatly affect the physical characteristics of the crystals formed. The typical characteristics altered are purity, morphology, stability, and phase. In some cases the impurities are

---

* a paper published by M. K. Cerreta and K. A. Berglund in ISCAP 1987, p.53, 1987.

introduced intentionally and are of great benefit, while in other cases extreme care is required to exclude them. The source of impurities can also be the crystallizer itself, or they may enter with the feed solution. Because of the latter possibility, the impact of impurities on product recovery must be considered in upstream process design, since the viability of the entire process may be determined by the presence of a single impurity. For this reason, and since some extraneous material will always be present in solution, it is of considerable importance to understand the interaction between the crystal, the solute molecules, and the impurities. The purpose of this work is to study the effects of $CrCl_3$, $FeCl_3$, $AlCl_3$, and changing pH on the crystal and aqueous solution structures of ammonium dihydrogen phosphate (ADP) using UV-VIS absorption, laser Raman and Fourier transform infrared spectroscopies. Previously, Cerreta and Berglund [1] have shown that the majority of dihydrogen phosphate anions in pure, concentrated aqueous solution are coupled together by hydrogen bonds in a fashion dissimilar to those of the crystal. This result is briefly reviewed.

5-3. Experimental

Saturated aqueous solutions of ADP at 30°C were prepared by dissolving one of solid $CrCl_3$, $FeCl_3$, or $AlCl_3$ at 1000 ppm in water and adding crystals of analytical grade ADP to slight excess. The water used was doubly distilled and passed through Barnstead D8904 and D8901 cartridges to remove any organic or ionic impurities. Saturated solutions of ADP at 30^{o}C and various pH were prepared by adding several milliliters of 85% H_3PO_4 or 30% NH_4OH to 75 ml of water and then adding ADP crystals to slight excess. The pH was measured on an Orion model 501 pH meter. Undersaturated solutions were prepared gravimetrically.

Raman excitation was provided by a Spectra Physics model 175 argon ion laser operating at 514.5 nm. The sample cell held solutions at 28.00^{o}C ±0.05^{o}C and is described in Chapter 3. Spectra of solids were obtained from capillary tubes. The Raman scattered light was collected with standard 90^{o} collection optics (Spex model 1459) and dispersed in a Spex model 1877 spectrometer. Detection was accomplished with an EGG PARC OMA III system equipped with a model 1421 detector. The resolution is 0.8 cm^{-1}.

The FTIR spectra of solutions and solids were obtained with a Perkin-Elmer model 1750 FTIR at 4 cm^{-1} resolution. Solutions were held in a Spectra Tech ATR CIRCLE cell equipped with a ZnSe bar, while solids were suspended in Nujol between NaCl plates. A Perkin-Elmer model 3840 Lambda Array provided the UV-VIS spectra.

5-4. ADP Crystals and Crystal Growth

Figure 4-1 shows the unit cell of pure ADP looking down the c-axis [2]. The small squares represent tetrahedral phosphate groups. The small open circles are hydrogen atoms and hydrogen bonds are depicted by broken lines. It should be noted that each phosphate group is hydrogen bonded to four other phosphates. The natural habit of pure ADP consists of a tetragonal prism capped at either end by tetragonal pyramids and is shown in Figure 4-2.

Mullin and Amatavivadhana [3] studied the growth characteristics of pure ADP. They found the growth rate of any face varied parabolically with supersaturation, suggesting that ADP grows by a surface limited mechanism. Growth in the z-direction is faster than in the x- or y-directions and begins at a lower supersaturation. Because of this, the {100} faces taper in the [001] direction at low supersaturation. The tapered habit is shown in Figure 5-1.

The natural pH of ADP is 3.8. Mullin and others [4] and Davey and Mullin [5] studied the effects of pH and Cr^{+3}, Fe^{+3}, and Al^{+3} ions on the habit of ADP. No changes in crystal habit were detected below pH 3.8. However, increasing the pH to approximately 5 gradually diminished the tapering at low supersaturation and growth in the x or y directions increased many times over the values observed at lower pH. Tapering was also observed in the presence of the metal ions, the degree of tapering being more pronounced in the order $Cr^{+3} > Fe^{+3} > Al^{+3}$. It was determined that the ions were incorporated in the {100} and {010} faces.

5-5. UV-VIS, Raman, and FTIR Spectroscopies

UV-Visible absorption occurs as a result of the interaction between the electric vector of a photon field and the electron distribution of a molecule. Electrons are

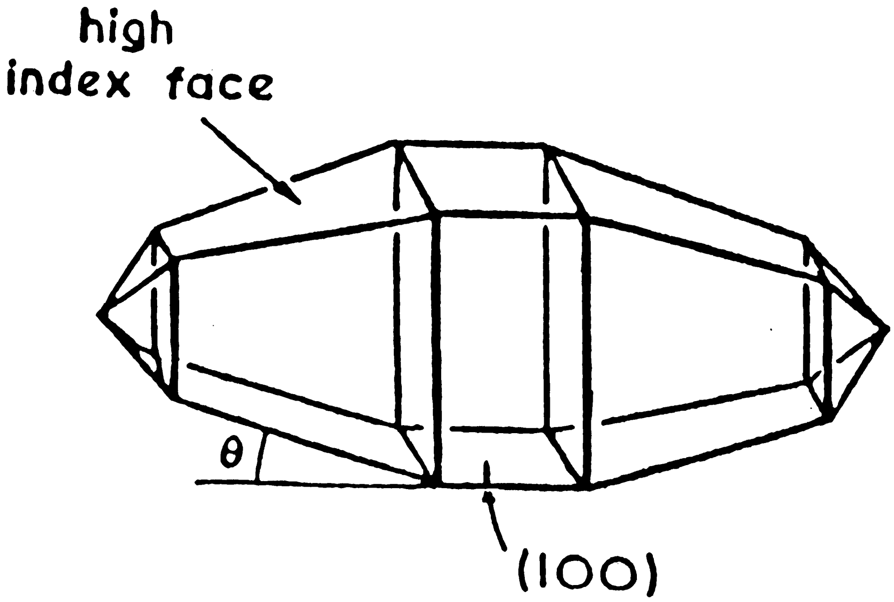

Figure 5-1. The tapered habit of ADP and KDP.

promoted from one orbital to another, the difference in energy between orbitals being exactly equal to the energy of the photon absorbed. This energy difference is dependent upon the environment of the molecule. Infrared absorption is similar except that the interaction is between the electric vector of the photon field and the oscillating dipole moment of a vibrating molecule. The energy difference here is between vibrational states and is again a function of the molecular environment. The Raman process is also dependent upon molecular vibrations, but in this case the passing electric field of the photon induces a dipole moment in the vibrating molecule. The dipole induced is proportional to the polarizability of the electron cloud about the molecule. The molecule then extracts only enough energy from the light to move between vibrational states, and re-emits a photon of correspondingly lower energy. Thus, the Raman event is an inelastic scattering process.

In general, the selection rules for IR and Raman transitions dictate that asymmetric and bending vibrations are best observed in the IR, while symmetric modes are strongest in the Raman.

Group theory arguments show that the aqueous dihydrogen phosphate molecule is of approximate C_{2v} symmetry with 15 non-degenerate fundamental vibrations, all of which are Raman active, and 13 are IR active. Most prominent in the Raman are the $(OH)_2P{=}(O)_2$ symmetric stretch (1075 cm^{-1}) and the $(O)_2P{-}(OH)_2$ symmetric stretch (875 cm^{-1}). In the infrared the strongest bands observed are the $(OH)_2P=(O)_2$ asymmetric (1150 cm^{-1}) and symmetric (1075 cm^{-1}) stretches, and the $(O)_2P-(OH)_2$ asymmetric stretch (940 cm^{-1}). The O-H stretching region near 3000 cm^{-1} is of little diagnostic value since the water bands in this region obscure the phosphate O-H stretch in both the Raman and IR.

5-6. Results and Discussion

5-6.1 Pure Solutions

The Raman spectra of sodium, potassium, and ammonium dihydrogen phosphates (NaDP, KDP, and ADP, respectively) in pure, aqueous solution at various concentrations are shown in Figure 4-3. The $(O)_2P-(OH)_2$ symmetric stretch band moves from 875 cm^{-1} to 894 cm^{-1} (usually referred to as the 875 cm^{-1} band) and broadens with increasing phosphate concentration. The $(OH)_2P=(O)_2$ symmetric stretch band decreases in intensity relative to the 875 cm^{-1} band and develops extreme asymmetry to lower energy. These results are independent of the identity of the cation. Figure 5-2 shows the equivalence of the Raman spectra of all three salts at 1.87M. Further, addition of the chloride salt of the cations to dihydrogen phosphate solutions does not affect the spectra [6].

The spectral changes are explained by the formation of hydrogen bonds between the phosphate groups. As the bonds form, electron density is removed from the O-H bond, which increases the strength of the P-OH bond. This causes the

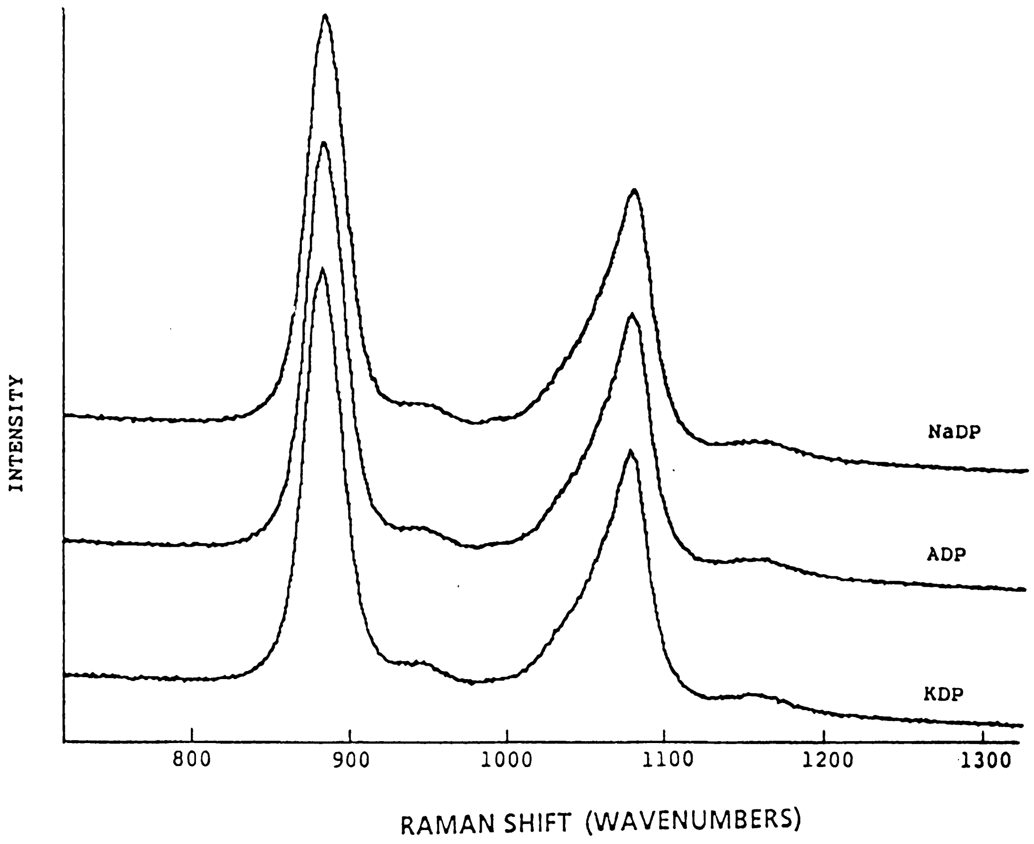

Figure 5-2. The Raman spectra of 1.87 M NaDP (top), ADP (middle), and KDP (bottom).

875 cm^{-1} band to move to higher energy. Electron density is also withdrawn from the P=O bond, thereby weakening it and reducing the energy of the $(OH)_2P=(O)_2$ symmetric stretch vibration. This results in the asymmetry that develops in the 1075 cm^{-1} band, indicating the formation of a new species in solution.

The infrared spectra of ADP solid and supersaturated aqueous ADP corroborate the argument above (Figure 5-3). Upon going from solution to solid, the $(O)_2P-(OH)_2$ symmetric stretch moves from 877 cm^{-1} to 898 cm^{-1} and the asymmetric stretch moves from 942 cm^{-1} to 955 cm^{-1}. In solution, the $(OH)_2P=(O)_2$ symmetric stretch at 1069 cm^{-1} displays some asymmetry centered at about 1031 cm^{-1}; in the solid, the bands are nearly resolved at 1025 cm^{-1}, 1056 cm^{-1}, and 1075 cm^{-1}. Other bands present in the solution are the NH_4+ symmetric bend (1450 cm^{-1}) and the O-H bend of water (1637 cm^{-1}).

Raman band intensities are proportional to the concentration of the species responsible for the band, provided the Raman transition parameters do not vary with concentration. The 1075 cm^{-1} band fades relative to the 875 cm^{-1} band as phosphate monomers enter into hydrogen bonding. The intensity of the 875 cm^{-1} band is not so strongly affected since the $(O)_2P-(OH)_2$ vibration is two bonds removed from the site of the hydrogen bond. In dilute solution, where only "free" aquated ions exist, the bands at 875 cm^{-1} and 1075 cm^{-1} are of equal intensity and half-width at

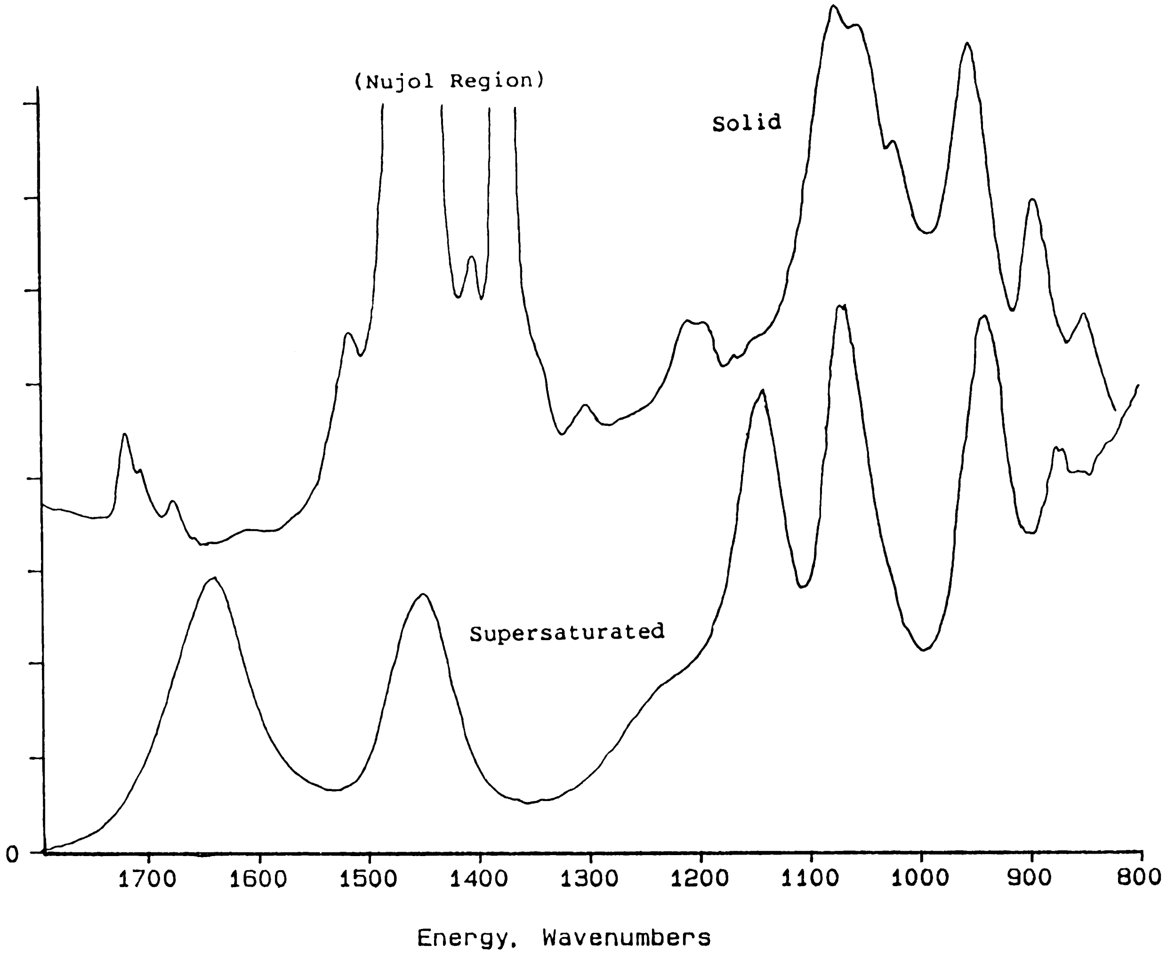

Figure 5-3. The IR spectra of solid (top) and supersaturated aqueous ADP (bottom).

half-maximum. The ratio of the integrated intensity of the 875 cm^{-1} band to the entire 1075 cm^{-1} envelop remains constant at approximately 1:1 with increasing concentration, up to 2M for KDP and NaDP and up to 3M and possibly higher for ADP [6]. This means that the Raman transition parameters are reasonably constant over the concentration ranges specified. Therefore, the ratio of the area of the band giving rise to the asymmetry to the area of the total 1075 cm^{-1} band envelop is the fraction of phosphate anions in solution participating in hydrogen bonds. Cerreta and Berglund [1] fit the experimental band profiles to synthetic Lorentzian-Gaussian sum functions by an iterative least-squares procedure. The band position of the new species varies from 1062 cm^{-1} at low concentrations to 1038 cm^{-1} in supersaturated NaDP (for convenience, referred to as the 1050 cm^{-1} band). The area ratio $A_{1050}/[A_{1050} + A_{1075}]$, where A is the integrated intensity of the band identified by the subscript, shows that 60% and 80% of the phosphates are involved in hydrogen bonding in supersaturated KDP and ADP solutions, respectively. An example of the spectral deconvolution is presented in Figure 4-5, and the results of the band fitting procedure are presented in Figure 4-6.

The Raman spectra of powdered crystals of KDP and ADP between 750 cm^{-1} and 1350 cm^{-1} show only a single band at about 920 cm^{-1} [1]. The fitting of supersaturated-solution band profiles does not require a band at this position. At 30°C, the spectra of all three salts at 1.87M are the same

(Figure 5-2) even though NaDP would crystallize as the dihydrate and KDP is supersaturated. It must be concluded that the Raman spectra offer no evidence of quasi-crystalline entities in dihydrogen phosphate solutions. Instead, there is evidence for the structure shown in Figure 4-7 [7-9], although other structural types are possible.

Cerreta and Berglund [1] calculated an association constant for each of the concentrations studied, assuming the value of n in Figure 4-7 is 2. The resulting "constant" varied widely and unsystematically. The assumption that n is 2 is therefore questionable, and so the association process probably proceeds past the dimer. Preliminary results from light scattering experiments have failed to detect particles greater than 10 angstroms in diameter in saturated solutions of NaDP. This suggests that the species formed by the association process may be limited to a few molecules.

5-6.2 The Effect of pH

The Raman and infrared spectra of supersaturated ADP from pH 2.12 to pH 7.30 are presented in Figures 5-4 and 5-5, respectively. Consider first the Raman spectra. At pH 2.12, the $(O)_2P-(OH)_2$ symmetric stretch appears at 896 cm^{-1} (up from 885 cm^{-1} at pH 3.8) and the 1075 cm^{-1} band decreases in intensity relative to the 896 cm^{-1} compared with the same bands at pH 3.8. The asymmetry in the 1075 cm^{-1} band is more pronounced at pH 2.12 than at pH 3.8.

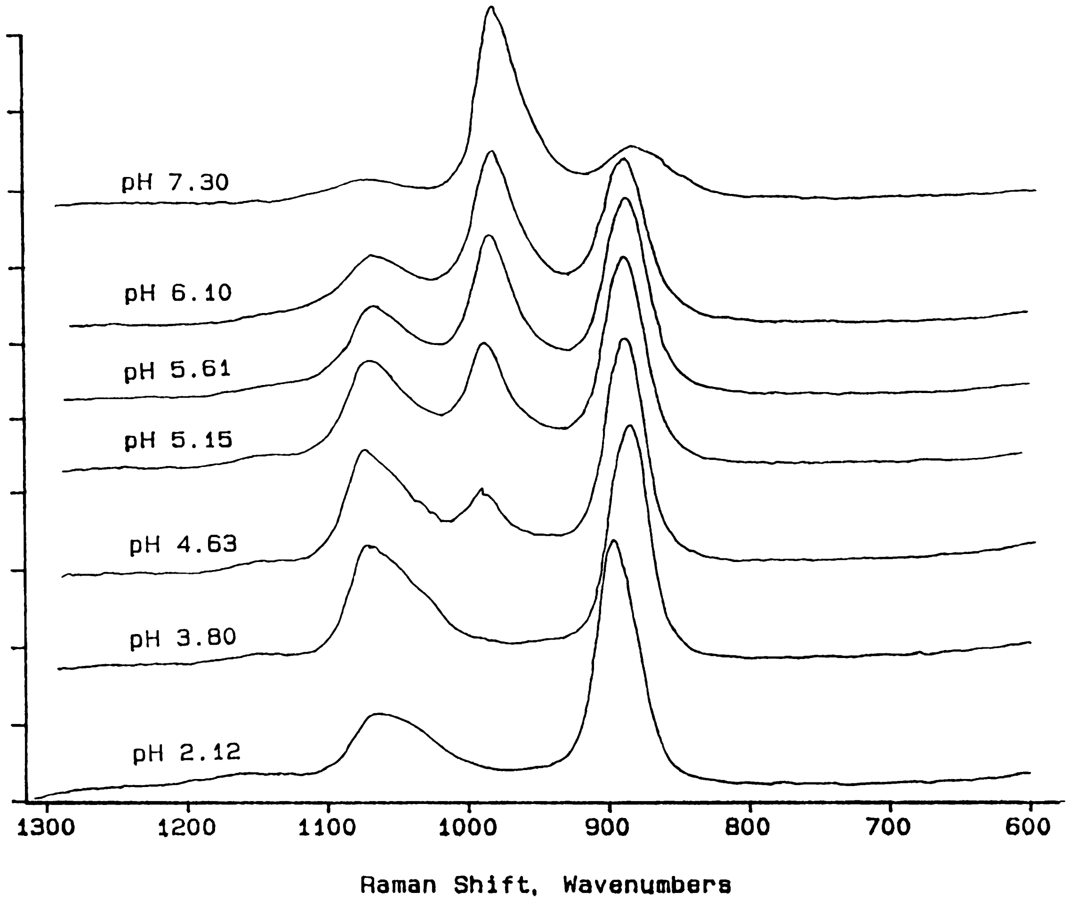

Figure 5-4. The Raman spectra of supersaturated ADP at various pH.

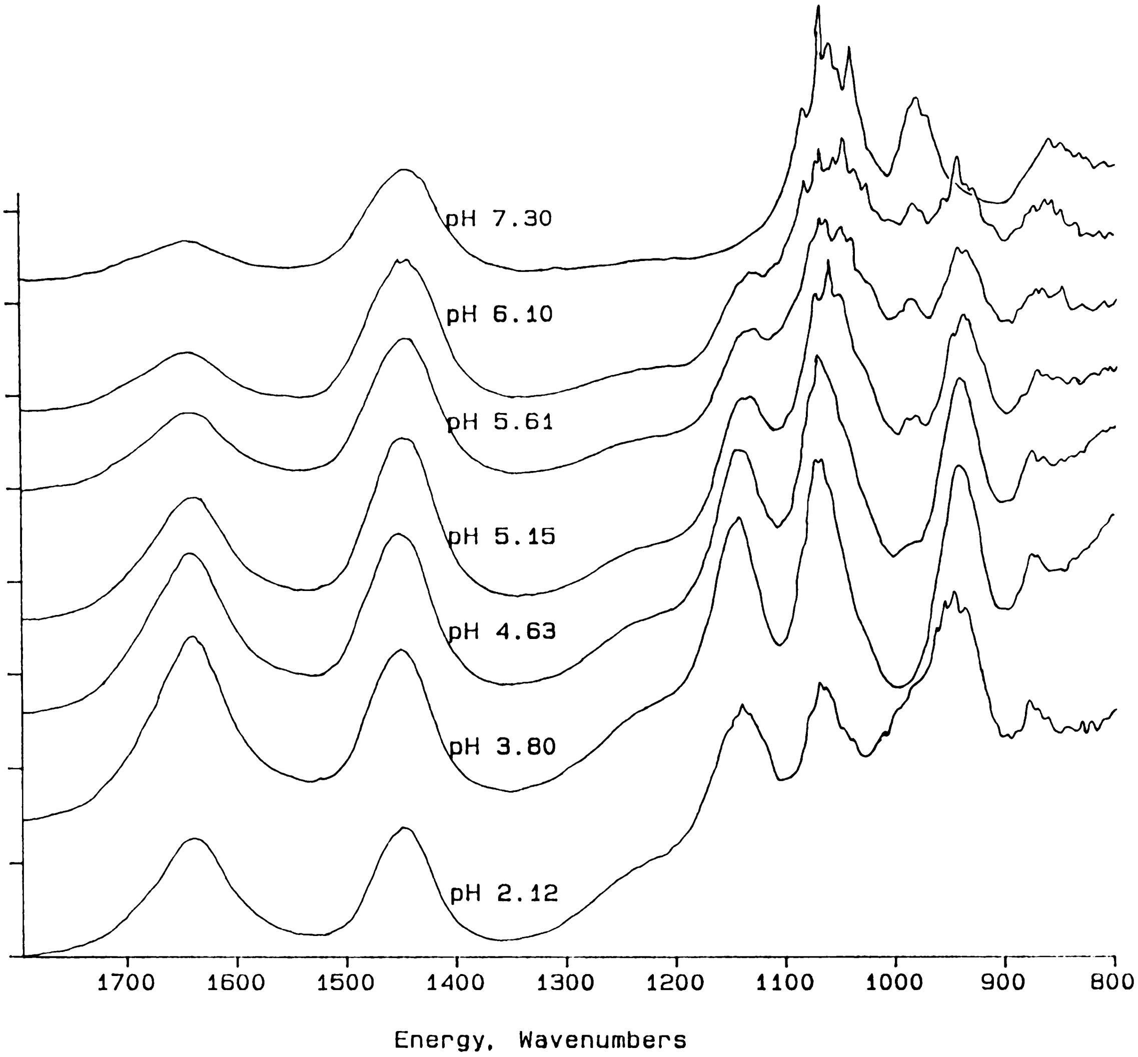

Figure 5-5. The IR spectra of supersaturated ADP at various pH.

These results are consistent with the continued dimer formation expected at the lower pH. As the pH increases above 3.8, the most obvious change is the appearance of a new band at 989 cm^{-1}. This is the $(OH)P-(O)_3$ symmetric stretch of the HPO_42- ion. Asymmetry in this band is most evident at pH 7.30, although not to the same degree as for the $(OH)_2P=(O)_2$ symmetric stretch. The same arguments used for H_2PO_4- dimer formation may be invoked for dimerization of the HPO_42- ion. From the spectra, it is clear that the concentration of HPO_42- in the pH range 4.5 to 5.5 is substantial. It is also obvious that considerable H_2PO_4- is present at pH 6.1, and the ion lingers even at pH 7.30. At elevated pH, the relative intensities of the 1075 cm^{-1} band to the 875 cm^{-1} band remain fairly constant. Although the 989 cm^{-1} band obscures the 1075 cm^{-1} band, it appears that the asymmetry of the 1075 cm^{-1} band is relieved very slightly with increasing pH.

The behavior of the infrared bands with increasing pH in Figure 5-5 complements the Raman spectra. As the pH increases, the 877 cm^{-1}, 945 cm^{-1}, and 1150 cm^{-1} bands associated with the H_2PO_4- ion fade, but not completely until pH 7.30. The formation of the 989 cm^{-1} band is evident, as are the many bands in the 1000 cm^{-1} to 1100 cm^{-1} region due to various asymmetric $(OH)P-O_3$ stretching vibrations. The NH_4+ bending vibration at 1450 cm^{-1} becomes quite strong (compare with the water bending mode) due to the addition of NH_4OH. At elevated pH, the 870 cm^{-1} band due to $(O)_3P-(OH)$ stretching is present.

The increased perfection and ease of ADP crystal growth at pH 5 has been explained by Davey and Mullin [5] as resulting from removal of $(H_3O)^+(H_2O)_3$ adsorption at kink sites on the {100} faces. Since fewer of the sites are blocked, growth is faster. If hydrated hydronium ion adsorption is blocking the growth sites, then a critical number of them must be blocked at approximately pH 4. The presence of excess ammonium ion (due to the addition of NH_4OH) and the divalent $HPO_4 2-$ ion were not considered in the study cited above.

The Raman and IR spectra of the dihydrogen phosphate anion do not change significantly over the pH range studied until pH 7.30. The slight inflection change of the 1075 cm^{-1} band in the Raman indicates some breakup of the pure solution structure at higher pH, but the hydrogen-bonded anion structure appears stable at pH 5. Because of the increased presence of ammonium ion at high pH, it is difficult to accept the view that surface removal of the hydronium ion accounts for the increase in crystal growth rate. Instead, the answer may lie in the changing nature of the adsorbed material near the crystal surface. Comparison of Figures 4-1 and 4-7 show that at least two hydrogen bonds must be broken on transition from the anion in solution to anion in the crystal. In pure solution, the hydrogen bonded species may inhibit crystal growth since it is not of the proper structure to fit in the crystal lattice. As the pH is raised, enough of this structure is disrupted to allow the crystal to grow more rapidly. The role (if any) of the ammonium ion and of $HPO_4 2-$ in the process is not clear.

5-6.3 Effects of Metal Ions

The UV-VIS absorption spectrum of supersaturated aqueous ADP is shown in Figure 5-6. It is rather uneventful, as is expected of nearly all colorless solutions. The vast window from 300 nm to 900 nm provides a means for observing the absorption spectra of the aqueous metal ions.

The spectra of aqueous $CrCl_3$ (500 ppm) and the same solution supersaturated with ADP are shown in Figure 5-7. The presence of ADP quenches the strong absorption at 270 nm, moving it to 300 nm. Likewise, absorptions at 400 nm and 585 nm are shifted to lower energy at 430 nm and 625 nm, respectively. Clearly, the chromium ion is interacting with the phosphates in the solution; it does not simply block the surface of a crystal. Figure 5-8 displays the spectra of aqueous $FeCl_3$ (100 ppm) and aqueous $FeCl_3$ in the presence of supersaturated ADP. Major absorptions at 215 nm and 290 nm meld into one at 244 nm when ADP is present. A moderate absorption at 490 nm in the "pure" $FeCl_3$ solution is completely missing in the $FeCl_3$/ADP spectrum. Again, it is evident that the Fe^{+3} ion is interacting strongly with the phosphates present in solution, not just at a crystal surface.

$AlCl_3$ solutions are colorless and show no absorptions other than a moderate one at 190 nm. Thus, the UV-VIS

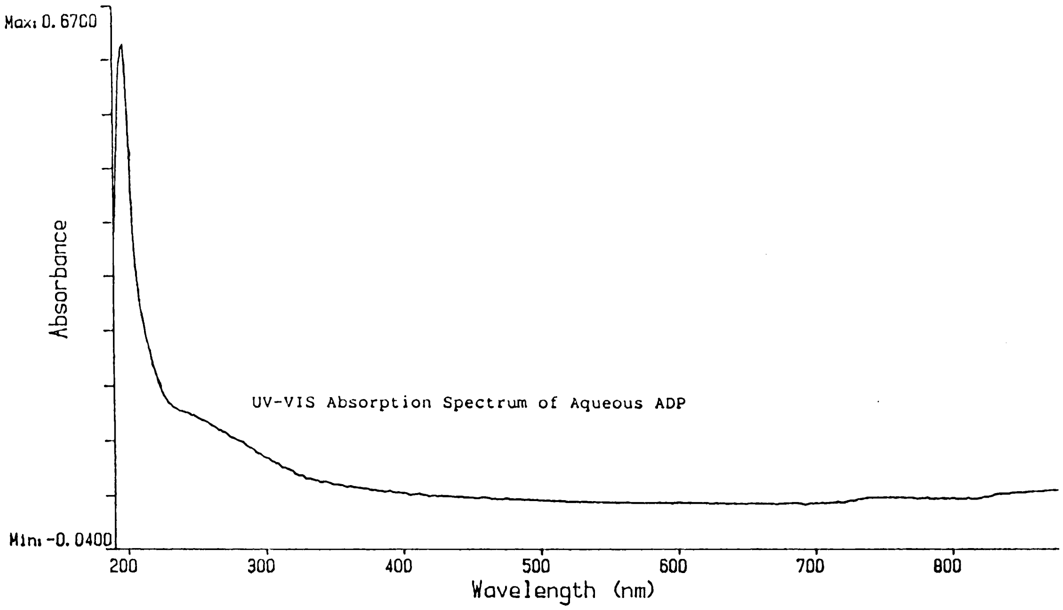

Figure 5-6. The UV-Vis absorption spectrum of supersaturated ADP.

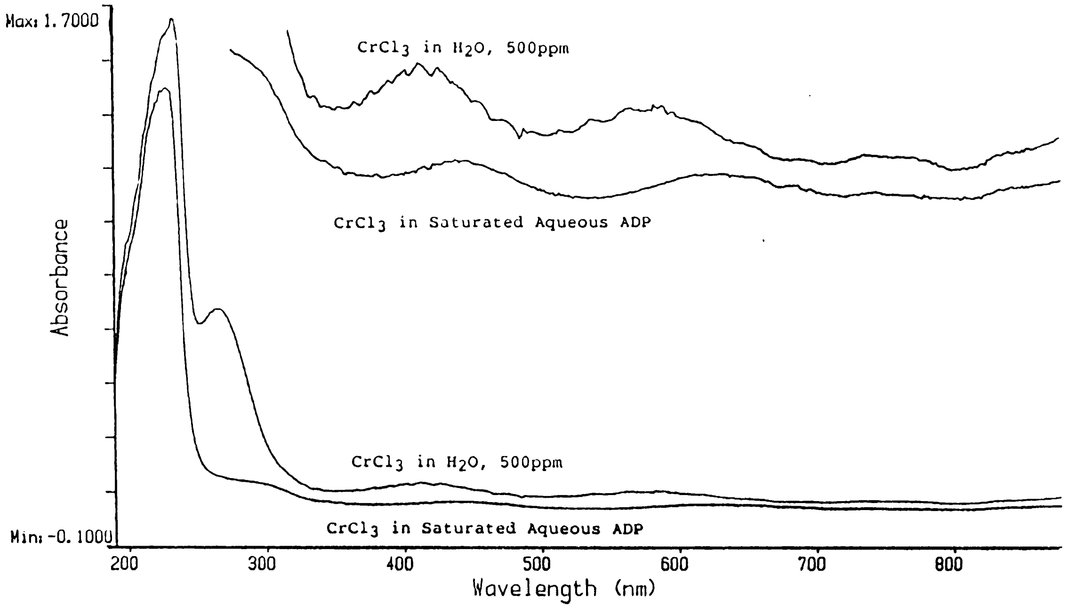

Figure 5-7. The UV-Vis spectra of Cr^{+3} (500 ppm) in water (top) and in supersaturated ADP (bottom).

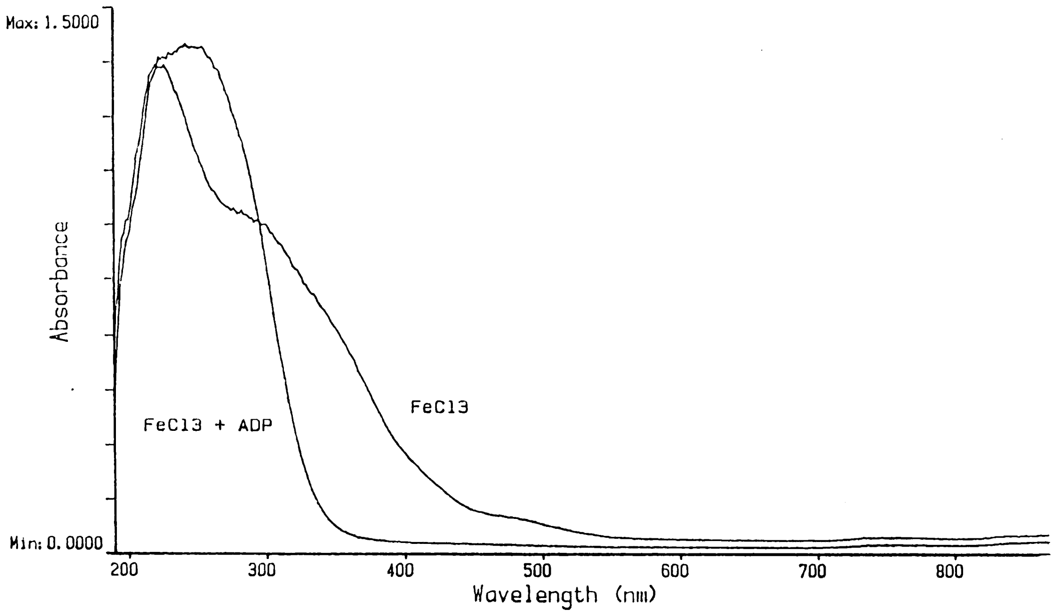

Figure 5-8. The UV-Vis spectra of Fe^{+3} (100 ppm) in water (top) and in supersaturated ADP (bottom).

spectrum of $AlCl_3$ in supersaturated ADP did not show any noteworthy changes compared to aqueous $AlCl_3$.

It was disappointing that the Raman and IR spectra of supersaturated ADP showed absolutely no changes in the presence of any of the three impurities. It is apparent that the impurities were too dilute to be detected and their influence was overwhelmed by the large number of dihydrogen phosphate molecules present. However, the absorption bands of $CrCl_3$ in ADP solutions suggest an avenue of attack. In the Raman experiment, the laser was tuned to 514.5 nm, which is directly between the 430 nm and 625 nm absorption (Figure 5-7). Using the 415 nm and 647 nm emission lines of a krypton laser will allow resonance Raman to occur, whereby vibrations of the chromium-dihydrogen phosphate complex are selectively enhanced approximately 3 orders of magnitude.

5-7. Conclusions

UV-VIS, Raman and FTIR spectroscopies have been used to show that the structure of supersaturated ADP solutions at various pH consists of dihydrogen phosphate molecules linked into dimeric form. These dimers are at least moderately stable at elevated pH, although perhaps broken down somewhat. pH 5 solutions, where it is easiest to grow relatively perfect ADP crystals, contain significant amounts of monohydrogen phosphates. The difficulty to growing ADP crystals at natural pH 3.8 is probably related to the difficulties in disrupting the dimeric structures.

The UV-VIS spectra show that Cr^{+3} and Fe^{+3} interact strongly with phosphate anions in supersaturated solutions. The fate of Al^{+3} is undetermined.

5-8. Acknowledgment

The authors gratefully acknowledge the support of the National Science Foundation through grant number CPE-8409458. Appreciation is also expressed to the Upjohn Company for the graduate fellowship support of Michael K. Cerreta. This work was performed in the Shared Laser Laboratory of Michigan State University.

5-9. Literature Cited

1. M. K. Cerreta and K. A. Berglund. Accepted for publication in J. Crystal Growth.
2. A. A. Khan and W. H. Baur, Acta Crystallogr., B29, 1973, 2721.
3. J. W. Mullin, and A. Amatavivadhana, J. App. Chem., 17, 1967, 151.
4. J. W. Mullin, A. Amatavivadhana, and M. Chakraborty, J. App. Chem., 20, 1970, 153.
5. R. J. Davey and J. W. Mullin, Kris. Tech., 11(6), 1976, 625.
6. C. M. Preston and W. A. Adams, J. Phys. Chem., 83(7), 1979, 814.
7. D. L. Wertz and G. A. Cook, J. Sol. Chem., 14(1), 1985, 41.
8. M. Catti and G. Ferraris, Acta Crys., B30, 1974, 1.
9. A. Goypiron, J. de Villepin, and A. Novak, J. Chemie Phys., 75(9), 1978, 889.

CHAPTER 6

LASER RAMAN AND FOURIER TRANSFORM INFRARED SPECTROSCOPIC STUDIES OF THE CRYSTAL AND AQUEOUS SOLUTION STRUCTURES OF SOME AMINO ACIDS*

6-1. Abstract

Laser Raman and Fourier transform infrared (FTIR) spectroscopies have been used to study the crystal and aqueous solutions of alpha glysine, L-lysine, and L-glutamic acid. The spectra prove that the amino acids exist in the solid and in solution as zwitterions. Comparison of the spectra of dilute and supersaturated amino acids indicates that there is little change in structural association between the two concentration extremes. Contrasts in the solid-state spectra and that of supersaturated solutions show that the molecules in solution do not associate in the same manner as in the crystal.

6-2. Introduction

Needle shaped crystals of sodium chloride will not flow from a salt shaker. Well-formed crystals of beryllium oxide are inert, while the dust of poorly-formed beryllium oxide crystals is lethal. Improper crystal morphology can range from a nuisance to a deadly problem. Control of crystal shape by impurity addition is usually conducted by

---

* a paper presented by M. K. Cerreta and K. A. Berglund at the 79th Annual Meeting of AIChE, New York, New York, Nov. 15-20, 1987.

trial-and-error. However, several works have appeared [1, and references therein] describing systematic methods for growing crystals of desired morphology. "Tailormade" impurities have been designed to bind at a preselected crystal face and so inhibit growth in a predictable manner. Weissbuch and others [2] have extended the technique to the separation of D- and L-amino acids on the opposite faces of centrosymmetric glycine crystals. The purpose of this work is to investigate the structure of pure crystal and aqueous solutions of glycine, glutamate, and lysine by laser Raman and Fourier transform infrared (FTIR) vibrational spectroscopies as a precursor to studies of amino acid crystal nucleation and growth in the presence of impurities.

6-3. Experimental

Solid lysine (in the hydrochloride form, but referred to here simply as lysine), glycine, and glutamic acid from Sigma Chemical were used without further purification. Saturated aqueous solutions at 30°C were prepared by adding one of the three solids in excess to doubly distilled water that had been purified by passing through Barnstead D8904 and D8901 cartridges. Undersaturated solutions were prepared gravimetrically. Acidic and basic solutions of glycine were made by adding a few milliliters of 4M HCl or 4M NH_4OH to a saturated solution.

Raman excitation was provided by a Spectra Physics model 175 argon ion laser operating at 514.5 nm. The sample cell held solutions at 28.00°C ±0.05°C and is described in

Chapter 3. Spectra of solids were obtained from capillary tubes. The Raman scattered light was collected with standard 90^{o} collection optics (Spex model 1459) and dispersed in a Spex model 1877 spectrometer. Detection was accomplished with an EGG PARC OMA III system equipped with a model 1421 detector. The resolution is 0.8 cm^{-1}.

The FTIR spectra of solutions and solids were obtained with a Perkin-Elmer model 1750 FTIR at 4 cm^{-1} resolution. Solutions were held in a Spectra Tech ATR CIRCLE cell equipped with a ZnSe bar, while solids were suspended in Nujol between NaCl plates.

6-4. Raman and Infrared Spectroscopies

If a vibrating molecule possesses a permanent electric dipole moment, that dipole will oscillate with the normal modes of the molecule. The electric vector of a passing light wave can couple to the molecular dipole if the frequency of the light corresponds to the energy difference between two vibrational states of the same normal mode. The light is absorbed, and the process is termed infrared absorption. Vibrational transitions may also occur if an electric dipole moment can be induced in a molecule. This is possible whenever light of nearly arbitrary energy passes a molecule and polarizes the molecular electron cloud. The induced dipole then oscillates with the frequency of the normal modes of the molecule. Beats are produced between the frequencies of molecular vibration and the frequency of the light. The molecule can extract energy from the light in an amount just enough to allow a change of vibrational state, and then re-emits a photon of correspondingly lower energy. This is the Raman process.

The selection rules governing the two processes usually require that asymmetric or bending vibrational transitions occur by IR absorption and symmetric vibrational transitions are favored in the Raman, but this is by no means rigorous.

With the individual atoms locked into place in the solid state, the vibrations are well-defined and usually sharp. Because of strong intermolecular interaction, there are more vibrations possible in the solid state than in solution. On passing from solid to solution, several vibrations may fade, especially some skeletal, bending and twisting modes.

None of the amino acids possess symmetry elements in solution, so band assignments must come from characteristic group frequencies, isotopic substitution, Raman depolarization ratios, and intuition. Edsall [3] published an elegant series of Raman studies over a 30 year period and definitely assigned approximately half the vibrations of all the amino acids in aqueous solution. For glycine, the simplest amino acid, there are 24 possible normal modes, and some overtones and combinations as well. Suzuki and others [4] have assigned vibrations in the IR spectra of amino acids and performed a normal mode coordinate analysis for glycine.

6-5. Studies of Crystal and Aqueous Glycine

There are three crystalline modifications of glycine, known as the alpha, beta, and gamma forms. The phase obtained depends on the conditions of crystallization. The alpha form is by far the most common, grown by evaporation from water, and only that form will be considered here. Marsh [5] has performed extensive x-ray studies of the crystal. Figure 6-1 shows the structure of the molecule, and Figure 6-2 depicts the unit cell. The molecule exists as a zwitterion in the crystal. The $C\text{-}C\text{-}(O)_2$ group is planar with the amine group deviating from the plane. Strong hydrogen bonds between the amino and carboxylate groups join the molecules into a layer lying principally in the ac plane. Another layer connects to the first by hydrogen bonds between the amino and carboxylate groups in a centrosymmetric fashion. It is this fact that allows racemic molecular mixtures to be separated. Finally, the double-layers are joined into pairs by van der Waals forces. The natural habit of alpha glycine is shown in Figure 6-3.

The infrared spectra of solid, supersaturated, dilute, acidic, and basic glycine is given in Figure 6-4. The Raman spectra for the same conditions is given in Figures 6-5a, 6-5b, and 6-5c. In acidic solution, the strong, broad Raman band at about 1750 cm^{-1} is due to the C=O stretching motion. This band is completely missing in the base solution; the band at 1410 cm^{-1} is caused by the symmetric stretch of the ionized carboxylate group. The smaller band at 1445 cm^{-1} in

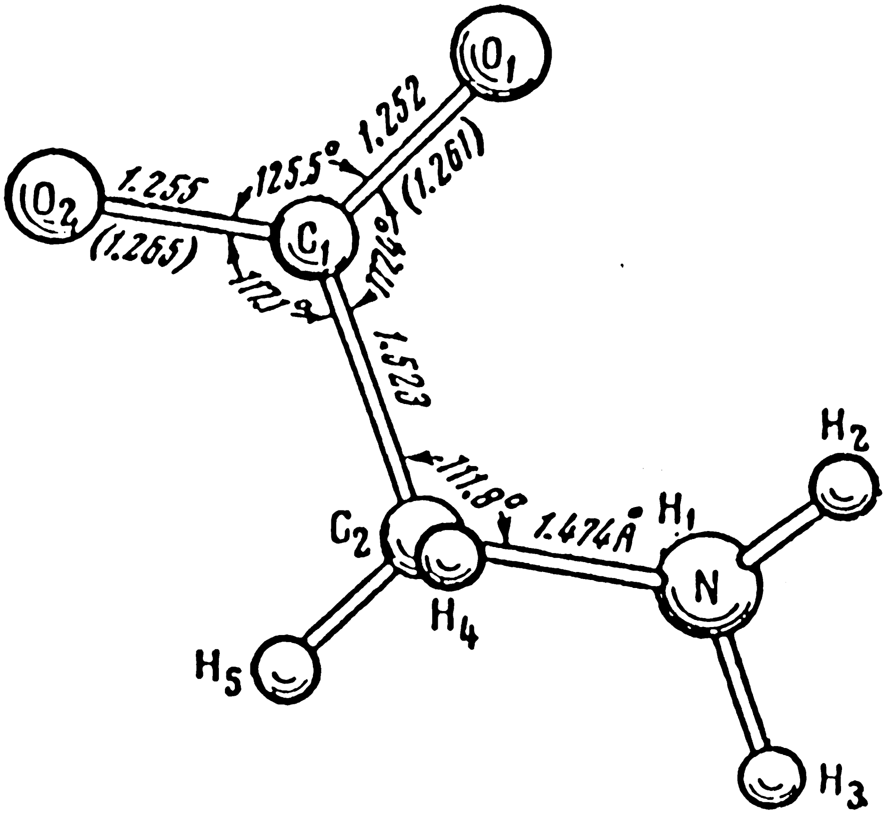

Figure 6-1. The glycine molecule.

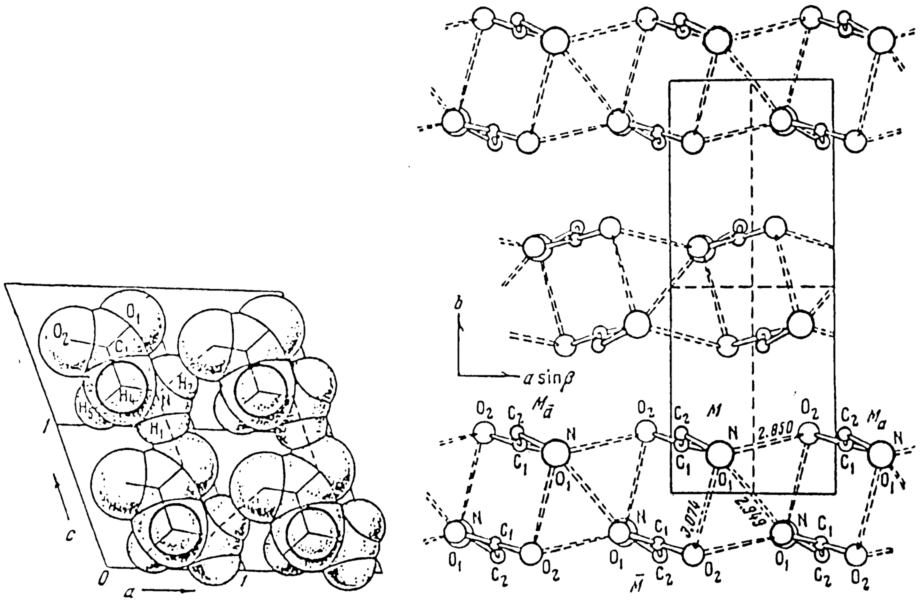

a

Figure 6-2. The unit cell of glycine.

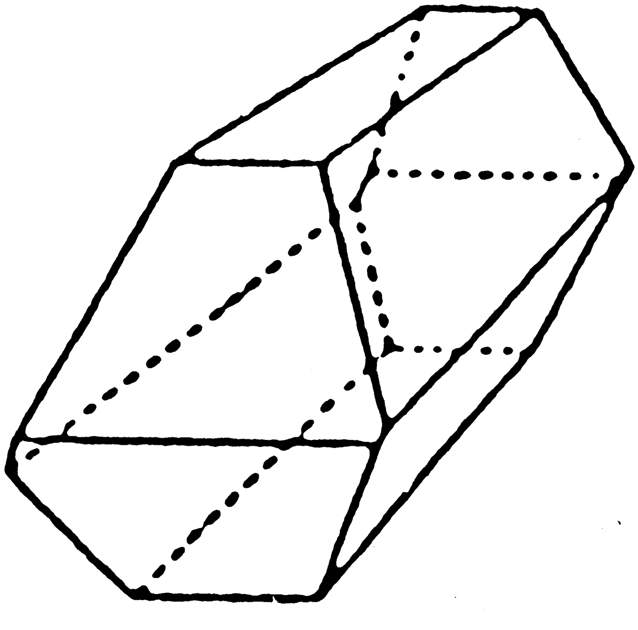

Figure 6-3. The characteristic habit of glycine.

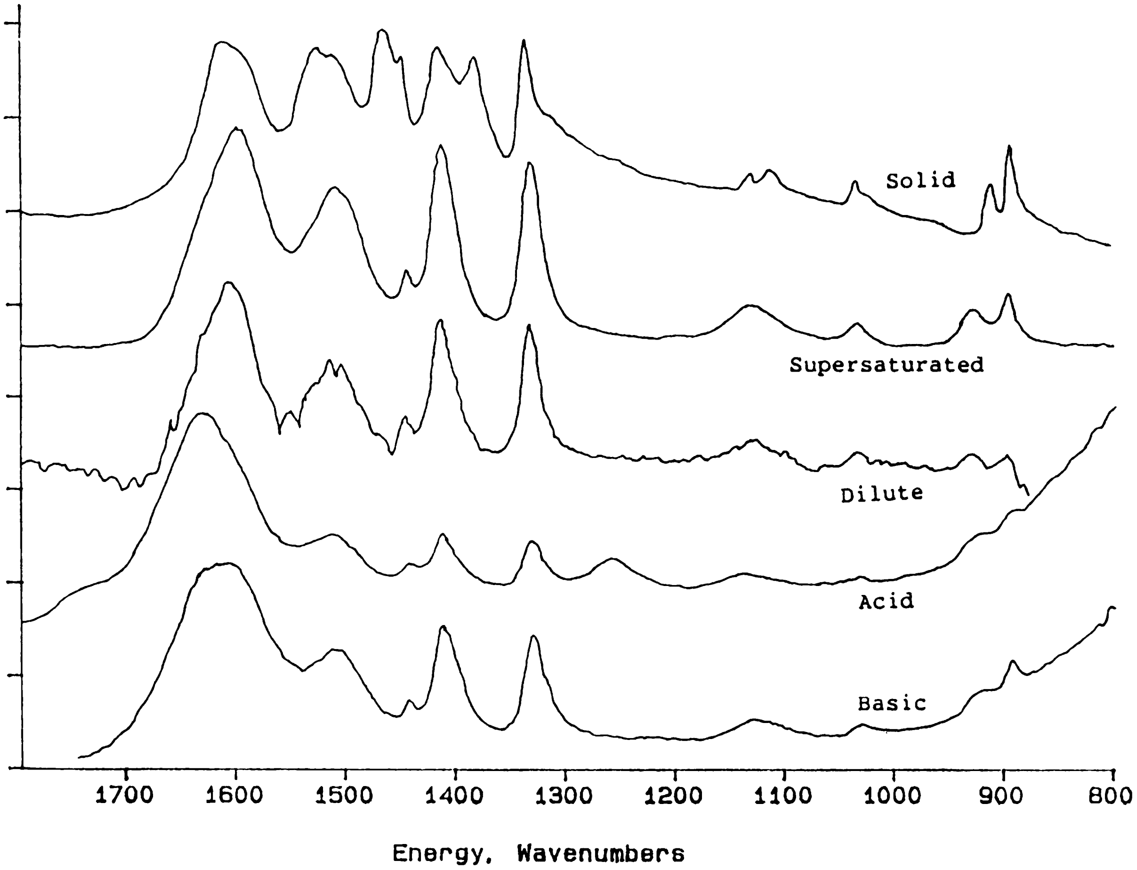

Figure 6-4. The IR spectra of glycine in various states.

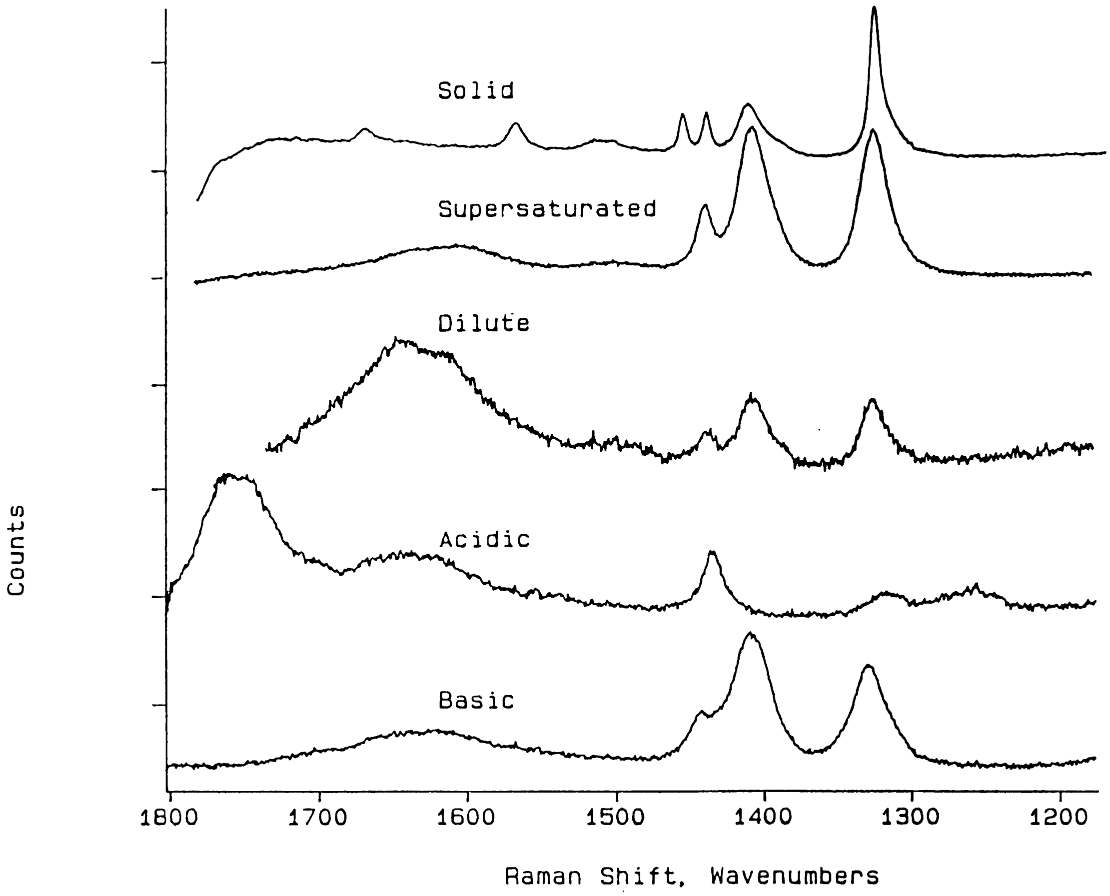

Figure 6-5a. The Raman spectra of glycine in various states, 1200-1800 cm^{-1}.

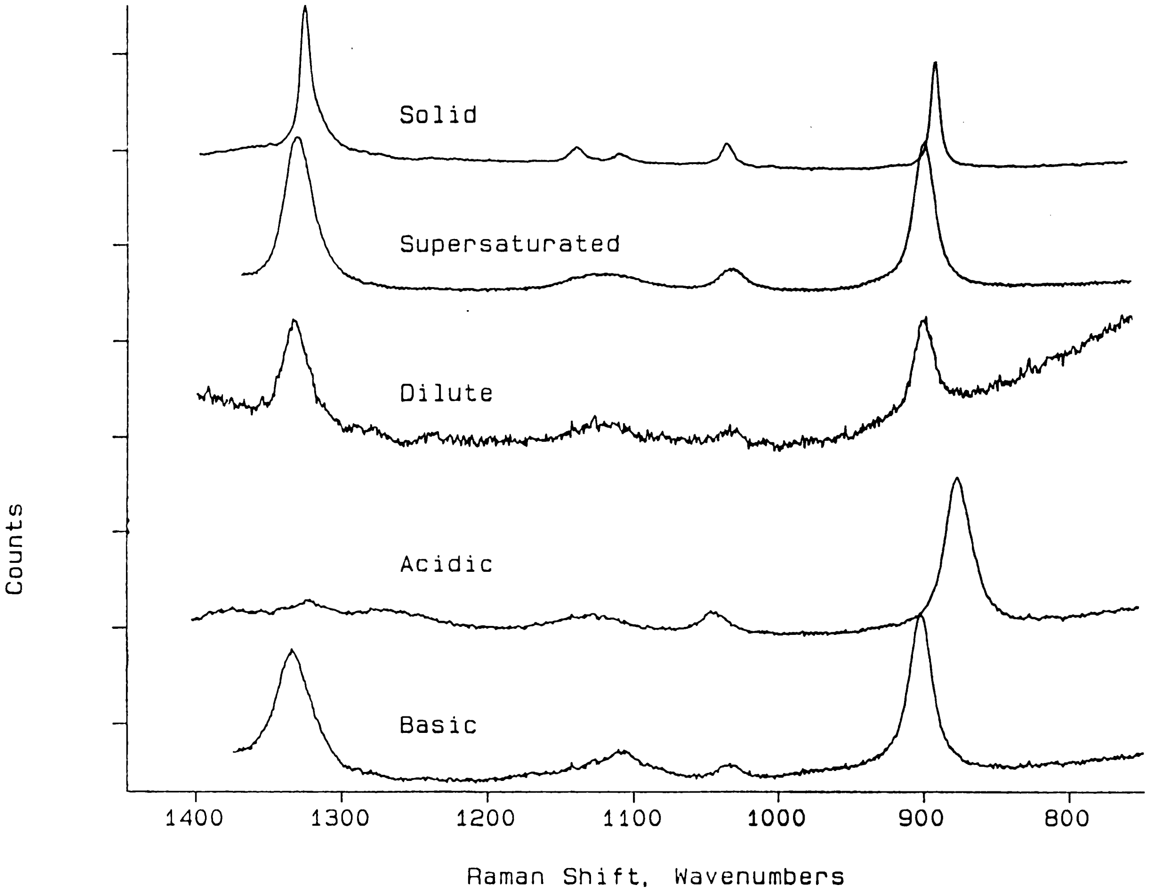

Figure 6-5b. The Raman spectra of glycine in various states, 800-1350 cm^{-1}.

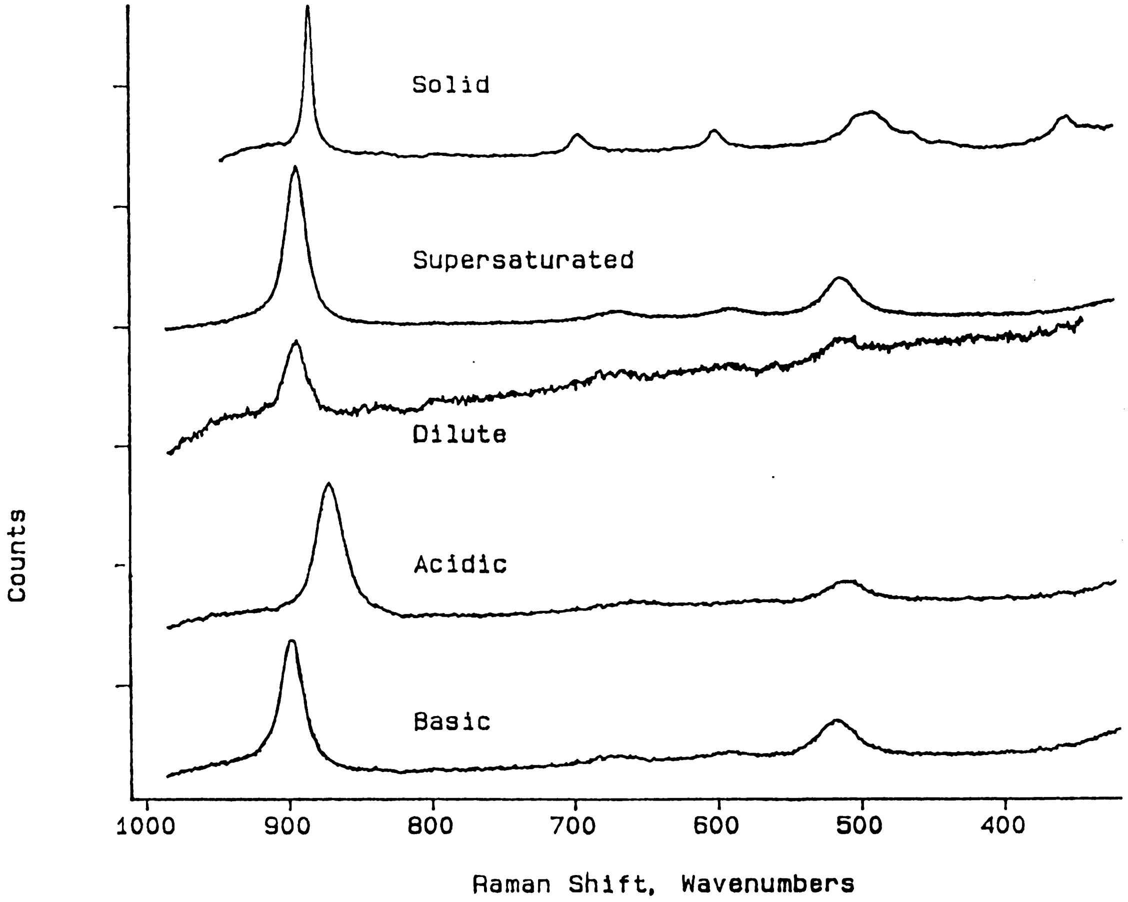

Figure 6-5c. The Raman spectra of glycine in various states, 350-950 cm^{-1}.

both the Raman and IR is the CH_2 bending mode. The strong Raman band at 1330 cm^{-1} has been assigned to a skeletal stretching mode. Comparison of its intensity in all the spectra, comparison of the 1410 cm^{-1} bands in the Raman, and the lack of a Raman band in the 1700 cm^{-1} region in all but the acidic solution prove without doubt that in ordinary solutions and solids, glycine exist as the zwitterion. This argument is also supported by the behavior of the band near 900 cm^{-1} in all the spectra. Similar results were found for lysine and glutamic acid.

In both the IR and the Raman, there is a one-to-one correspondence between the bands in supersaturated solution and dilute solution. It might be thought that there are differences in the Raman 1630 cm^{-1} region; however, the strong band at about 1650 cm^{-1} in the dilute solution spectrum is the water bending mode, made more prominent by the dilution effect. Therefore, within the sensitivities of the two techniques, there is no change in structural association patterns with concentration. Both the IR and Raman bands at 1410 cm^{-1} show some asymmetry to lower energy. This is indicative of hydrogen bonding between the carboxylate group and either water or other glycine molecules.

There is a fairly close correspondence between the solid and supersaturated solution spectra. However, the differences in intensity ratios and the appearance of a new Raman band in the solid spectrum in the 1400 cm^{-1}-1500 cm^{-1}

region indicate significant structural changes in transition from crystal to solution.

6-6. Studies of Crystal and Aqueous Lysine

Because of the basicity of the two amine groups present, L-lysine is most often crystallized by evaporation from aqueous solutions containing HCl. The structure of the molecule is shown in Figure 6-6. The unit cell contains two water molecules [6] as well as an HCl molecule and is shown in Figure 6-7. L-lysine in the crystal is present as a zwitterion in which both amino groups have the NH_3^+ form. The aliphatic chain and $N_{(2)}$ form a plane, as does the carboxylate group. There is extensive hydrogen bonding between all the electronegative elements present, involving all the hydrogens on the amino and water groups. The characteristic habit is nearly trigonal prismatic, and its projection in the ab plane is presented in Figure 6-8.

The IR and Raman spectra of lysine are shown in Figures 6-9, 6-10a, and 6-10b. Comparison of the dilute and supersaturated solution spectra in both the IR and the Raman indicate that, as with glycine, there is little structural change with changing concentration. The missing region in the dilute IR spectrum between 1600 cm^{-1} and 1700 cm^{-1} is due to the subtraction of the water O-H bending mode.

There are enormous differences between the solid-state spectra and the solution spectra. This must be ascribed to the freedom to rotate about C-C and C-N bonds for lysine in solution. Again, as with glycine, the molecule may

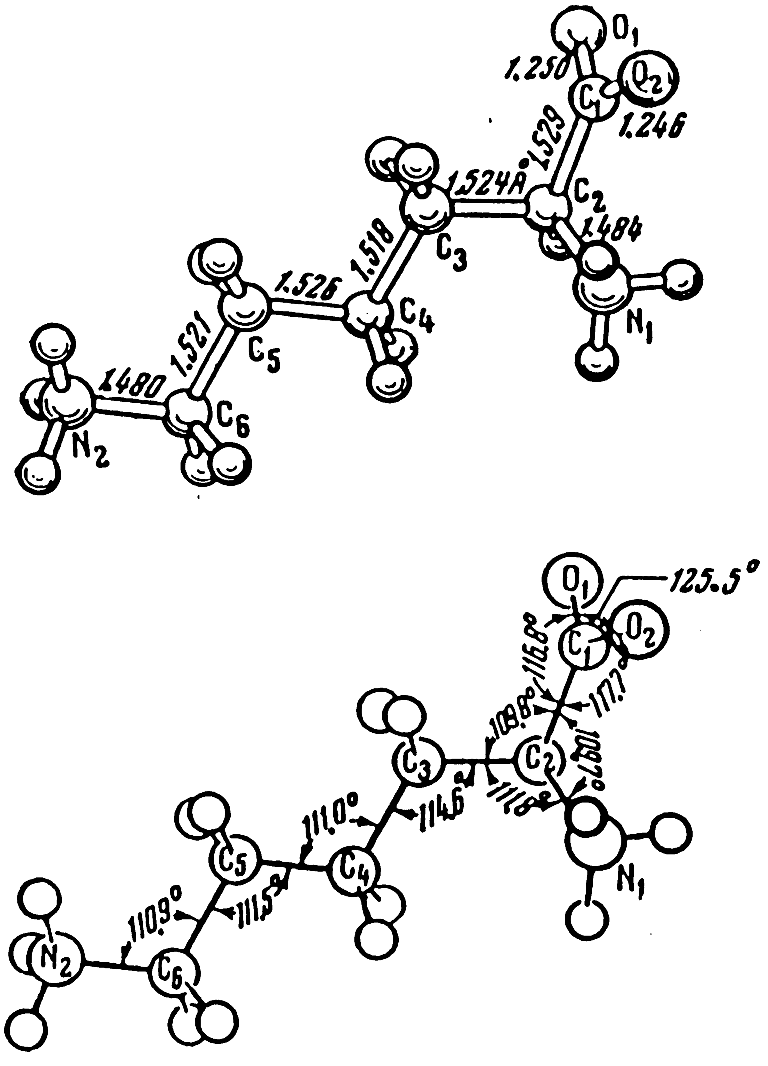

Figure 6-6. The lysine molecule.

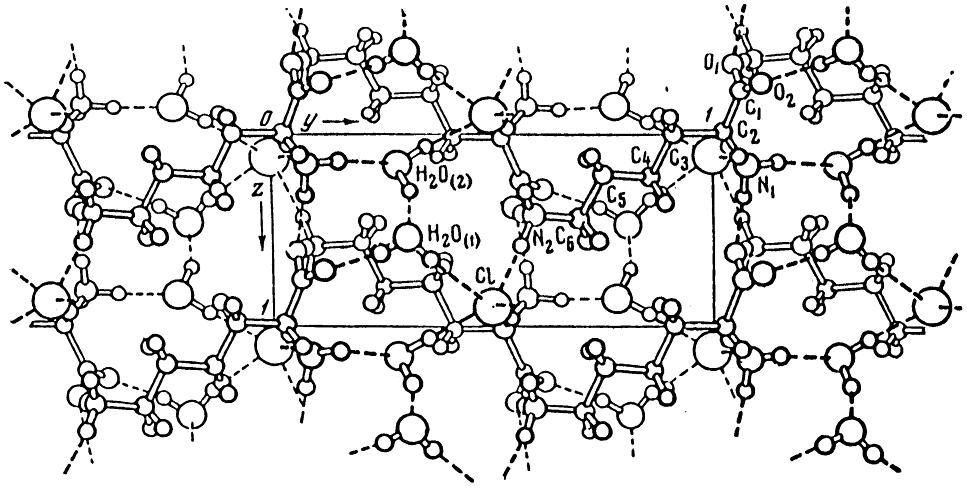

Figure 6-7. The unit cell of lysine:HCl:$2H_2O$.

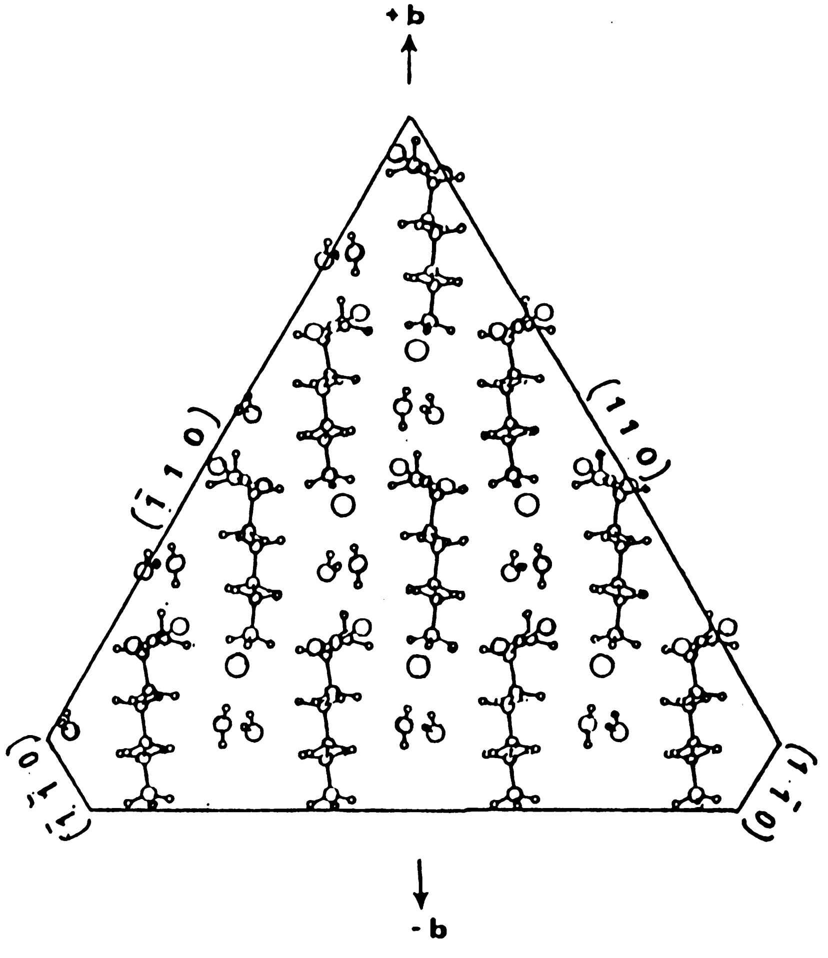

Figure 6-8. The natural habit of lysine:HCl:$2H_2O$.

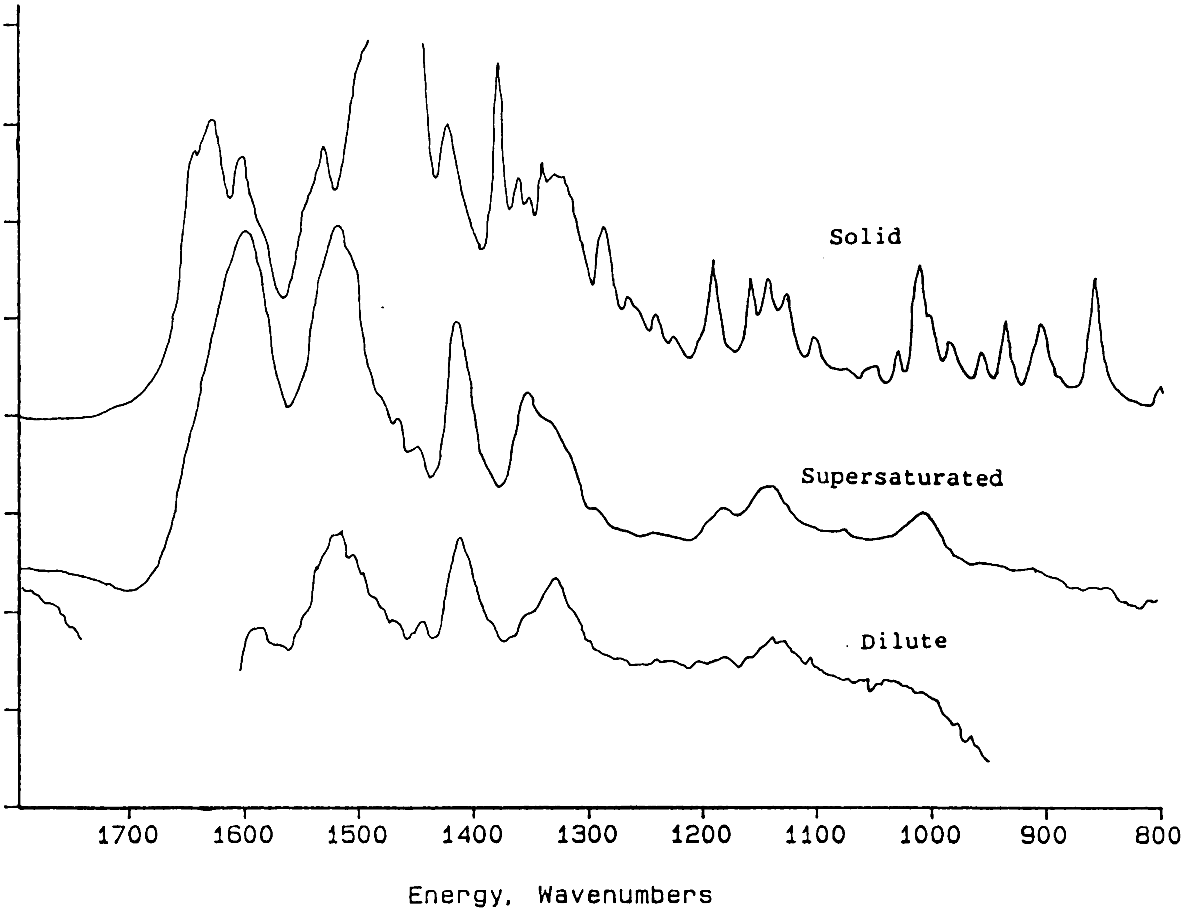

Figure 6-9. The IR spectra of lysine in various states.

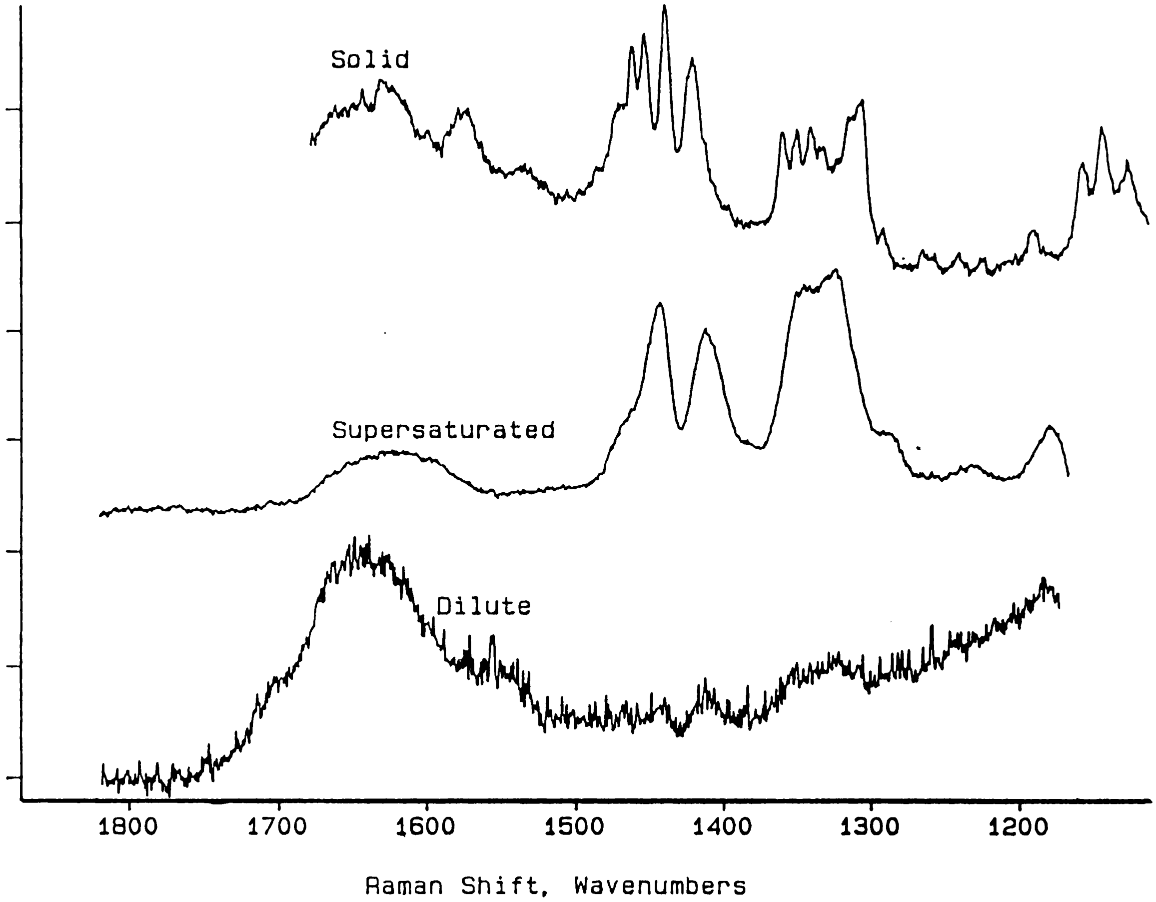

Figure 6-10a. The Raman spectra of lysine in various states, 1200-1700 cm^{-1}.

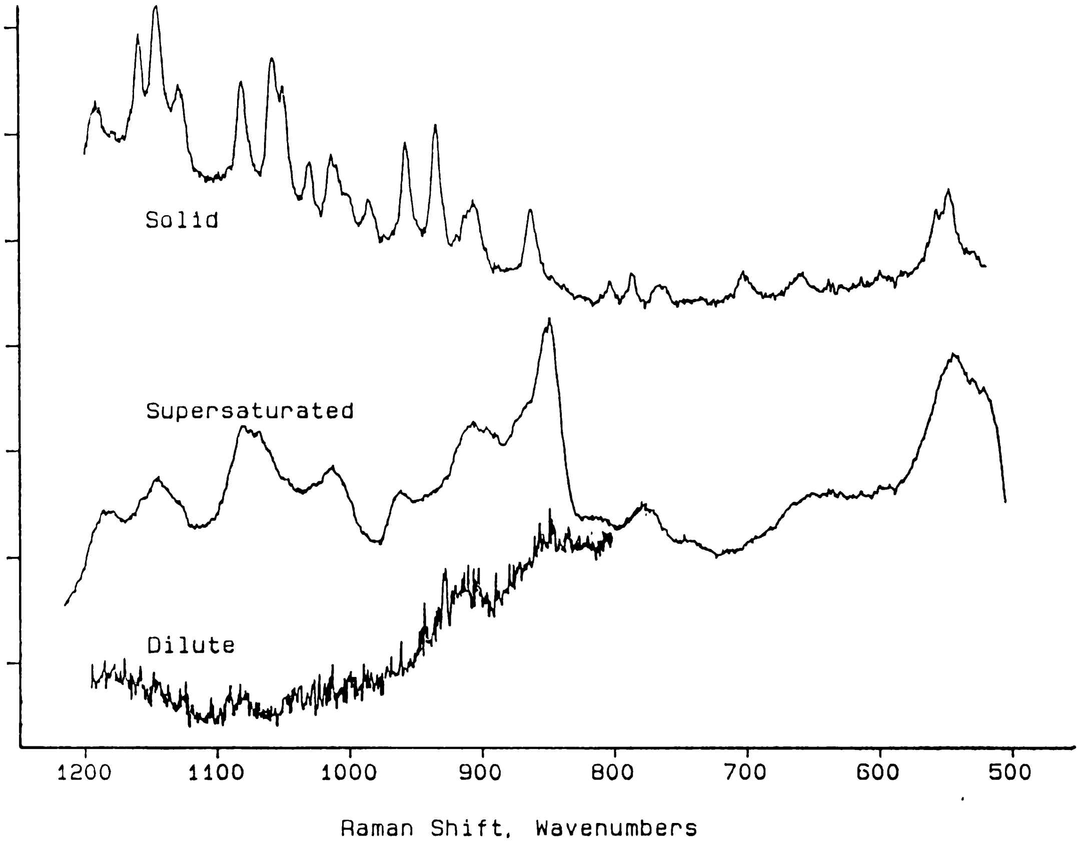

Figure 6-10b. The Raman spectra of lysine in various states, 550-1200 cm^{-1}.

associate in forms different than the crystal.

6-7. Studies of Crystal and Aqueous L-Glutamic Acid

L-glutamic acid is crystallized by evaporation from water. Actually, it is quite difficult to grow well-formed crystals, and the resulting solid is much more like a powder. The molecule is shown in Figure 6-11. The molecular structure in the unit cell is rather complicated and the interested reader is referred to [7]. The most salient features of the unit cell are as follows: it exists as a zwitterion with carbon 1 ionized; the C-N bond lies at an angle of 43^{o} to the plane of the carboxylate ion; very short (2.54 A) OH-O hydrogen bonds join the molecules into chains while NH-O bonds (~2.9 A) connect the chains into a framework; and there are also close N-O contacts (2.86 A) arising from amino-carboxylate interaction between different molecules.

The IR and Raman spectra of glutamic acid are shown in Figures 6-12, 6-13a, and 6-13b. The IR plots are very busy, and it is difficult to draw many conclusions from them. It should be mentioned that it is difficult to obtain good quality aqueous spectra of glutamic acid in either the IR or Raman since the solubility of this amino acid is relatively low. The Raman profiles are easier to interpret. As with the other two amino acids, there appears to be little structural change with solution concentration. Glutamic acid seems to be more akin to lysine than to glysine when

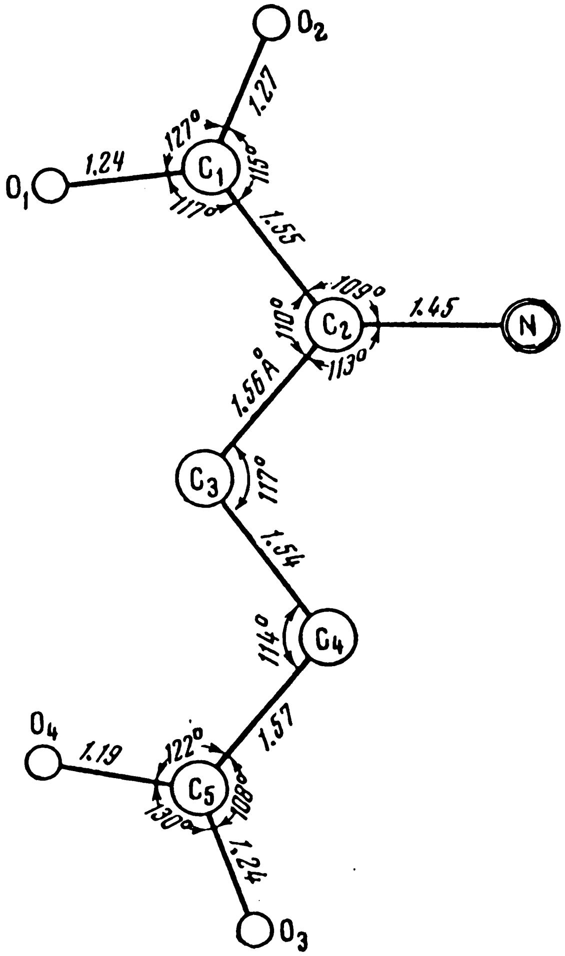

Figure 6-11. The glutamic acid molecule.

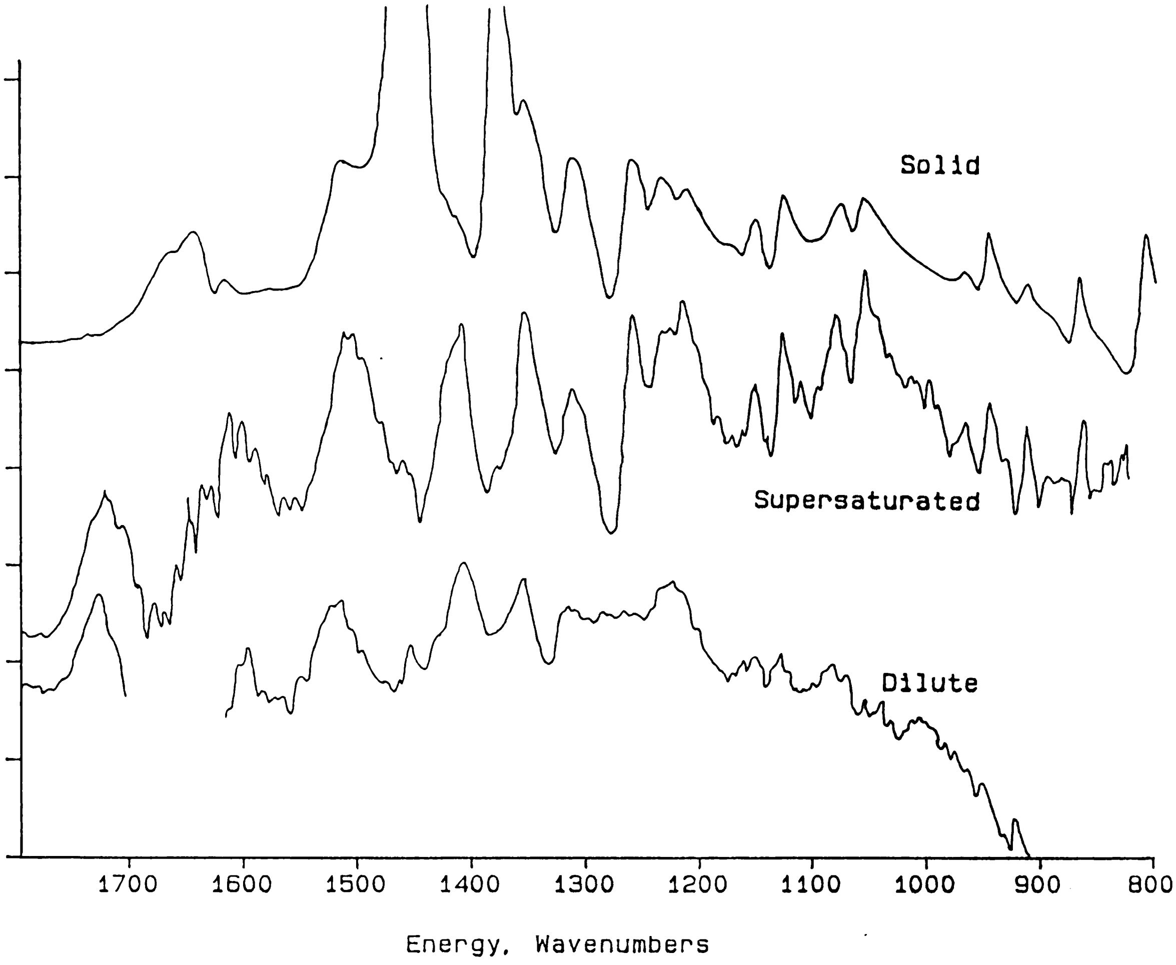

Figure 6-12. The IR spectra of glutamic acid in various states.

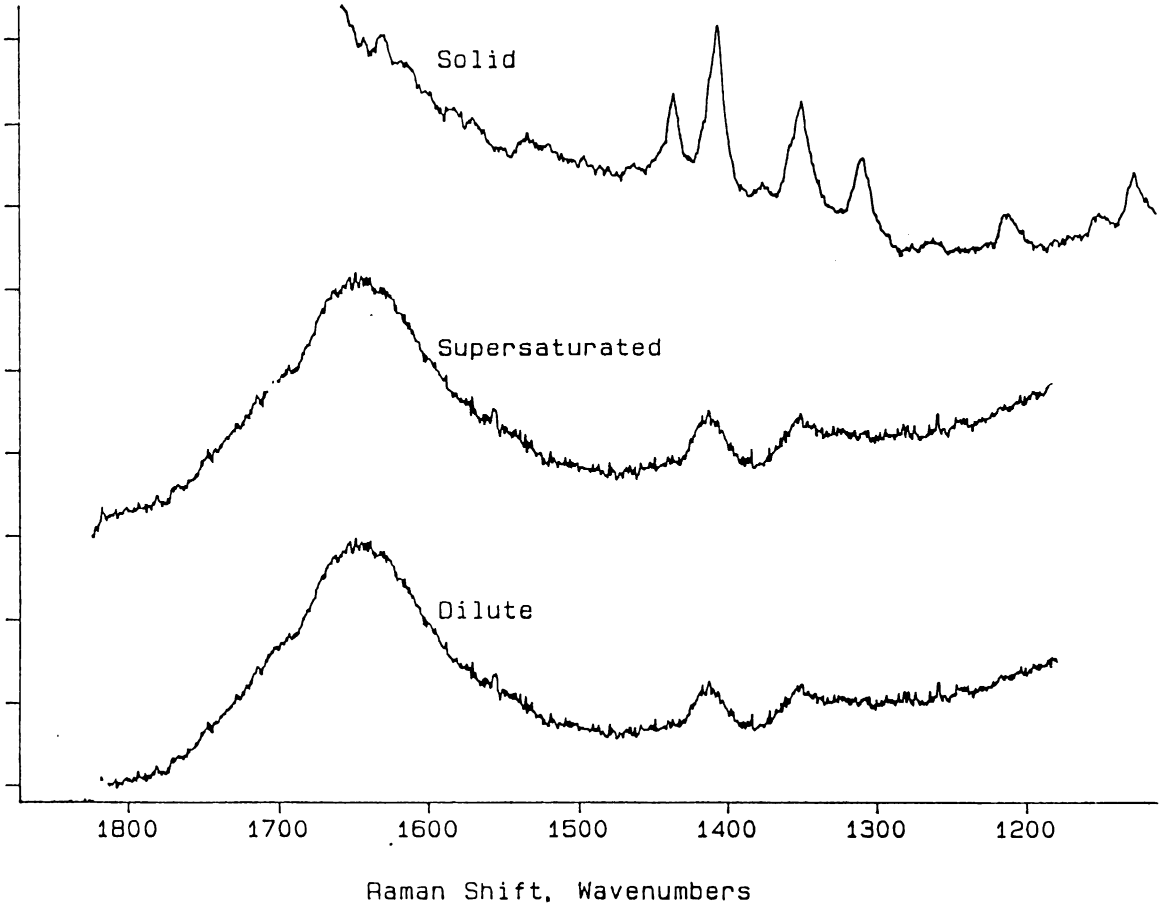

Figure 6-13a. The Raman spectra of glutamic acid in various states, 1200-1700 cm^{-1}.

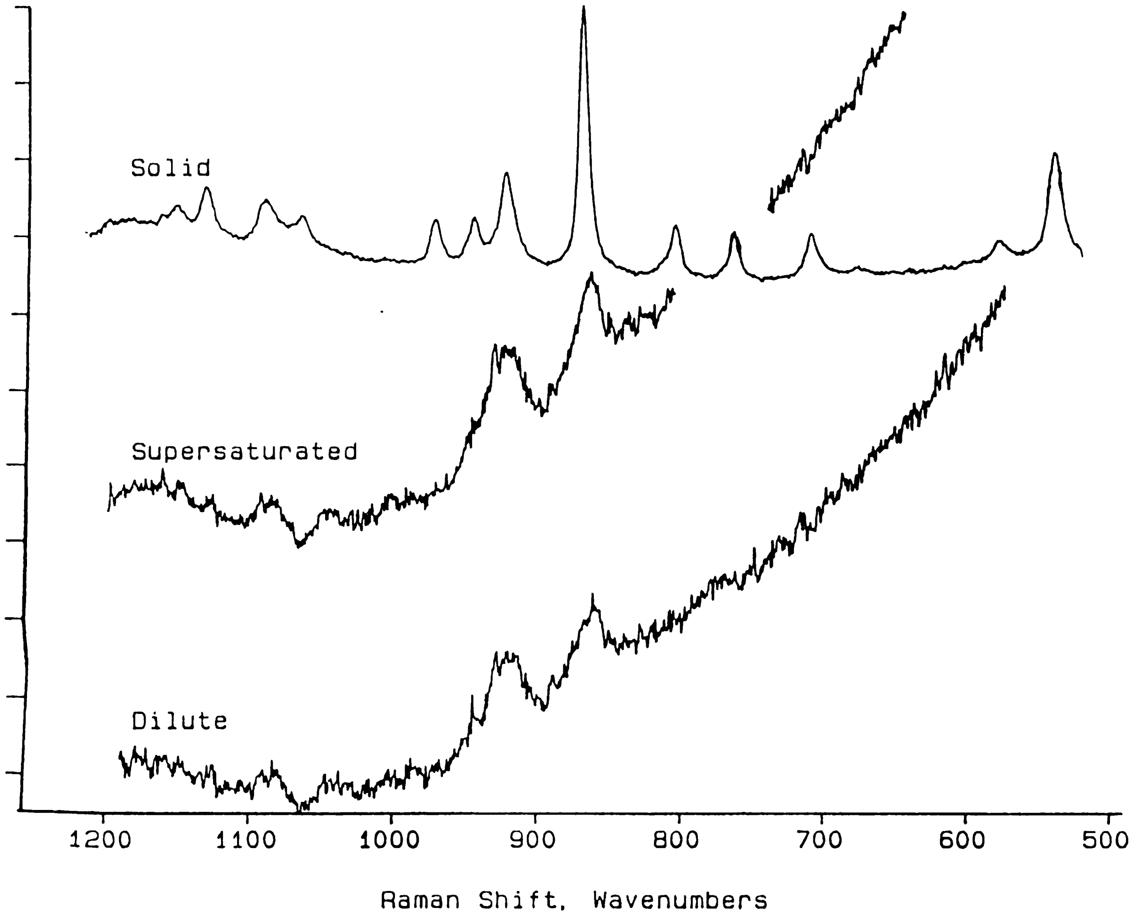

Figure 6-13b. The Raman spectra of glutamic acid in various states, 550-1200 cm^{-1}.

its solid-state and solution profiles are compared; that is, there is once again major differences between the spectra, especially below 1200 cm^{-1}.

6-8. Conclusions

The Raman and IR spectral profiles show, by comparison and contrast, that the three amino acids under investigation exist in the crystal and in solution as the zwitterion; that there is essentially no major structural change between the species in dilute and concentrated solution; and that the molecules in solution do not associate in a like-manner as in the crystal.

6-9. Acknowledgment

The authors gratefully acknowledge the support of the National Science Foundation through grant number CPE-8409458. Appreciation is also expressed to the Upjohn Company for the graduate fellowship support of Michael K. Cerreta. This work was performed in the Shared Laser Laboratory of Michigan State University.

6-10. Literature Cited

1. I. Weissbuch, L. J. W. Shimon, E. M. Landau, R. Popovitz-Biro, Z. Berkovitch-Yellin, L. Addadi, M. Lahav, and L. Leiserowitz, Pure and Appl. Chem., 58, 1986, 947.

2. I. Weissbuch, L. Addadi, Z. Berkovitch-Yellin, E. Gati, M. Lahav, and L. Leiserowitz, Nature, 310, 1984, 161.

3. J. T. Edsall, S. A. S. Ghazanfar, and D. V. Myers, J. Am. Chem. Soc., 86, 1964, 3439.

4. S. Suzuki, T. Shimanouchi, and M. Tsuboi, Spectrochim. Acta, 19, 1963, 1195.

5. R. E. Marsh, Acta Crystallogr., 11, 1957, 654.

6. R. E. Marsh and D.A. Wright, Acta Crystallogr., 15, 1962, 54.

7. S. Hirokawa, Acta Crystallogr., 8, 1955, 637.

CHAPTER 7

CONTACT NUCLEI FORMATION IN AQUEOUS DEXTROSE SOLUTIONS*

7-1. Abstract

A laser Raman microprobe was used to determine the growth of alpha dextrose monohydrate crystals on crystals of alpha anhydrous dextrose in supersaturated aqueous solutions. Below 28.1°C, the Raman spectra indicated growth occurs readily, but in solutions saturated above 40.5°C, no growth could be found. Contacts of parent anhydrous crystals yielded only monohydrate nuclei below 28.1°C, while contacts in solutions saturated at 40.5°C and 45.0°C gave both crystalline forms, and contacts in solutions saturated at 49.5°C gave only anhydrous nuclei. The inability of the monohydrate to grow on anhydrous crystals in the same solution that forms the two crystalline phases with a single contact precludes an attrition mechanism of nuclei formation. For the same reason, the hypothetical mechanism involving parent crystal stabilization of pre-crystalline clusters, allowing the clusters to grow into nuclei, is also contradicted. A third, unknown mechanism is believed to apply.

---

* a manuscript submitted by M. K. Cerreta and K. A. Berglund for publication in J. Crystal Growth.

7-2. Introduction

Operation of industrial crystallizers is characterized by high suspension densities and supersaturations (1^oC to 3^oC) well below those required for primary nucleation (which occurs from zero suspension density solutions at $>10^oC$ undercooling). Nucleation in these circumstances is referred to as "secondary" to reflect the fact that the presence of crystals in solution is required prior to any nucleation. Strictly speaking, only materials of moderate to high solubility follow secondary nucleation mechanisms. Botsaris [1] suggested that secondary nucleation may be conveniently regarded as two separate processes. The first is production of nuclei that involves the parent crystal in some way, and the second is the removal of the nuclei from the parent crystal to the bulk solution. There is no doubt as to the mechanism responsible in greatest measure for the removal of the nuclei; it is a contact between the parent crystal and another crystal or the crystallizer [2-4]. However, there is much disagreement over the source of the nuclei. One view holds that the nuclei were once an integral part of the parent crystal, while another holds that the nuclei originate from solution as pre-crystalline clusters stabilized by the surface of the parent crystal.

It has been found [5] that dextrose (D-glucose), a common and important sugar that is highly water soluble, nucleates in both its anhydrous and monohydrate forms from a single contact of an anhydrous parent crystal between about

38°C and 50°C. This result precludes any kind of attrition mechanism unless the monohydrate form can grow on anhydrous attrition nuclei. It is the purpose of this work to determine if the dextrose monohydrate can grow on anhydrous dextrose crystals under various conditions of tempera-ture and undercooling using a laser Raman microprobe. The microprobe technique has been demonstrated [6] capable of distinguishing between crystalline phases present in supersatu-rated solution as they are produced (i.e., *in situ*).

7-3. Production of Secondary Nuclei

A thorough treatment of the knowledge concerning the production and removal of secondary nuclei can be found in many reviews [1,7-10]. Based on studies of aqueous sucrose crystallization by fluid shear, Powers [11] in 1956 was the first to suggest that aggregates of molecules in solution which have not yet attained regular crystal lattice formation might be stabilized by the parent crystal surface and act as crystal nuclei. The homogeneous nucleation theory of Gibbs [12] pre-supposes the existence of such embryos. Mason and Strickland-Constable [13] in 1963 gently contacted crystals of $MgSO_4 7H_2O$ in aqueous solution to produce nuclei. They called this "attrition" breeding.

Two major criticisms of the attrition mechanism are 1) very gentle contacts, of $MgSO_4 7H_2O$ for example, do not produce visible damage to the crystal [14], and 2) smaller (<10μm) attrition nuclei do not grow or grow very slowly.

The first criticism has been contradicted by direct photographic evidence showing breakage of $KAl(SO_4)_2 12H_2O$ and $MgSO_4 7H_2O$ parent crystals [15]. Besides the fact that the second criticism should apply to either mechanism, it is not necessary that all the small crystals grow to populate the crystallizer. Recent work with the sucrose-water system [16] has revealed that the entire crystal size distribution (CSD) can be represented by a bimodal gamma distribution with 90% of the crystals in the small size range.

The major argument against the cluster concept is that they have never been detected experimentally. In experiments involving quiescent columns of supersaturated solutions, first conducted by Mullin and Leci [17] with citric acid and later with other substances by Larson and Garside [18], solution density differences between top and bottom were ascribed to molecular clusters that somehow descended the column. Whether or not this curious phenomena is explained by clustering, there is no basis for giving the clusters the structure of the crystal. Raman spectroscopic studies of solutions of dihydrogen phosphates [19], fructose [20], and amino acids [21] have shown the molecules in solution do not associate as in their crystals.

The attrition mechanism does have some degree of experimental verification. Seeds of optically active sodium chlorate in stirred solutions produced nuclei with the same optical activity virtually 100% of the time [22], although it might be that a seed stabilizes only clusters of the same handedness. The same experiment performed in stagnant solutions gave both L- and D- crystals at low (1°C to 3°C) supersaturation. Contacts with $KAl(SO_4)_2 12D_2O$ parent crystals in H_2O gave nuclei with large concentrations of deuterium that could only be attrition fragments [23]. Unfortunately, the nuclei were not or could not be examined individually to determine if growing nuclei contained deuterium. A study of potassium dihydrogen phosphate contact nucleation reported that all attrition fragments grew [24].

The definitive experiment to differentiate between the two proposed mechanisms has not yet been devised.

7-4. Secondary Nucleation and Raman Studies of Dextrose

Young [25] determined the phase diagram for the dextrose-water system between -30°C and 62°C. Below 50°C the alpha monohydrate form crystallizes, and above 50°C the alpha anhydrous form crystallizes. Beta anhydrous dextrose may also crystallize at the higher temperatures. Here, alpha and beta refer to the anomers of dextrose, both of which exist in solution, which is why ordinary commercial anhydrous dextrose contains about 5% beta anhydrous crystals. Dean [26] found an unstable phase that formed between 38°C and 50°C and transformed into the alpha monohydrate between 32°C and 38°C.

Alpha anhydrous dextose crystals are prismatic and easy to handle. The monohydrate forms slender needle crystals that are very fragile and difficult to manipulate. Figure 7-1 shows both crystalline phases. Elankovan and Berglund [5] conducted secondary nucleation experiments with alpha anhydrous parent crystals. At a solution temperature of 41°C and 4°C undercooling, contacts gave anhydrous and monohydrate nuclei together in the same solution.

The vibrational spectra of sugars studied by infrared, Raman, and normal coordinate analysis techniques have been reviewed in great detail [27]. The vibrations of dextrose in aqueous solutions have been assigned using Raman [28] and infrared [29] experimental methods. Vibrations of crystalline alpha anhydrous dextrose have been assigned in the Raman and infrared, and a normal coordinate analysis has been performed [30]. The vibrations of dextrose monohydrate have not been investigated.

Delhaye and Dhamelincourt [31] have given a complete description of the Raman microprobe and the technique of Raman microspectroscopy. The microprobe is simply an optical microscope capable of employing either ordinary white light for visual work or laser light for Raman experiments. When the microprobe is attached to an optical spectrometer, the system can produce Raman vibrational spectra of objects on the order of 2 μm in size. Every substance has a characteristic Raman spectrum that depends on, among other things, molecular environment. A special feature of Raman spectroscopy is that studies may be performed in water, which is a serious limitation in

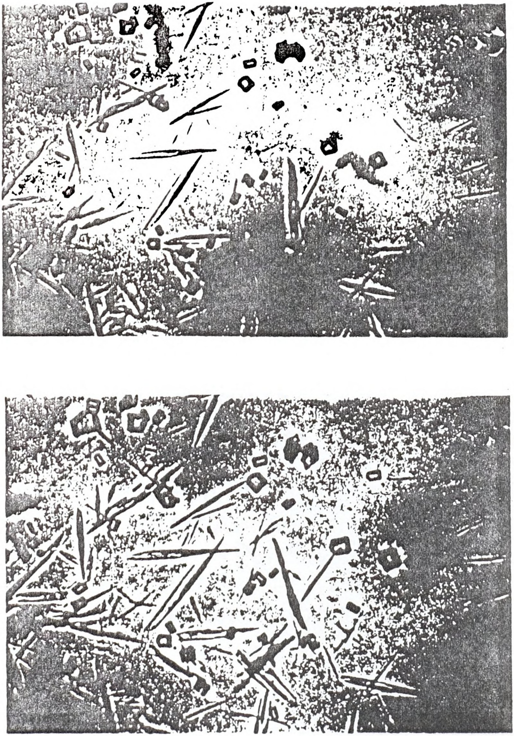

Figure 7-1. Crystals of dextrose monohydrate (needles) and anhydrous dextrose (prisms).

infrared spectroscopy.

7-5. Experimental Methods and Materials

Saturated solutions were made using ACS reagent grade dextrose purchased from Sigma. The water used was doubly distilled and passed through two Barnstead D8901 deionization columns. A sealed 250 ml Pyrex erlenmeyer flask was immersed in a Fischer Model 80 Water Bath with vigorous agitation provided by a plastic impeller. Solutions were considered saturated when excess crystals were present for at least 48 hours at the saturation temperature. The temperature was monitored to ± 0.01^{o}C with an Omega Precision Thermistor ON 700 and an Omega Digicator 410B. Solutions were passed through a .45 µm filter after removal from the saturating bath and again just prior to use. Parent crystals of well-formed alpha anhydrous dextrose were kindly provided by Dr. Ponnampalam Elankovan who has described their preparation [5]. They were typically 1 mm to 2 mm in size. It was not possible to employ monohydrate dextrose as parent crystals due to their fragile nature. The parent crystal was glued with the least amount of epoxy possible to a stainless-steel rod. The contacting chamber was thermostated and consisted of all glass or plastic materials except for an epoxy-coated thermistor. A schematic of the contacting cell is shown in Figure 7-2 and is described in greater detail elsewhere [6].

Laser excitation was provided by either a Coherent Innova 100 or Spectra Physics 165 argon ion laser operated

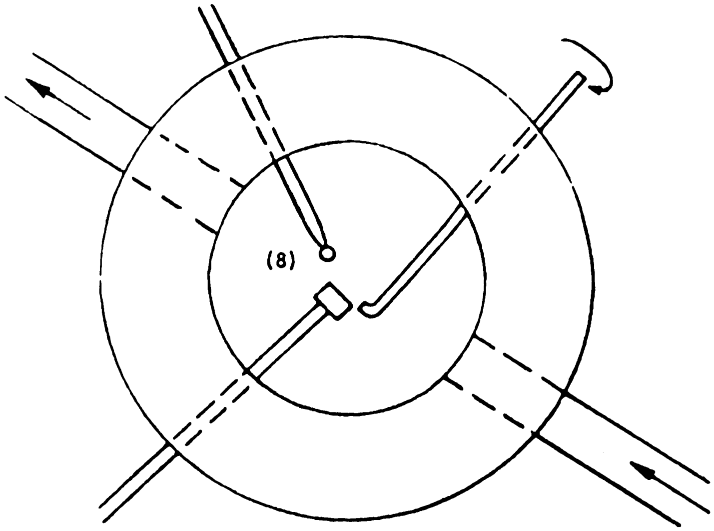

(A) TOP VIEW

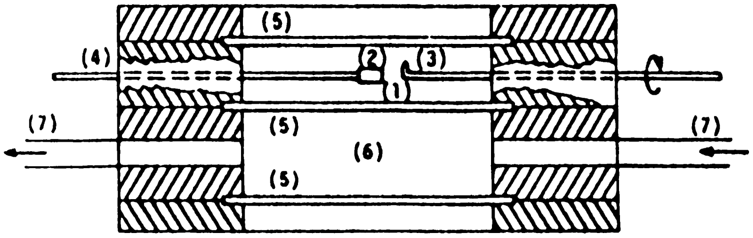

(B) SIDE VIEW

Figure 7-2. The contacting cell.

(1) Solution, (2) glass cover slip (upon which parent was contacted), (3) contacting rod (to which parent was glued), (4) support rod, (5) cover glass, (6) constant-temperature water, (7) water inlet and outlet, (8) thermistor.

at 514.5 nm and 1 W. A prism and iris combination was used to separate plasma lines. The microprobe was a Spex 1482D fitted with a Zeiss research-grade microscope. In this configuration, the Raman scattering is inherently 180° back-scattering. Because of the long working distance required, an Ealing X15/.23 cassegrain reflecting objective lens was used. The laser power at the sample was 500 mW. No severe heating effects were encountered, since varying the laser power did not change the spectra, and impinging the beam on the thermistor did not raise the solution temperature by more than .08°C. A Spex 1877D triple spectrometer with 1800 grooves/mm gratings blazed at 500 nm dispersed the Raman scattered light. An EG&G PARC 1421 multi-channel detector and 1460 OMA system collected and computerized the Raman spectra. Spectra were calibrated using the established Raman lines of toluene, and all peak positions reported are accurate to within 1 cm^{-1}. All spectra presented were recorded between 600 cm^{-1} and 1400 cm^{-1} (encompassing the so-called "finger-print" region) and have not been smoothed or otherwise modified.

With the multi-channel detector, 20 signal-averaged scans could be accomplished at any point on a crystal in less than five minutes. The spectrum of the parent crystal was recorded before and just after solution was added to the contact chamber. The solution was heated slightly above saturation to dissolve any surface irregularities, then cooled to the desired undercooling. Spectra were then collected at various times at random points all over the crystal, and often at the same point. Because of the relatively slow growth rate of dextrose, it was possible to interrogate every region of the parent crystal.

A search for growth of the monohydrate on the anhydrous parent crystal was made in solutions saturated at 20.8, 28.1, 40.5, 45.0, and 49.5°C, and undercoolings of 2, 4, and 6°C. After several hours, the parents were contacted. In addition, a small boiling chip was used as a "parent crystal placebo" in the solutions saturated at 20.8 and 45.0°C.

7-6. Results and Discussion

For reference, spectra of a saturated solution and powders of the monohydrate and anhydrous solids are given in Figure 7-3. During the course of an experiment, it was important to be able to quickly determine whether the laser beam was focused on the crystal surface or in the solution. The position of the C-C ring stretching vibration (1074 cm^{-1} for anhydrous and monohydrate crystals, 1064 cm^{-1} in solution) and the sharpness of all the bands made this relatively easy (in general, for any substance, solid-state bands are much narrower than corresponding solution bands). The 1345 cm^{-1} CO-H bending vibration also assisted in this regard for the anhydrous crystal.

Figure 7-3 shows the region between 800 cm^{-1} and 950 cm^{-1} clearly distinguishes the monohydrate from the anhydrous crystal. The 857 cm^{-1} band (C_1-O stretch + C_1-C

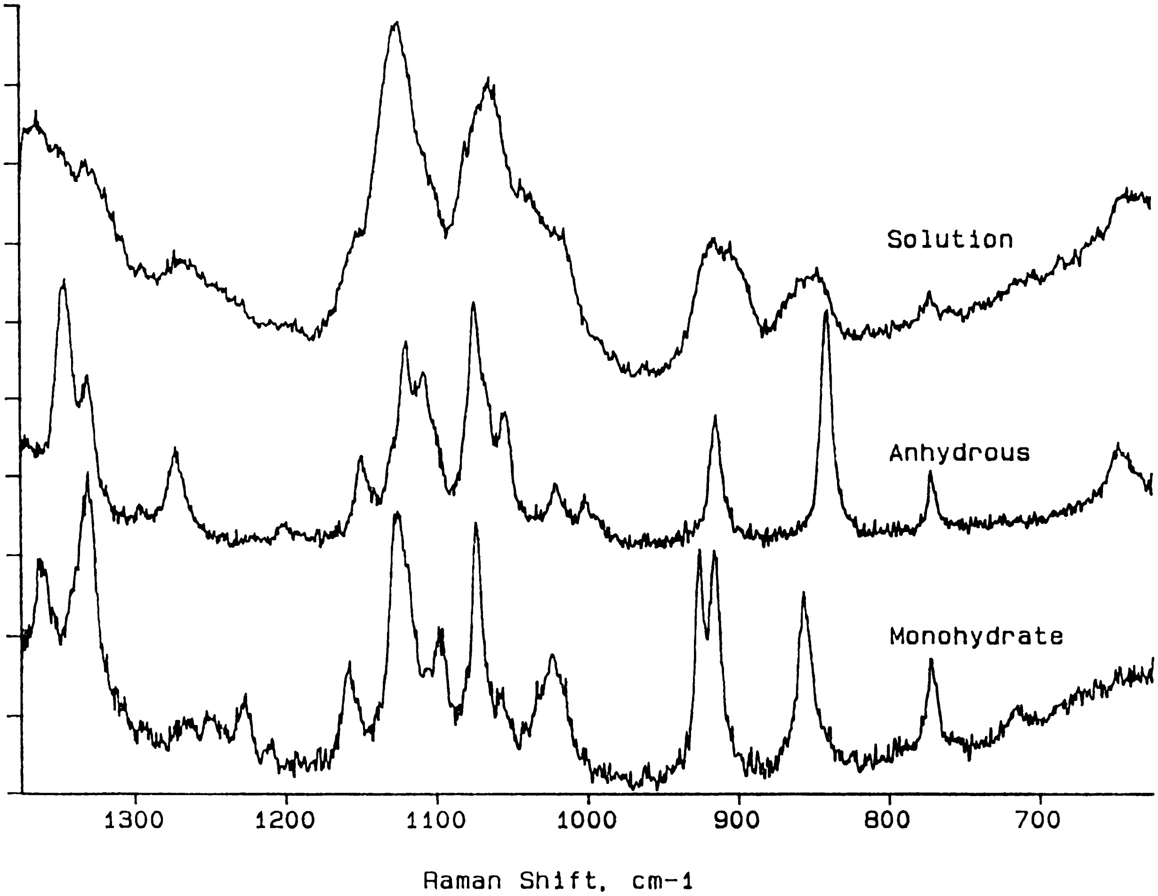

Figure 7-3. The Raman spectra of crystalline and aqueous dextrose.

bend, where C_1 is the anomeric carbon) in the monohydrate spectrum is well-removed from essentially the same vibration at 841 cm^{-1} in the anhydrous crystal. The monohydrate band at 925 cm^{-1} (not assigned) is also characteristic. The peak intensity of the 841 cm^{-1} vibration relative to the 914 cm^{-1} (pure C_1-O stretch) band in the anhydrous spectrum is opposite that of the 857 cm^{-1} to 915 cm^{-1} (pure C_1-O stretch) relative band intensity in the monohydrate spectrum. These differences allow the monohydrate phase to be identified on an anhydrous crystal.

It was expected that the solution saturated at 20.8°C would allow the monohydrate phase to grow on the anhydrous phase if the solution supersaturation were driven high enough. Besides an estimate of the supersaturation needed for heterogeneous growth, experiments with this solution provided a test of the sensitivity of the Raman microprobe. However, it was found that with only 2°C undercooling, the monohydrate crystal could be detected on the surface of the anhydrous crystal within 30 minutes after the supersaturation had been achieved. In 1 to 2 hours the needle crystals could be seen with the microscope, and usually after 3 hours a moss-like growth about the parent crystal was visible to the unaided eye.

The time development of the spectra for the crystal in solution at 18.8°C and 2°C undercooling are presented in Figures 7-4a to 7-4i. Comparison of Figure 7-4a (the solution) with Figure 7-4b (the parent crystal in air) and

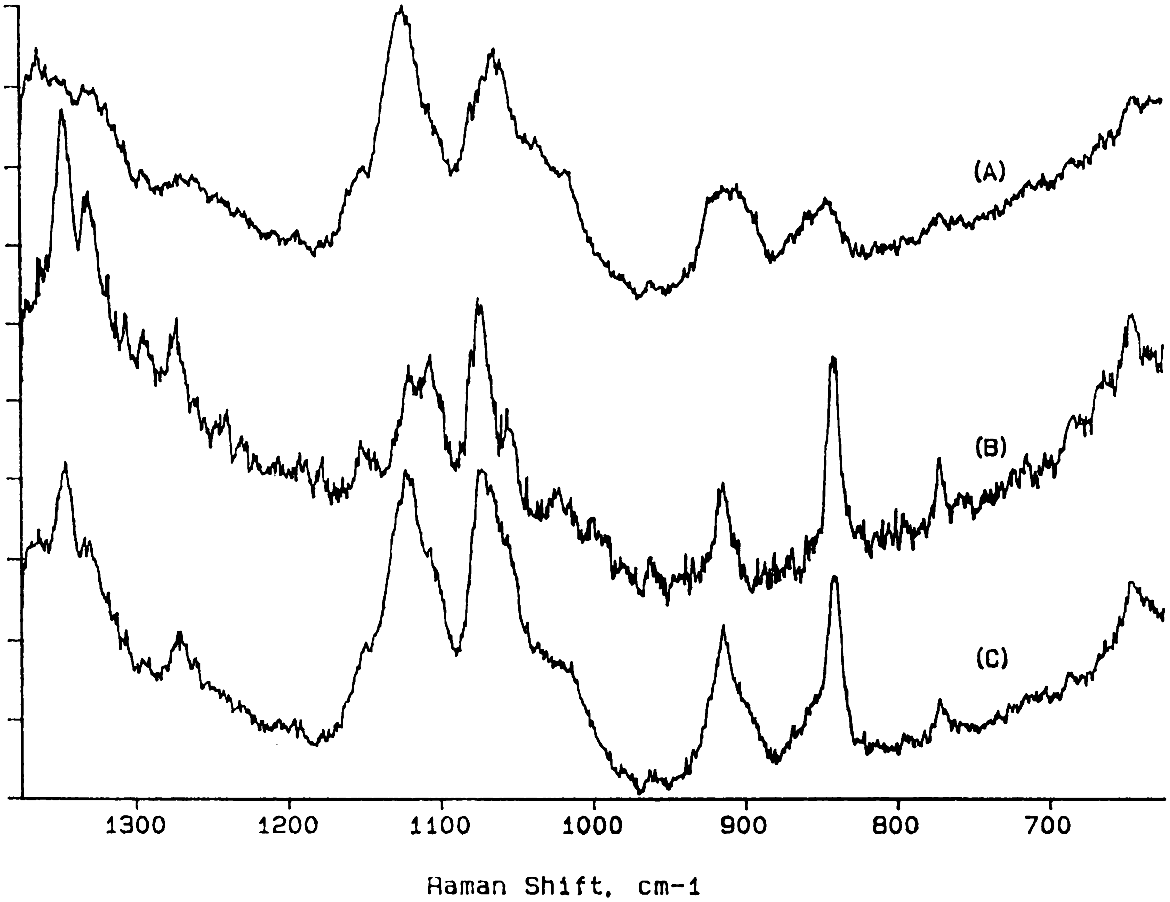

Figure 7-4. Time development of the Raman spectra of an anhydrous dextrose parent crystal in solution at 18.8°C, 2°C undercooling.

(A) The saturated aqueous solution,
(B) the parent crystal in air,
(C) the parent crystal in solution at t=0,

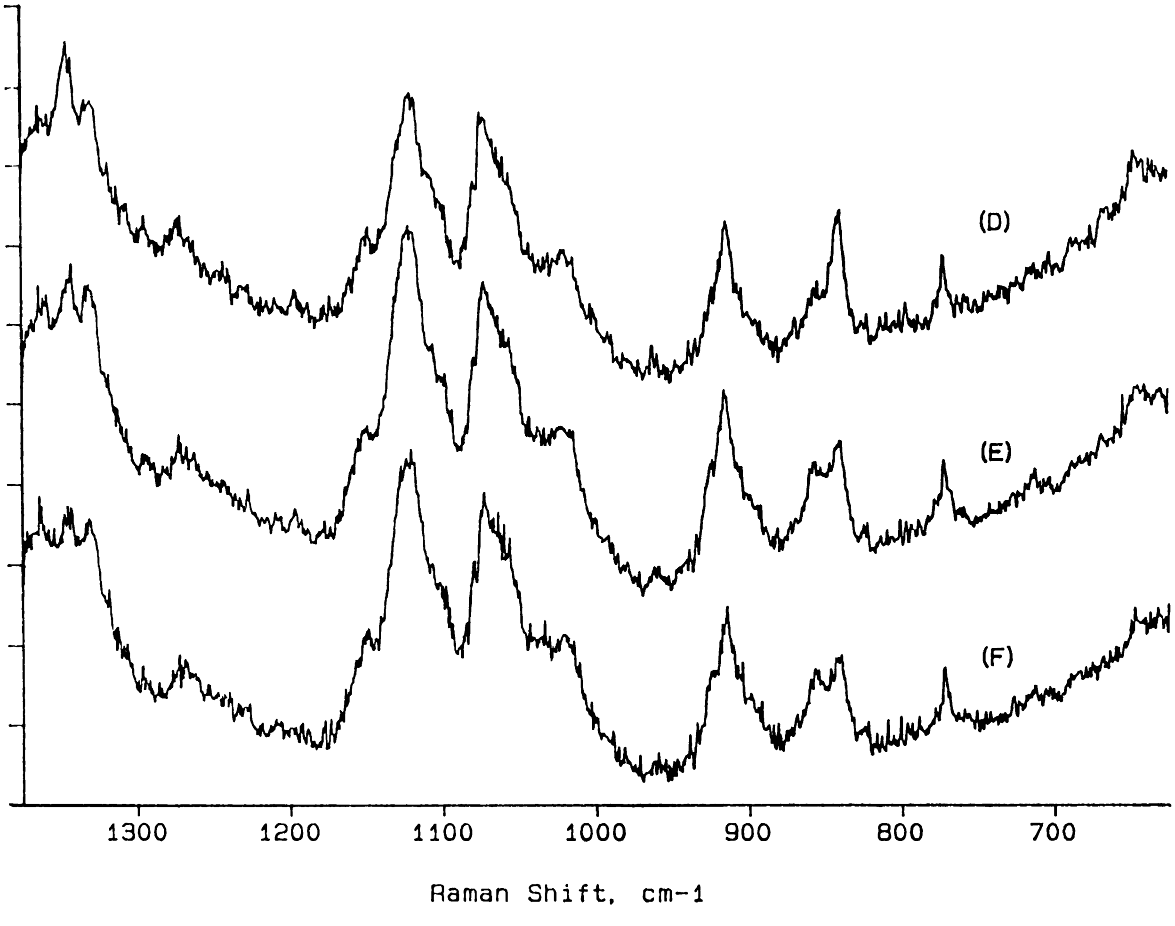

Figure 7-4 (cont'd.).

(D) the parent crystal in solution at t= 30 min.,
(E) the parent crystal in solution at t= 1 hr.,
(F) the parent crystal in solution at t= 2 hrs.,

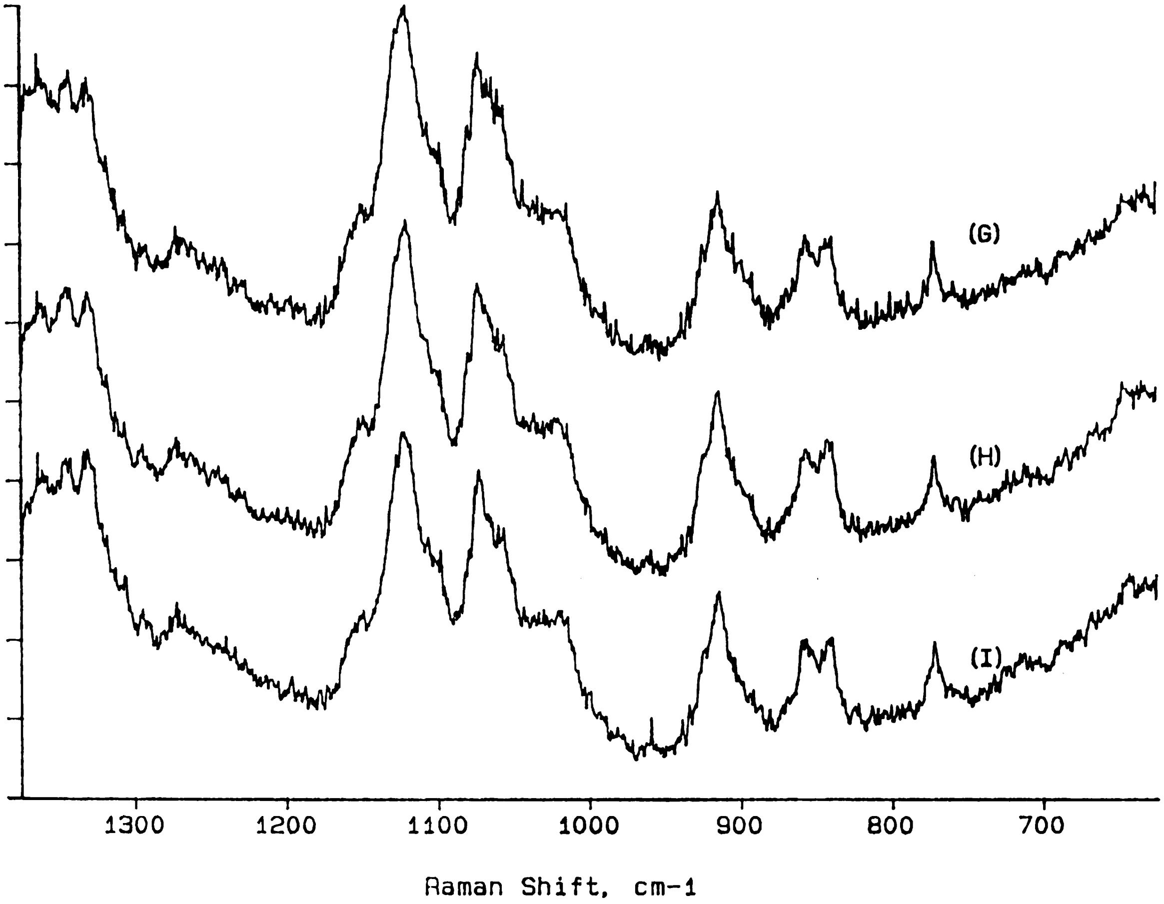

Figure 7-4 (cont'd.).

(G) the parent crystal in solution at t= 3 hrs.,
(H) the parent crystal in solution at t= 4 hrs.,
(I) the parent crystal in solution at t= 5 hrs.

Figure 7-4c (the parent crystal in solution), reveals that there is some intensity contribution from the solution in Figure 7-4c, especially in the 950-1200 cm^{-1} region. This is responsible for the asymmetry of the 841 cm^{-1} and 914 cm^{-1} bands in Figure 7-4c. In Figure 7-4d, a band is emerging at 857 cm^{-1} and the intensity of the 914 cm^{-1} band relative to the 841 cm^{-1} band is increasing. Figures 7-4e to 7-4i show the increasing intensity of the 857 cm^{-1} band with time and reversal of the 914 cm^{-1}/ 841 cm^{-1} relative peak intensity. The band at 914 cm^{-1} develops very slight asymmetry in Figures 7-4e to 7-4i. This is the 925 cm^{-1} monohydrate band obscurred by the additive intensity of the 914 cm^{-1} and 915 cm^{-1} bands.

The same results were found for experiments with the solution saturated at 28.1°C and 2°C undercooling, except that growth of the monohydrate generally took somewhat longer to first appear than with the solution saturated at 20.8°C. In both cases, contacts with the parent crystal made after 5 hours in solution always gave only monohydrate nuclei. Contacts made with parent crystals before any monohydrate could be detected did not produce nuclei.

Growth of the monohydrate on a boiling chip could not be detected at 18.8°C and 2°C undercooling, even after 24 hours in solution. This was also true for a boiling chip in solution at 39.5°C and 2°C undercooling. Supersaturations in excess of 10°C were required before crystal growth was observed, which occured on all surfaces once it began.

No growth of the monohydrate could be detected on the anhydrous parent when solutions saturated between 40-50^{o}C were investigated at 2^{o}C, 4^{o}C, and 6^{o}C undercooling, even after 24 hours. Figure 7-5 displays the results for an anhydrous parent in solution at 41.0^{o}C and 4^{o}C undercooling. No band appears at 857 cm^{-1}, and the relative intensities of the bands remain fixed with time. Contacts of the parent crystal gave both crystal phases at 4^{o}C and 6^{o}C undercooling in the solutions saturated at 40.5^{o}C and 45.0^{o}C. In the same solutions at 2^{o}C supersaturation, no nuclei were detected. For the solution saturated at 49.5^{o}C, only anhydrous nuclei formed at any supersaturation. Table 7-1 summarizes the results described above.

The experiments conducted below 30^{o}C verified that monohydrate dextrose growth on anhydrous dextrose can be detected, even when not visible under a microscope. Since it has been shown that monohydrate dextrose does not grow on anhydrous dextrose between 40^{o}C and 50^{o}C, an attrition mechanism cannot account for birth of monohydrate and anhydrous nuclei from an anhydrous parent. It cannot be concluded that the mechanism of new-particle formation is explained by the pre-crystalline cluster concept. A basic tenet of this hypothesis is that the parent surface stabilizes the clusters so they can grow to stable size; otherwise, all potential nuclei in the bulk solution would grow, too. But if the anhydrous parent surface is capable of stabilizing and producing monohydrate nuclei between

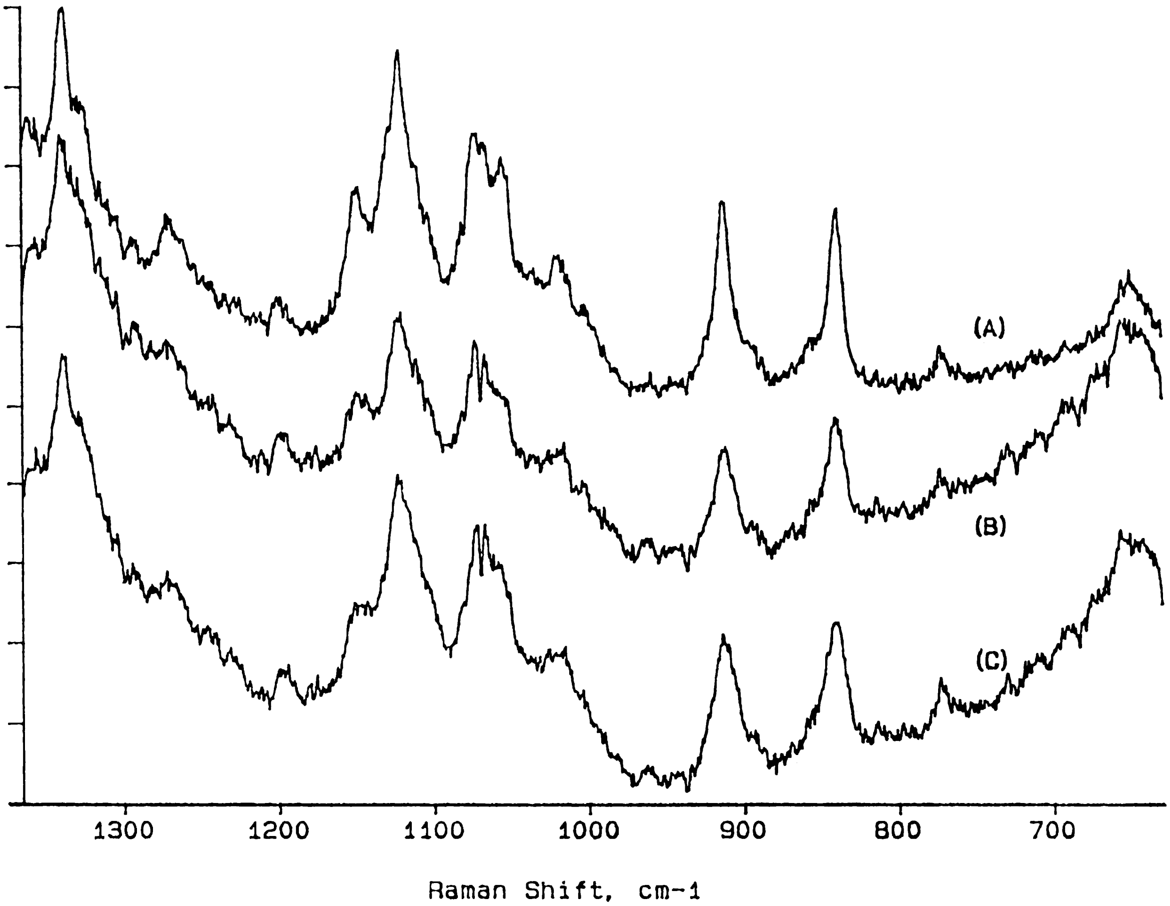

Figure 7-5. Time development of the Raman spectra of an anhydrous dextrose parent crystal in solution at 41.0°C, 4°C undercooling.

(A) The parent crystal in solution at t= 0,
(B) the parent crystal in solution at t= 3 hrs.,
(C) the parent crystal in solution at t= 24 hrs.

Table 7-1. Results of Dextrose Growth and Contact Experiments

Saturation Temperature	Degrees Undercooling 2°C Growth/Contact	4°C Growth/Contact	6°C Growth/Contact
20.8°C	Y/M	-	-
28.1°C	Y/M	-	-
40.5°C	N/X	N/B	N/B
45.0°C	N/X	N/B	N/B
49.5°C	N/A	N/A	N/A

Key to symbols:
Y= monohydrate grows on anhydrous parent
N= monohydrate does not grow on anhydrous parent
B= both monohydrate and anhydrous nuclei form after contact
M= only monohydrate nuclei form after contact
A= only anhydrous nuclei form after contact
X= no nuclei form after contact

40-45^{o}C, then it ought to be able to grow them.

We cannot yet give a hypothesis of secondary nuclei removal that is consistent with the experimental observations presented here. However, some facts may be helpful in its eventual formulation.

It was noted in [5] that the production of monohydrate and anhydrous nuclei in a single contact occured only when the solution was prepared from reagent-grade dextrose. When the solution was prepared from an industrial syrup, only the anhydrous nuclei formed. It is reasonable to assume that the industrial syrup contained some impurity not common to the reagent, and that this impurity retarded nucleation of the monohydrate. The identity of this impurity is not known. Its action must be one of either disrupting the monohydrate nuclei or encouraging the formation of anhydrous nuclei. This result points out the importance expected between the act of contact and the structure of the supersaturated solution.

Sugars are well-known for their ability to form different anomeric structures in solution (a notable exception is sucrose, in which a fructose and glucose molecule are joined through their anomeric carbons, and so cannot unfold), as well as inter- and intramolecular hydrogen bonded species. These structures are doubtless modulated by impurities and by a crystal surface. The role of the crystal surface is completely unknown.

As regards the monohydrate nuclei, the parent anhydrous crystal is a foreign surface, as is a boiling chip or piece of glass. The nuclei formation mechanism may be akin to the familiar procedure of scratching the bottom of a vessel to induce nucleation; here, the scratching rod is the anhydrous dextrose, which provides a highly sympathetic surface for the monohydrate.

This work expands the knowledge of nucleation processes in industrial crystallizers, but unfortunately not the understanding of them. It seems likely that just as contact nuclei removal may be brought about by a variety of mechanisms, one of which usually dominates, so too will nuclei production be subject to more than one means of formation.

7-7. Summary and Conclusions

A laser Raman microprobe is capable of collecting spectra on the surface a crystal in solution with minor solution interference. Anhydrous and monohydrate dextrose crystals can be distinguished by their Raman spectra. Growth of monohydrate dextrose on anhydrous dextrose occurs in supersaturated solutions below 28.1^{o}C, and contacts of parent crystals give only monohydrate nuclei. No growth of the monohydrate on anhydrous crystals can be detected in solutions saturated above 40.5^{o}C, while contacts can yield both crystalline phases. Therefore, a mechanism of nuclei formation involving only attrition of the parent crystal is not possible for the dextrose-water system between 40-50^{o}C. On grounds that a parent crystal must stabilize nuclei so they can grow, a mechanism of nuclei formation involving pre-crystalline clusters is cast into doubt. The actual mechanism at work is not known. Experiments with other systems capable of forming various hydrated phases will demonstrate whether this phenomenon is peculiar to dextrose or is more general.

7-8. Acknowledgments

The authors thank the National Science Foundation for support making this work possible through Grant No. CPE-8409458. Additional funding was provided by the RE/ED Fund of the State of Michigan. The Upjohn Company is also thanked for the graduate fellowship support of M.K. Cerreta. This work was performed in the Shared Laser Laboratory of Michigan State University.

7-9. Literature Cited

1. G. D. Botsaris, Industrial Crystallization, J. W. Mullin, Ed. (Plenum Press, New York, 1976), 3-22.
2. R. E. A. Mason and R. F. Strickland-Constable, Trans. Faraday Soc., 62, 1966, 455-461.
3. T. W. Evans, G. Margolis, and A. F. Sarofim, AIChE J., 20(5), 1974, 950-958.
4. R. T. Johnson, R. W. Rousseau, and W. L. McCabe, Chem. Eng. Prog. Symposium Series, 68(121), 1972, 31-41.
5. P. Elankovan and K. A. Berglund, AIChE J., 33(11), 1987, 1844-1849.
6. P. Elankovan and K. A. Berglund, Applied Spectrosc., 40(5), 1986, 712-714.
7. J. Garside, Chem. Eng. Sci., 40(1), 1985, 3-26.
8. M. A. Larson, Chem. Eng. Prog. Symposium Series, 80(240), 1984, 39-44.

9. J. Garside and R. J. Davey, Chem. Eng. Comm., 4, 1980, 393-424.

10. J. Estrin, Preparation and Properties of Solid State Materials, William R. Wilcox, Ed. (Marcel Dekher, Inc., New York and Basel, 1976), 1-42.

11. H. E. C. Powers, Nature, 178, 1956, 139-140.

12. J. W. Gibbs, Collected Works, 1, 1878, p. 325, Reprint, (Dover Publications, Inc., New York, 1961).

13. R. E. A. Mason and R. F. Strickland-Constable, Nature, 197, 1963, 897-898.

14. N. A. Clontz and W. L. McCabe, Chem. Eng. Symposium Series, 67(110), 1971, 6-17.

15. J. Garside and M. A. Larson, J. Crystal Growth, 43, 1978, 694-704.

16. K. A. Berglund and E. J. deJong, accepted for publication in AIChE J.

17. J. W. Mullin and C. Leci, Philos. Mag., 19, 1969, 1075.

18. M. A. Larson and J. Garside, Chem. Eng. Sci., 41(5), 1986, 1285-1289.

19. M. K. Cerreta and K. A. Berglund, K. A., J. Crystal Growth, 84, 1987, 577-588.

20. M. Mathlouthi and D. V. Luu, Carbohydrate Research, 78, 1980, 225-233.

21. M. K. Cerreta and K. A. Berglund. Paper presented at the Annual Meeting of AIChE, New York, New York, November 15-20, 1987.

22. E. G. Denk and G. D. Botsaris, J. Crystal Growth, 69, 1984, 623-626.

23. K. Shimizu, K. Tsukamoto, J. Horita, and T. Tadaki, J. Crystal Growth, 69, 1984, 623-626.

24. R. Wissing, M. Elwenspoek, and B. Degens, J. Crystal Growth, 79, 1986, 614-619.

25. F. E. Young, J. Phys. Chem., 61, 1957, 616-619.

26. G. R. Dean, Carbohyd. Research, 34, 1974, 315-322.

27. M. Mathlouli and J. L. Koenig, in Advances in Carbohydrate Chemistry and Biochemistry , R. Stuart Tipson and Derek Horton, Eds. (Academic Press, New York, 44, 1986), 7-90.

28. M. Mathlouthi, C. Luu, A. M. Meffroy-Biget, and D. V. Luu, Carbohyd. Research, 81, 1980, 213-223.

29. M. J. D. Low and R. T. Yang, Spectrochim. Acta, Part A, 29, 1973, 1761-1772.

30. J. P. Huvenne, G. Vergoten, G. Fleury, and P. Legrand, J. Molecular Structure, 74, 1981, 169-180.

31. M. Delhaye and P. Dhamelincourt, J. Raman Spectrosc., 3, 1975, 33-43.

CHAPTER 8

SUMMARY AND CONCLUSIONS

8-1. Summary and Conclusions

Dihydrogen phosphate anions in pure, aqueous solution form bi-dentate hydrogen-bonded structures, even at low concentrations, with >50% doing so by saturation at 30^{o}C for KDP (1.79 M), >80% for ADP (3.20 M), and ~100% for NaDP (6.00 M). These bonds must break and reform during the crystallization process, and so explains many characteristics of dihydrogen phosphate crystal growth and nucleation, including:

1. the rate-limiting surface growth mechanism;
2. the large activation energy for crystal growth;
3. the relatively slow growth in the x- or y-direction (the plane containing the hydrogen bonds) compared to the z-direction;
4. the unusually large supersaturations that can be achieved.

The solution spectra showed no evidence for solute clusters. The anion-anion structures are stable to pH 7. Their slight break-up at elevated pH may account for the increased ease and perfection of crystal growth at pH 5.5. Changing the pH did not bring any evidence of quasi-crystalline entities, but did show the evolution of the production of $HPO_4 2-$ ions.

Raman and infrared methods show the phosphate bulk solution structure is unaffected by the presence of Cr^{+3}, Fe^{+3}, or Al^{+3} ions below 500 ppm. However, the UV-VIS spectra show these impurities bind to H_2PO_4- in solution.

No structural changes with concentration were noted for glycine, lysine, or glutamic acid. Conversion to base or acid forms did induce considerable structure changes from the zwitterion. There was not very good agreement between the solution and crystal spectral profiles, indicating once again that solute clustering as in the crystal does not occur.

Below 30°C, monohydrate dextrose is easily detected growing on an anhydrous dextrose crystal surface. Between 40-45°C monohydrate dextrose will not grow on anhydrous dextrose under conditions where contact of the latter produces both phases. Therefore, an attrition mechanism of new-particle formation does not apply between 40-45°C. It is not necessarily true that the pre-crystalline cluster mechanism is at work; the anhydrous dextrose does not stabilize the monohydrate, a basic tenet of the hypothesis. A third, unknown mechanism may apply.

To date, only one solution study [1] indicates a solution with the structure of the crystal (aqueous KNO_3). Aqueous $NaNO_3$, dihydrogen phosphates, and amino acids [2, and this work] do not. This enforces the view that crystal growth and nucleation is a process governed most immediately by kinetic considerations, and only ultimately by equilibrium thermodynamics. That is, within the bulk supersaturated solution, the least-stable structure forms first; the most-stable structure (the crystal) forms last. The unstable structures should actually be considered as impurities.

In view of the above, the following physical model for growth and nucleation can be proposed. Within the bulk of a supersaturated solution, various structures exist depending on the history of the solution (age, for example). Most of what is present is either ionic, monomolecular or bound in a structure unlike the crystal. When a crystal has been growing for some time (long enough to achieve a constant growth rate), it will have surrounding it a sheath of "impurity structures" that cannot incorporate into the crystal lattice. The impurities block the "growth structures". When the crystal suffers a contact, some of the sheath is cut away, and attrition nuclei are exposed to conditions in the bulk that allow for a brief period of rapid growth before they, too, build up an impurity sheath. The process then repeats itself. The interplay between a crystal and the species in solution is of utmost importance.

8-2. Proposals for Future Research

Quantitative Raman study is difficult because exactly reproducing experimental conditions is virtually impossible. The variables responsible for this are the laser power, the point to which the laser light is focused, the orientation of the sample in the laser beam and with respect to the monochromator, the spectrometer calibration, and the slit settings (the bandpass). It is recommended that the sample cell be redesigned so as to allow for the addition of solute or solvent without disturbing the sample holder. Spectra may then be collected one after the other without changing the other parameters.

Even when the sample is interrogated successively without any alterations of these variables, the point-by-point variance of the intensity is at best about 1%. The best remedy for this is many scans. But time puts limits on how many scans may reasonably be collected. Optical multichannel analyzers (OMA) can collect a high quality spectrum in seconds, so future studies should be carried out employing this device. Currently available diode arrays have 1024 pixels providing about 1 cm^{-1} resolution, which is adequate for the dihydrogen phosphates.

The technique of Raman difference spectroscopy will be necessary for comparison of spectra in the supersaturated region. In this method a two-compartment sample cell spins each compartment in and out of the laser beam in succession. Each compartment would hold a solution of different supersaturation. The difference between the two spectra would give an indication of changing composition in the supersaturated region.

No studies in either the IR or the Raman have been made regarding the behavior of the low-energy bending and twisting modes (< 600 cm^{-1}) of the dihydrogen phosphate ion with concentration. This region should be investigated.

Micro Raman studies in the region of a growing crystal similar to those of Hussmann et al. [59] should be performed using an OMA system. This would elucidate changes in the solution structure between the bulk and the surface of the crystal.

It is necessary to determine if compounds capable of forming hydrated phases display regions of mixed-nuclei formation, as with dextrose. Magnesium sulfate heptahydrate and potassium aluminum sulfate dodecahydrate are the prime candidates for such a study, in view of the considerable work already done with them, their simple habit, and ease of growth. In addition, the sulfate ion is a good Raman scatterer.

8-3. Literature Cited

1. P. M. McMahon, K. A. Berglund, and M. A. Larson, Process Tech. Proc., 2, 1984, 229.

2. G. A. Hussman, M. A. Larson, and K. A. Berglund, Industrial Crystallization 84, S. J. Jancic and E. J. de Jong, Eds. (Elsevier Science Publishers, B.V., Amsterdam, 1984), 21.

APPENDICES

APPENDIX A

ON THE VIBRATIONAL BAND ASSIGNMENTS OF AQUEOUS DIHYDROGEN ORTHOPHOSPHATES

Shortly after beginning the work of Chapters 4 and 5, it was discovered that the origin of the asymmetry in the 1075 cm^{-1} band in the Raman spectra of aqueous phosphates was not settled. Steger and Herzog (SH) [1,2] proposed that it is a PO-H bending mode made prominent when the OH groups lock into place as a result of hydrogen bonding. There is good evidence for this. When the anion is in dilute solution, nothing holds the OH group in place, so the H should be free to rotate about the P-O bond, diminishing the normal coordinate character of the O-H bend. When the OH group is hydrogen bonded to another phosphate, the H becomes fixed and can no longer rotate, instead emphasizing the O-H bend. In addition, the shape of the band when deconvoluted is like that of a bending mode.

Apparently unaware of Steger and Herzog's work, Preston and Adams (PA) [3] interpreted the vibrational origin of the band asymmetry as the hydrogen-bonded $P=(O)_2$ symmetric stretch. This is also a reasonable conclusion, as discussed in Chapter 4. Both SH and PA agreed that the reason for the development of the band asymmetry is the formation of hydrogen bonds. However, the band deconvolution and analyses of this work depend heavily on the exact assignment of the band.

Fortunately, there is a very simple experiment that can differentiate between the two proposals, and it is somewhat surprising that SH and PA did not pursue it. By substituting deuterium for hydrogen in the anion, an O-H bend frequency should show a relative decrease by $1/(2)^{.5}$, i.e., by 0.714. For example, the water O-H bending mode shifts from 1634 cm^{-1} to about 1200 cm^{-1} when deuterated. Therefore, if the vibration is really an O-H bend, a concentrated solution of the deuterated phosphate should show the band at $0.714*1050\ cm^{-1} = 750\ cm^{-1}$. If the vibration is actually a $P=(O)_2$ symmetric stretch, deuteration should have little or no effect on the Raman spectrum.

A proper study of the problem would entail not just the experiment outlined above, but also a normal mode coordinate analysis, a review of the occurence of O-H bending modes and deuteration effects, a review of hydrogen bonding, and a similar experiment with sulfuric acid. It was not the purpose of this work to become involved in the disagreement over the band origin. Instead, the results of the simple experiment are presented in this appendix.

Saturated solutions of KDP, ADP, and NaDP were prepared by dissolving excess dihydrogen salt in D_2O, filtering, recrystallizing, and redissolving in D_2O. The salts were recrystallized from D_2O four times. The absence of hydrogen in the final salt was confirmed by the absence of any band in the O-H stretching region using Fourier transform infrared spectroscopy. The Raman spectra were collected as described in Chapter 4.

Figure A-1 shows the spectrum of deuterated NaDP in D_2O, which best illustrates the results. First, there is no band at 750 cm^{-1} or anywhere in its vicinity. The $P=(O)_2$ band is still found at 1060 cm^{-1}. The $P-(OD)_2$ symmetric stretch at 878 cm^{-1} has shifted 16 cm^{-1} from the same vibration in $P-(OH)_2$ at 894 cm^{-1}, which is as expected since hydrogen is definitely involved in this vibration. The O-D bending mode of D_2O is present at about 1200 cm^{-1}. The spike at 1122 cm^{-1} is roomlite, used for calibrating the spectrum. Exactly the same results were found for KDP and ADP.

The results provide unambiguous proof that the vibrational band in question cannot be due to O-H bending, but is the hydrogen-bonded $P=(O)_2$ symmetric stretch as proposed by Preston and Adams. With this established, the results of Chapter 4 are valid.

Literature Cited

1. E. Steger and K. Herzog, Z. Anorg. Allg. Chem., 331, 1964, 169.

2. E. Steger, K. Herzog, and J. Klosowski, Z. Anorg. Allg. Chem., 432, 1977, 42.

3. C. M. Preston and W. A. Adams, J. Phys. Chem., 83(7), 1979, 814.

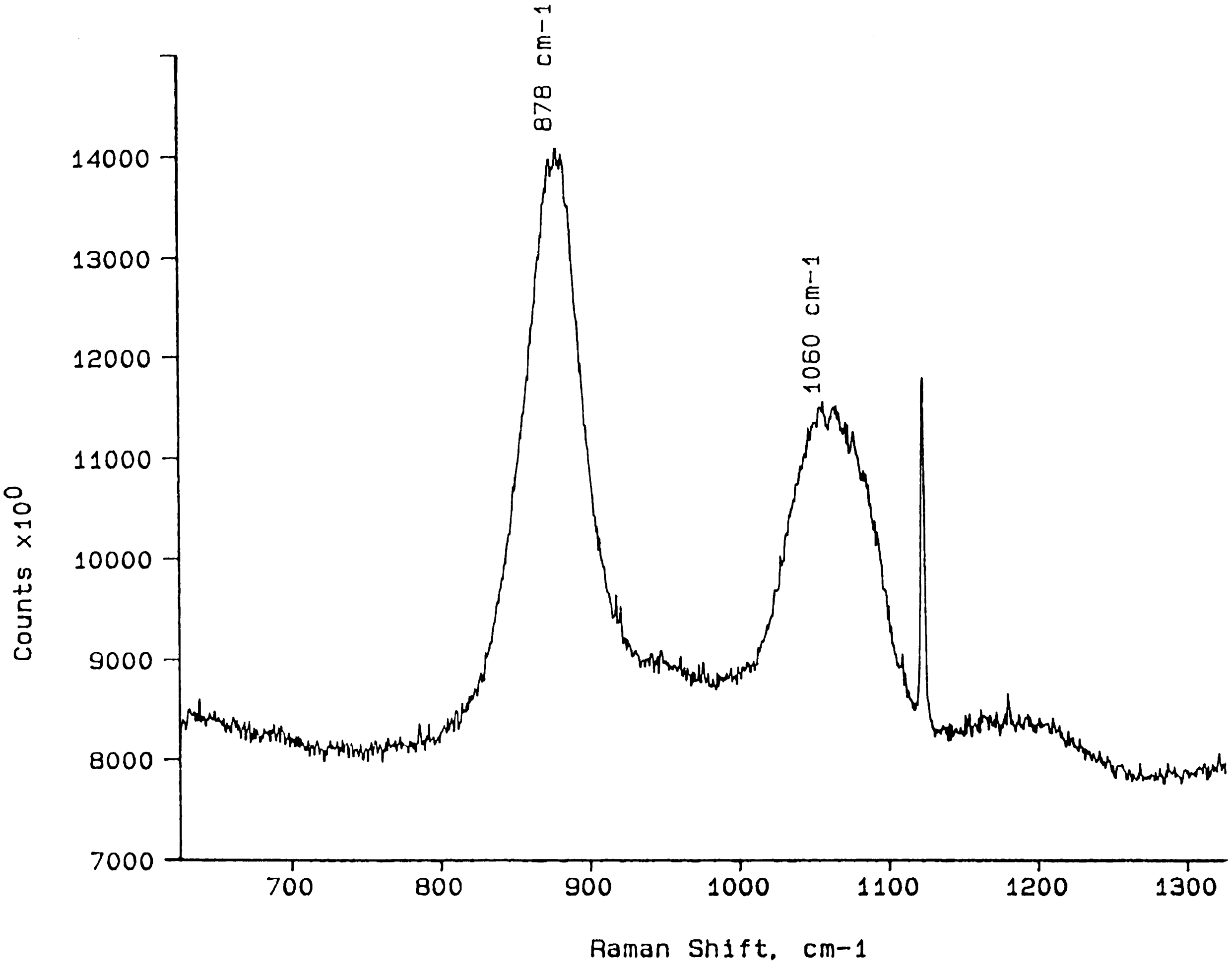

Figure A-1. The Raman spectra of deuterated NaDP in saturated D_2O at 30°C.

APPENDIX B

DISTINGUISHING FEATURES OF THE RAMAN SPECTRA OF CRYSTALLINE AND AQUEOUS DEXTROSE

Regarding the search for the growth of monohydrate dextrose on anhydrous dextrose, it was necessary to know (a) when the laser beam was focused in solution or on the parent crystal, and (b) whether the spectrum collected was that of the monohydrate or anhydrous phase. The means by which this was accomplished is discussed in Chapter 7. There were additional corroborating features in the time development of the spectra that could not be mentioned since brevity is a major concern in papers destined for publication. Those additional features are discussed here.

Referring to Figures 7-3 to 7-5, first note the band present in both crystalline phases and the solution at 772 cm^{-1}. It is weak relative to the 841 cm^{-1} band in the anhydrous spectrum. Relative to the 857 cm^{-1} band in the monohydrate spectrum, it is much stronger. In Figures 7-4c to 7-4i, it becomes stronger relative to the same bands, which is further proof of the growth of the monohydrate. In Figure 7-5 its intensity compared to the 841 cm^{-1} band remains constant, showing that the monohydrate is not present. Comparison of Figures 7-3a, 7-3b and 7-3c shows this band is much stronger and sharper in the crystal than in solution. This was an additional feature used to focus the laser on the crystal and is apparent in Figures 7-4 and 7-5.

There is a strong band at 1345 cm^{-1} in the anhydrous spectrum (Figure 7-3b). This band decreases in intensity in Figures 7-4c to 7-4i because the monohydrate is slowly covering the anhydrous crystal and blocking the laser beam. The same is true of the anhydrous bands at 1273 cm^{-1} and 646 cm^{-1}. In Figure 7-5, these three bands maintain their relative intensity because the monohydrate is not present.

The 1331 cm^{-1} band, present in the spectra of both crystalline phases but strongest in the monohydrate, increases in intensity with time in Figure 7-4. This is additional evidence for the growth of the monohydrate.

There is a weak band, present in the anhydrous spectrum only, at 1202 cm^{-1}. This band recedes in Figures 7-4c to 7-4i, but remains constant in Figure 7-5. Again, the former is proof of the growth of the monohydrate and the latter is proof of its absence.

APPENDIX C

RAMAN SPECTRA OF DIHYDROGEN ORTHOPHOSPHATES

The Raman spectra of dihydrogen orthophosphates that were used in analyses but not included in Chapter 4 appear on the following pages.

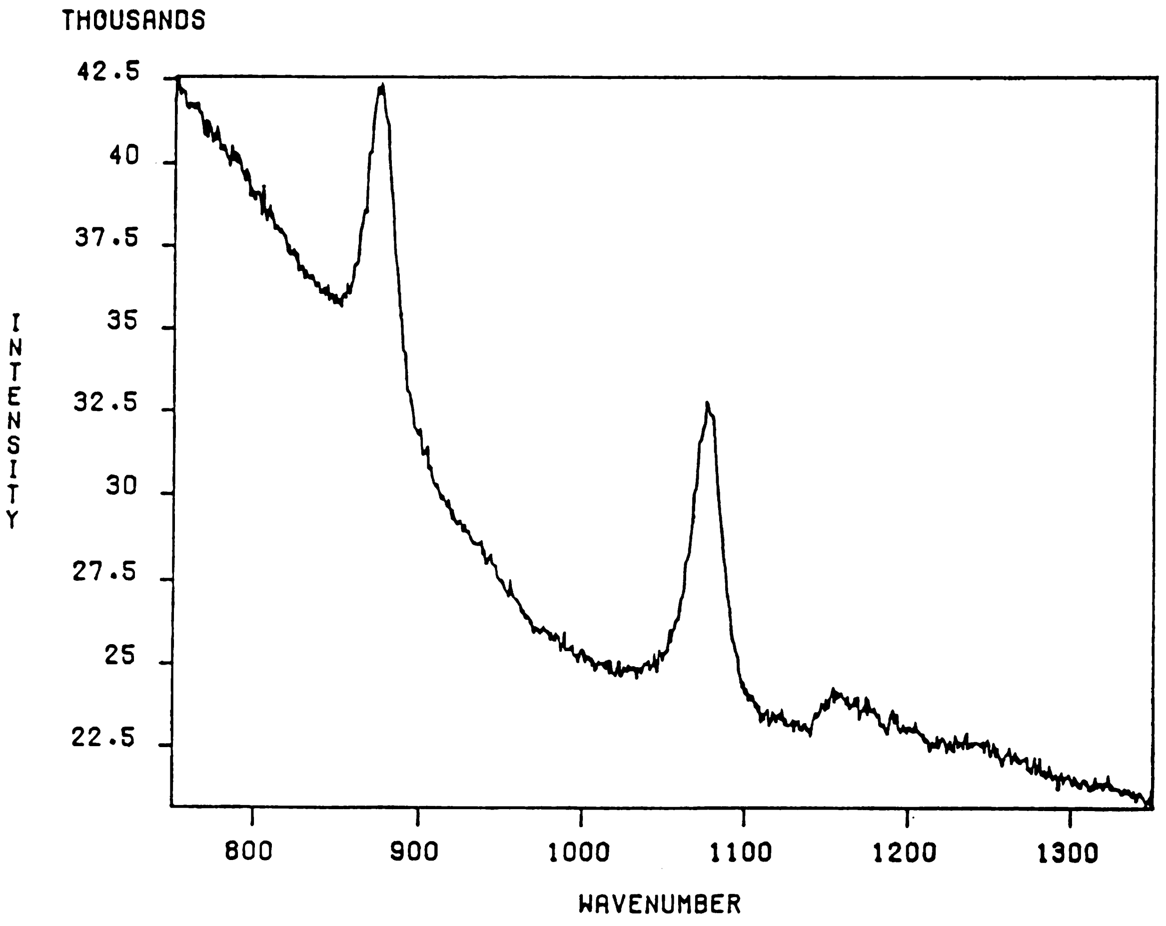

Figure C-1. The Raman spectra of 0.01 M ADP.

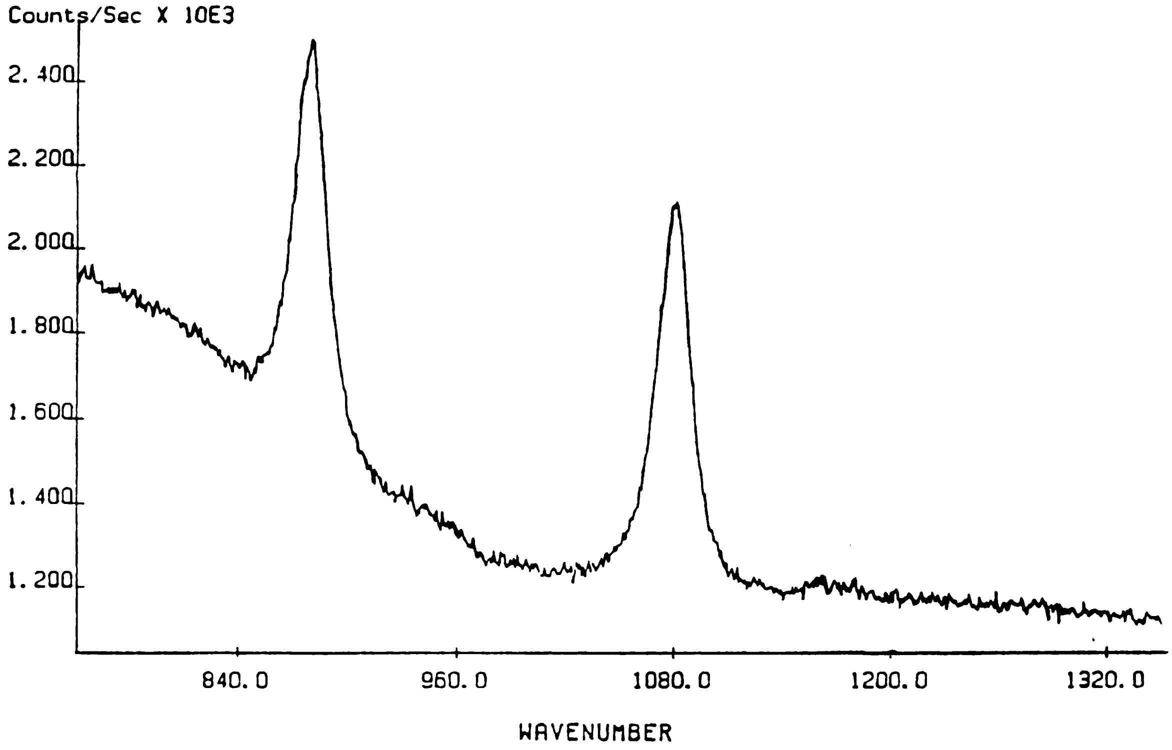

Figure C-2. The Raman spectra of 0.10 M KDP.

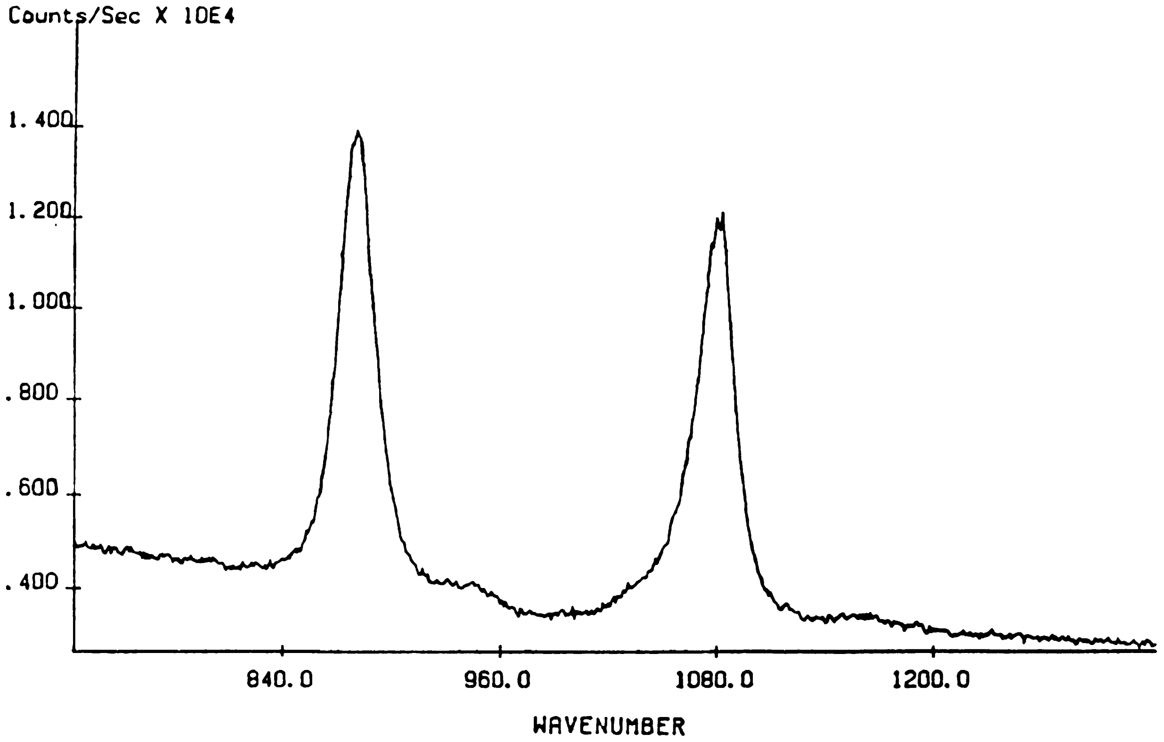

Figure C-3. The Raman spectra of 1.00 M ADP.

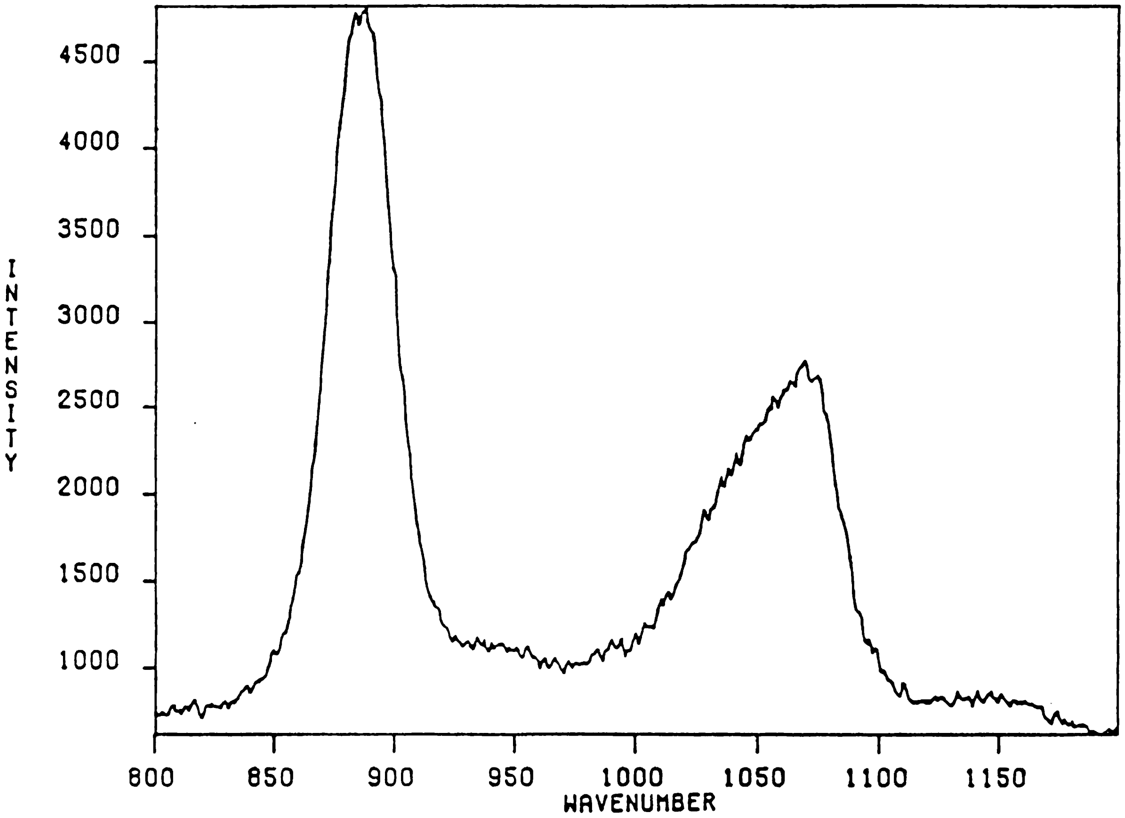

Figure C-4. The Raman spectra of 3.30 M ADP.

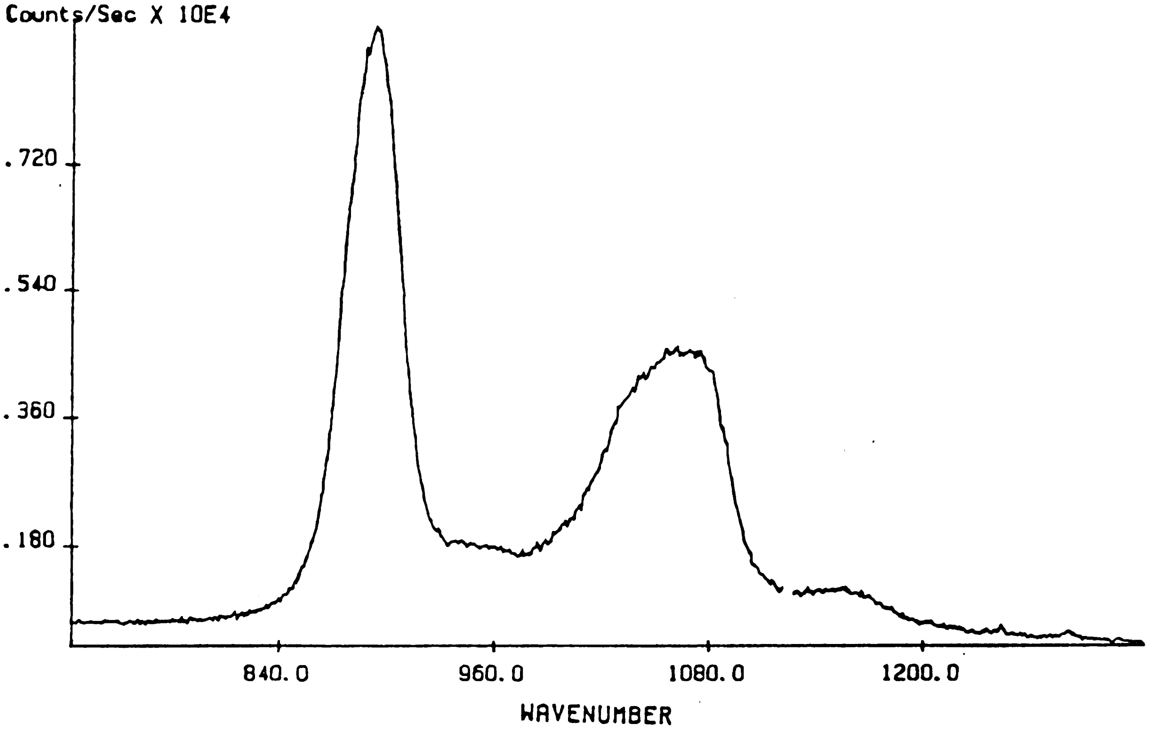

Figure C-5. The Raman spectra of 4.60 M NaDP.

APPENDIX D

RAMAN SPECTRA OF DEXTROSE

The Raman spectra of dextrose that were referred to but not included in Chapter 7 are presented on the following pages.

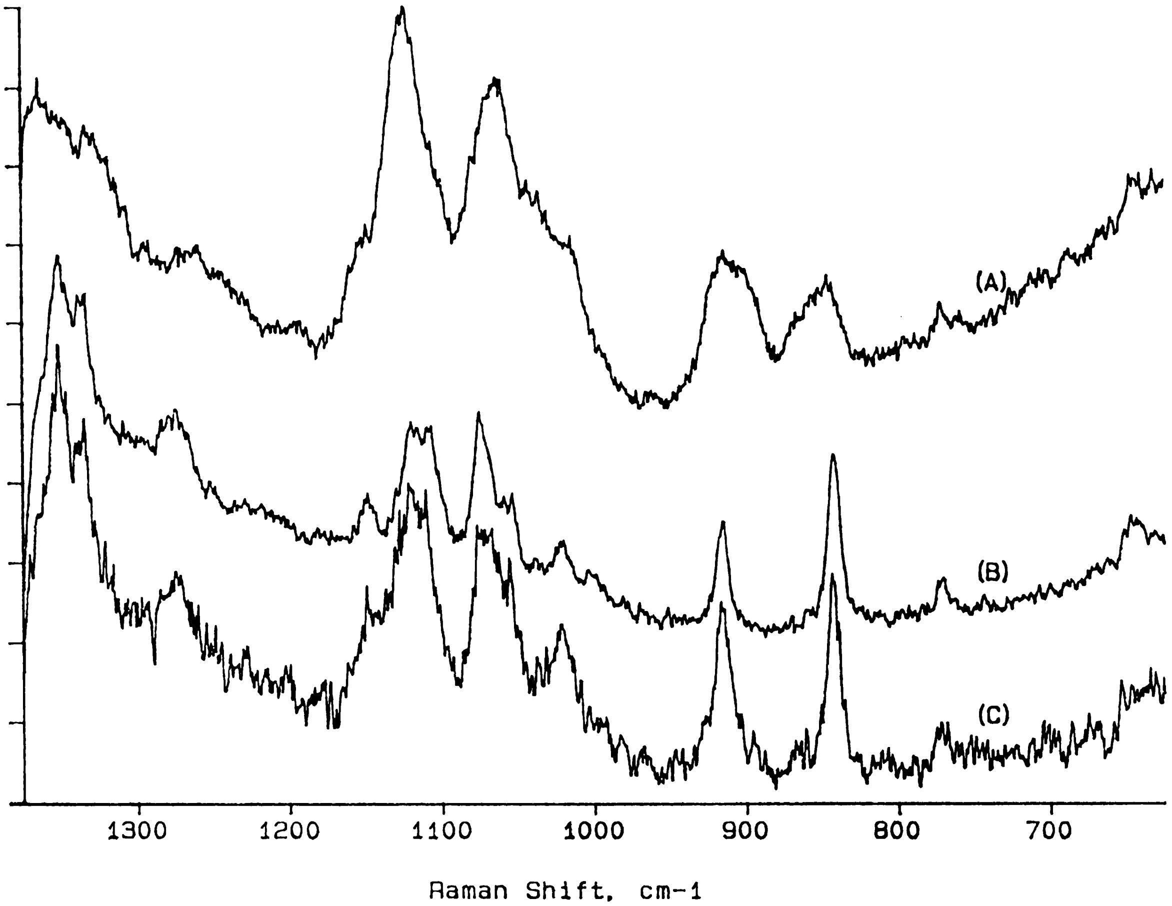

Figure D-1. The time development of the Raman spectra of an anhydrous parent dextrose crystal in solution at 26.1°C and 2°C undercooling.

(A) The saturated solution,
(B) the parent crystal in air,
(C) the parent crystal in solution at t= 0,

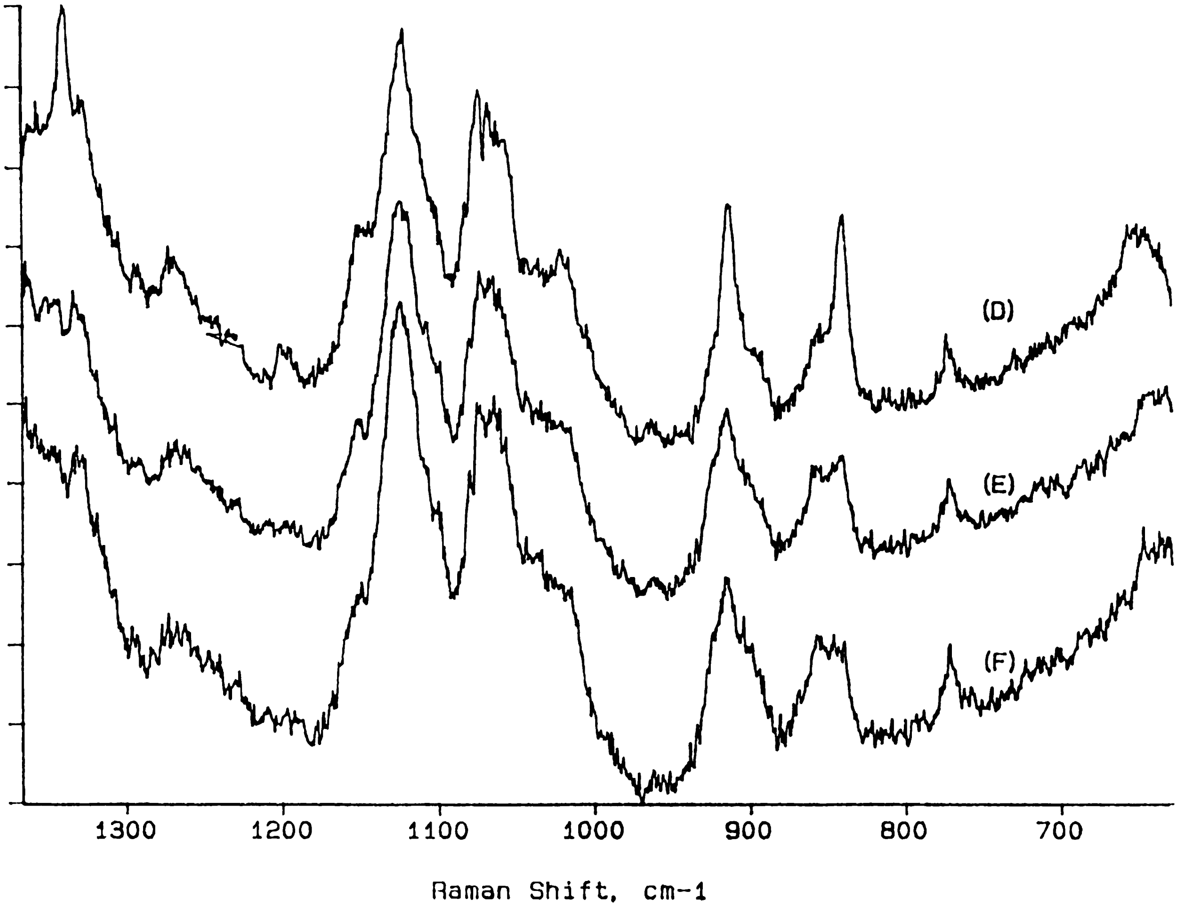

Figure D-1 (cont'd.).

(D) the parent crystal in solution at t = 2 hrs.,
(E) the parent crystal in solution at t = 3 hrs.,
(F) the parent crystal in solution at t = 4 hrs.

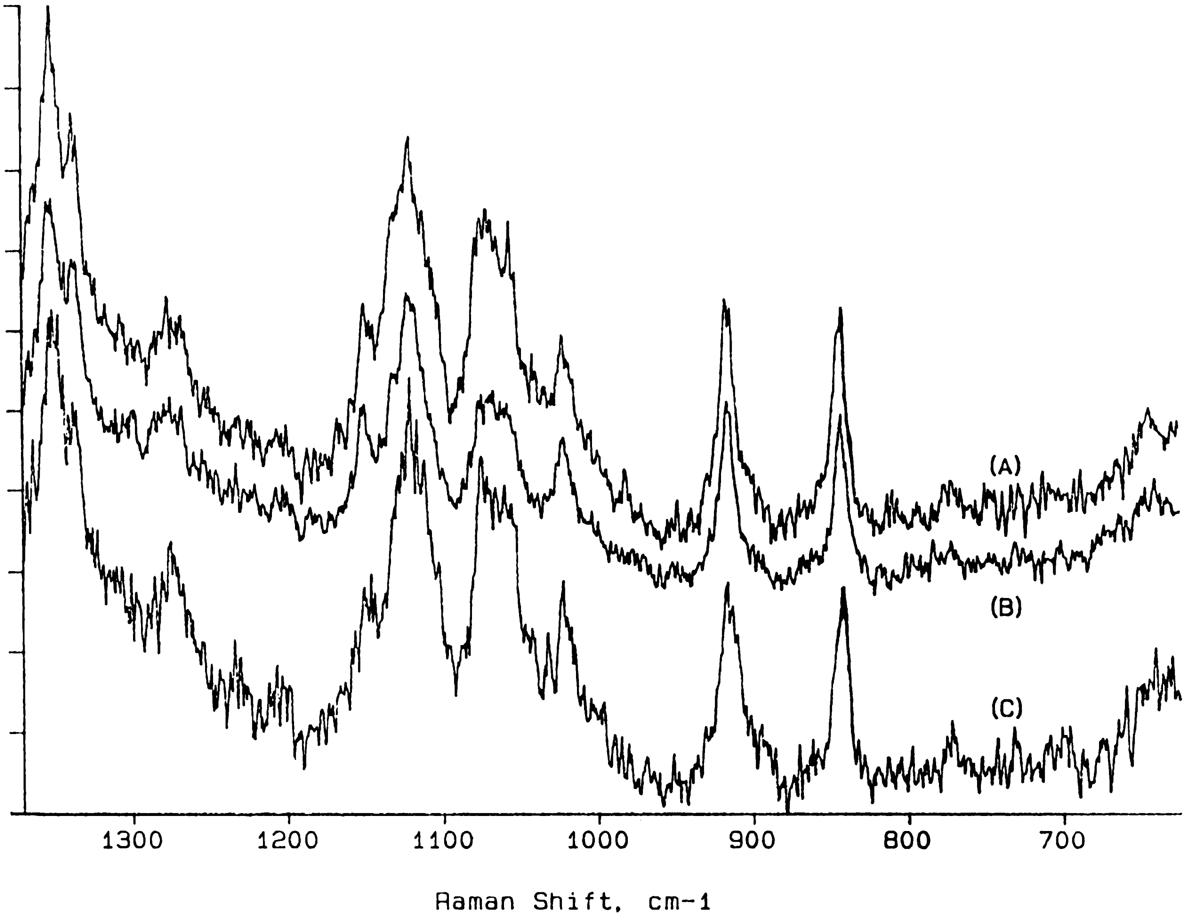

Figure D-2. The time development of the Raman spectra of an anhydrous parent dextrose crystal in solution at 38.5°C and 2°C undercooling.

(A) The parent crystal in solution at t= 0,
(B) the parent crystal in solution at t= 3 hrs.,
(C) the parent crystal in solution at t= 9 hrs.

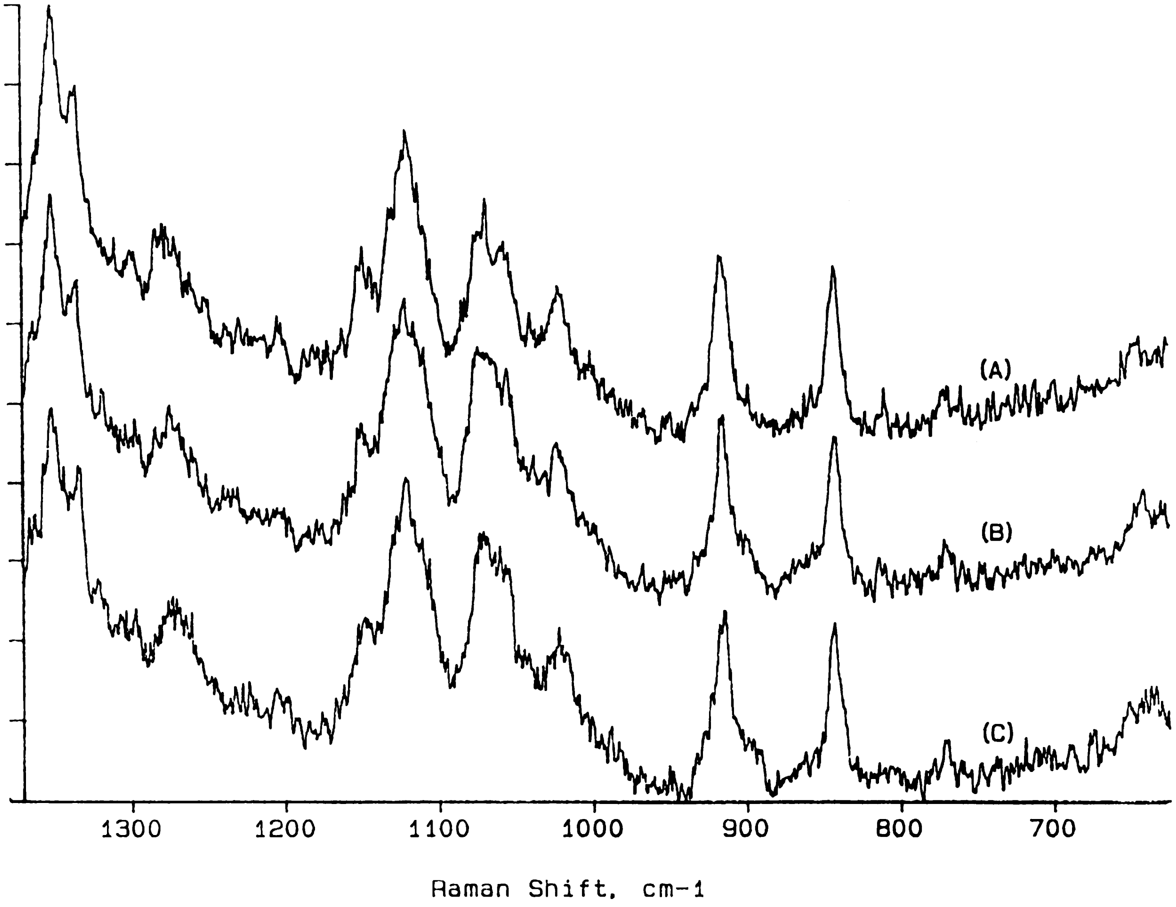

Figure D-3. The time development of the Raman spectra of an anhydrous parent dextrose crystal in solution at 36.5°C and 4°C undercooling.

(A) The parent crystal in solution at t= 0,
(B) the parent crystal in solution at t= 3 hrs.,
(C) the parent crystal in solution at t= 12 hrs.

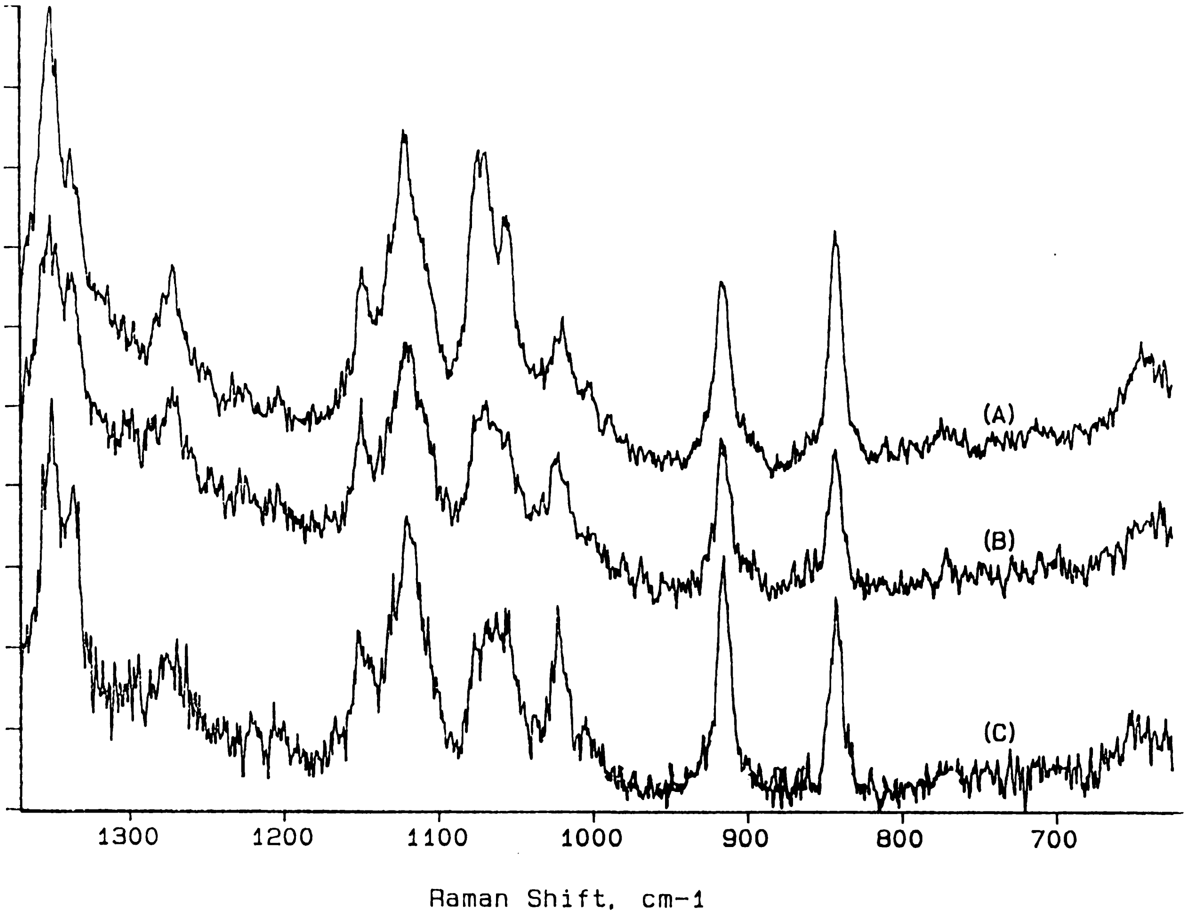

Figure D-4. The time development of the Raman spectra of an anhydrous parent dextrose crystal in solution at 34.5^{o}C and 6^{o}C undercooling.

(A) The parent crystal in solution at t= 0,
(B) the parent crystal in solution at t= 3 hrs.,
(C) the parent crystal in solution at t= 8 hrs.

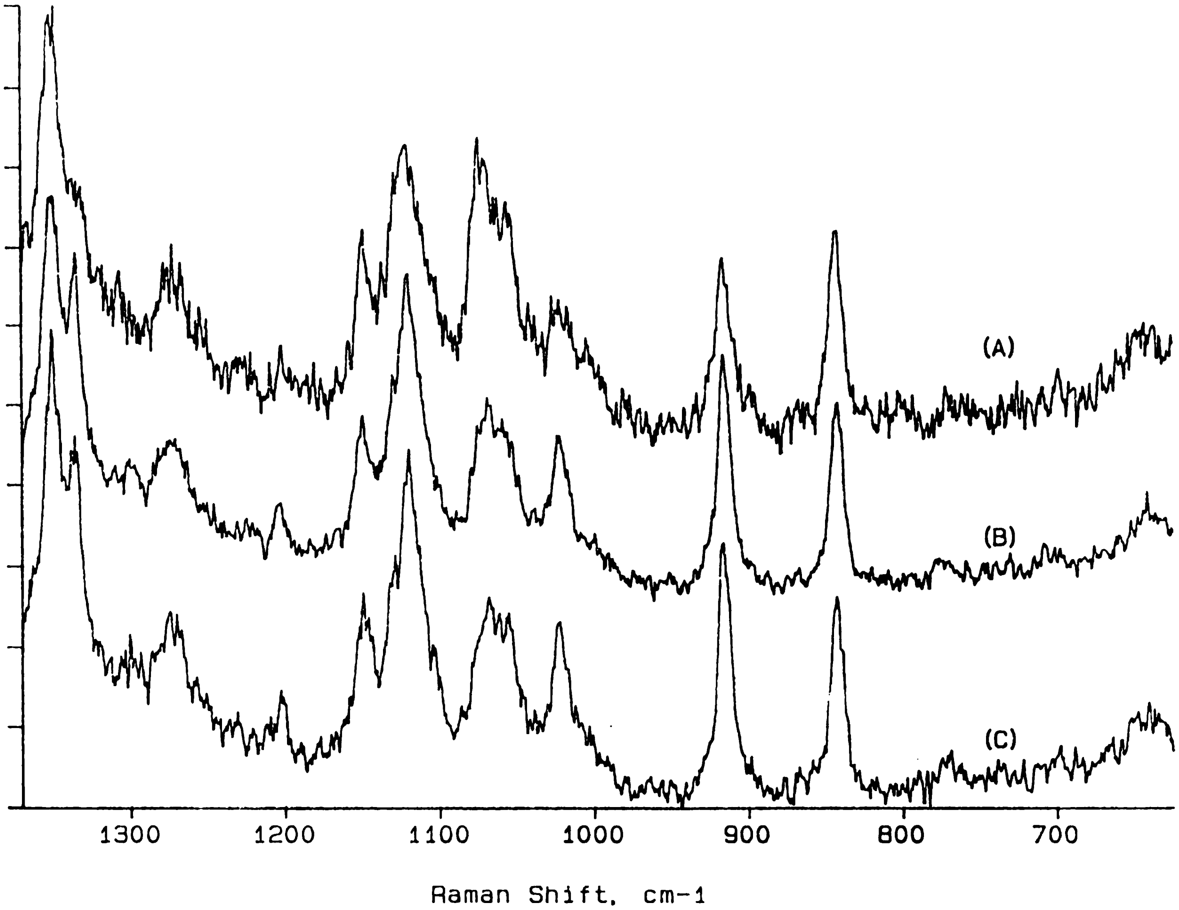

Figure D-5. The time development of the Raman spectra of an anhydrous parent dextrose crystal in solution at 43.0°C and 2°C undercooling.

(A) The parent crystal in solution at t= 0,
(B) the parent crystal in solution at t= 3 hrs.,
(C) the parent crystal in solution at t= 24 hrs.

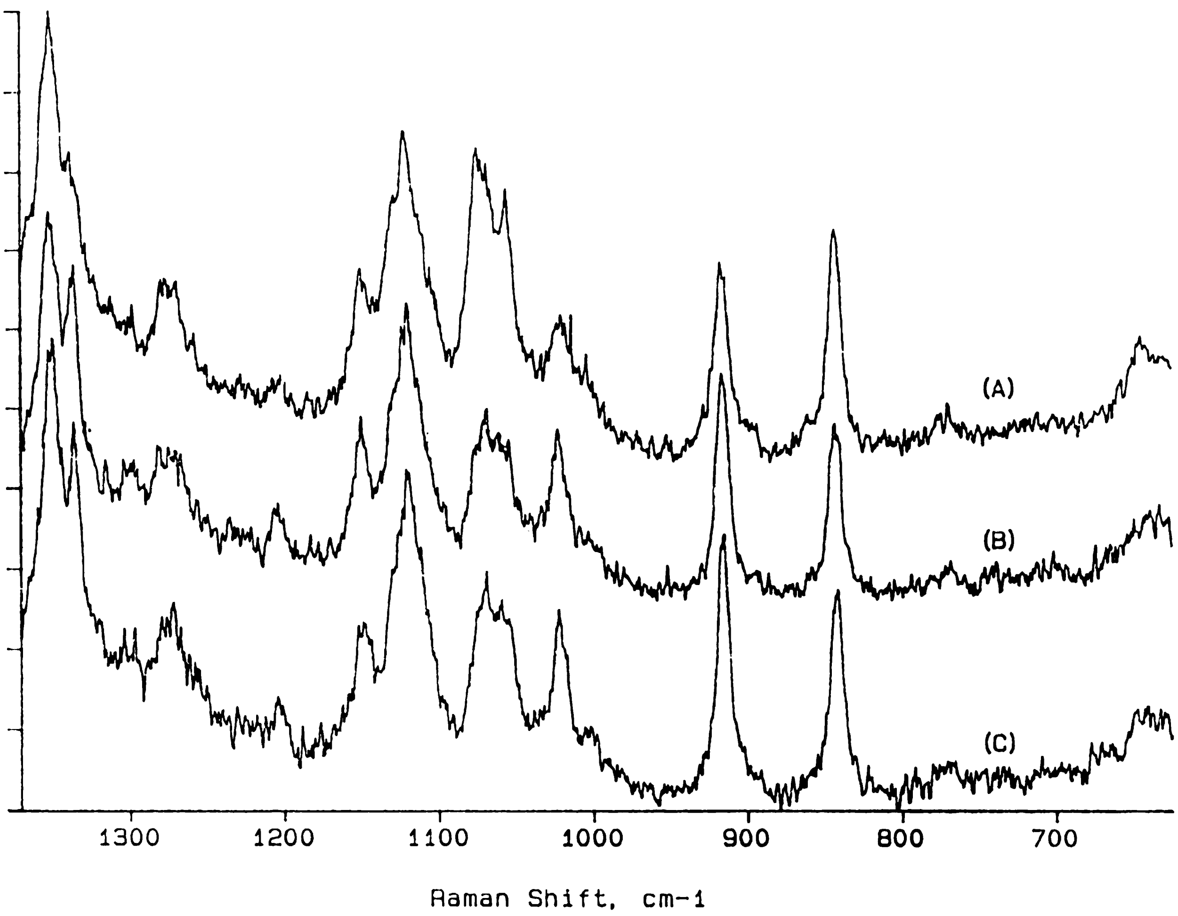

Figure D-6. The time development of the Raman spectra of an anhydrous parent dextrose crystal in solution at 39.0°C and 6°C undercooling.

(A) The parent crystal in solution at t= 0,
(B) the parent crystal in solution at t= 4 hrs.,
(C) the parent crystal in solution at t= 11 hrs.

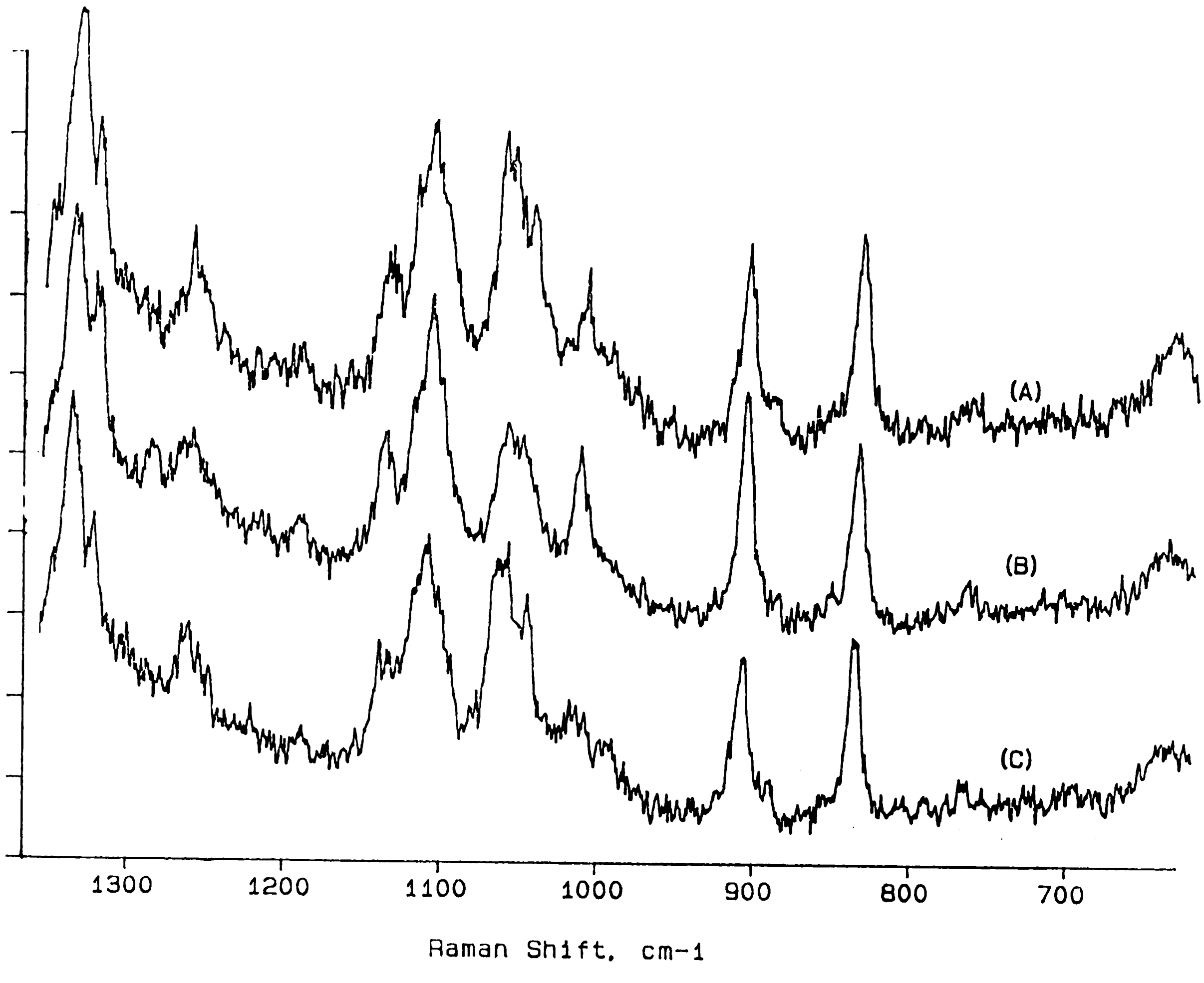

Figure D-7. The time development of the Raman spectra of an anhydrous parent dextrose crystal in solution at 47.0^{o}C and 2^{o}C undercooling.

(A) The parent crystal in solution at t= 0,
(B) the parent crystal in solution at t= 3 hrs.,
(C) the parent crystal in solution at t= 9 hrs.

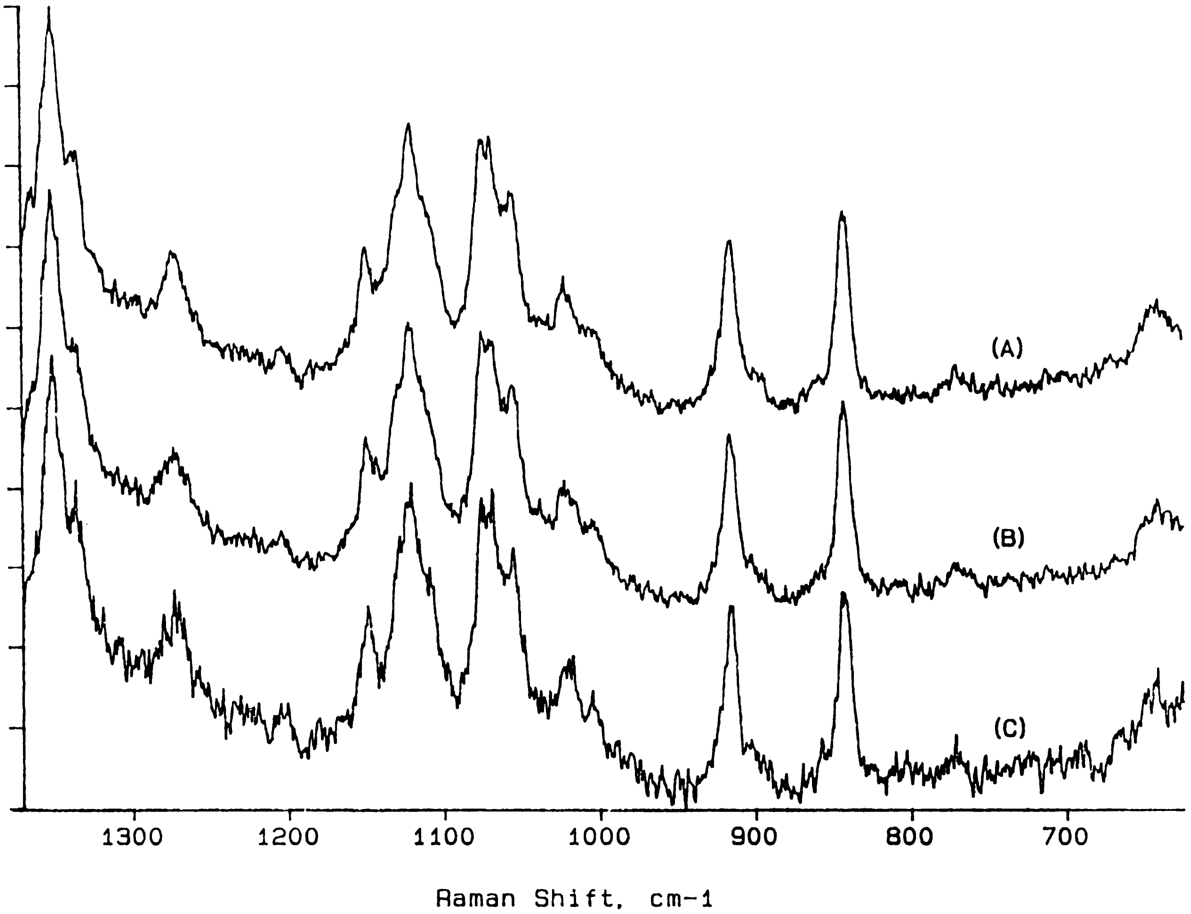

Figure D-8. The time development of the Raman spectra of an anhydrous parent dextrose crystal in solution at 45.0°C and 4°C undercooling.

(A) The parent crystal in solution at t= 0,
(B) the parent crystal in solution at t= 3 hrs.,
(C) the parent crystal in solution at t= 17 hrs.

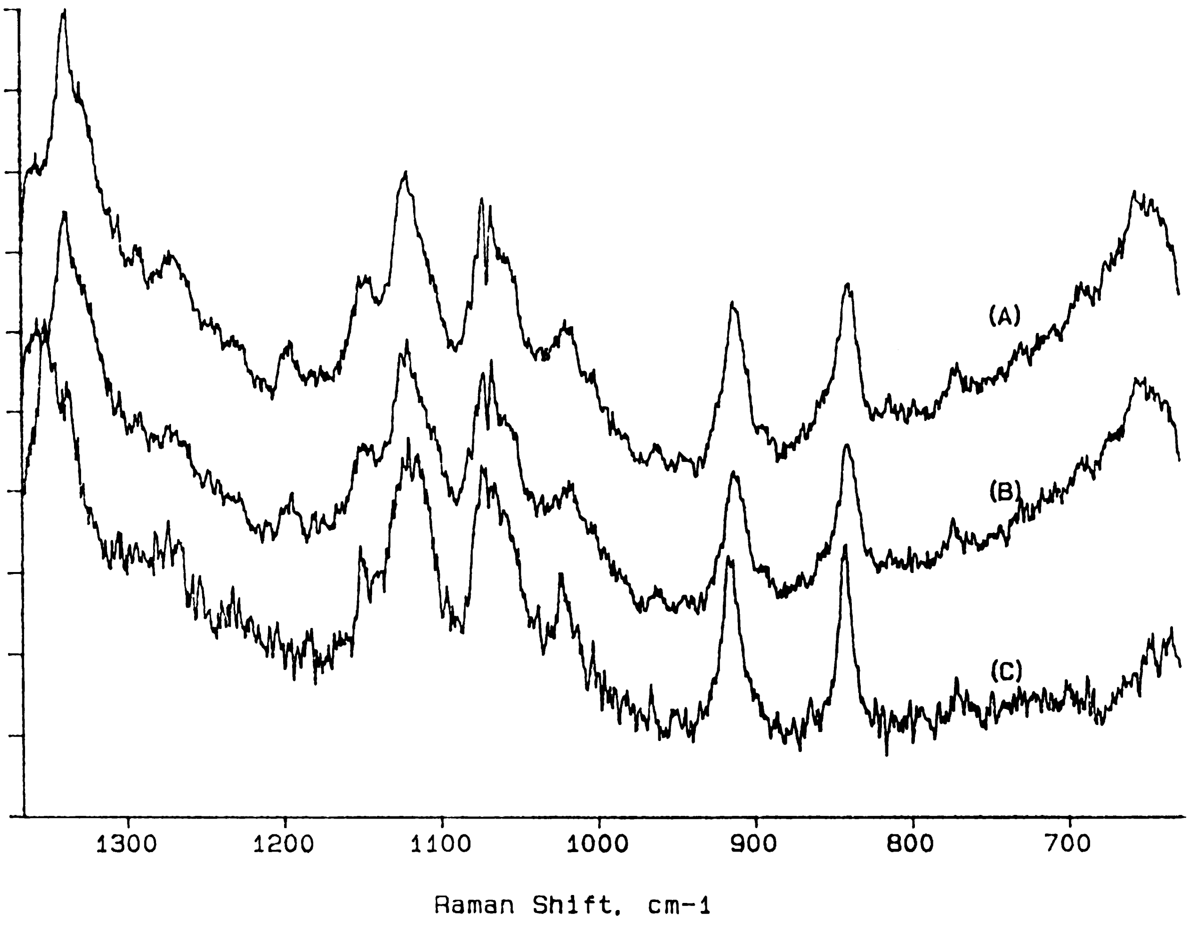

Figure D-9. The time development of the Raman spectra of an anhydrous parent dextrose crystal in solution at 43.0^{o}C and 6^{o}C undercooling.

(A) The parent crystal in solution at t= 0,
(B) the parent crystal in solution at t= 3 hrs.,
(C) the parent crystal in solution at t= 10 hrs.

MICHIGAN STATE UNIV. LIBRARIES
31293005703206